Mechanistic Modeling of Increased Oxygen Transport Using Functionalized Magnetic Fluids in Bioreactors

by

Bernat Ollé Pocurull

M.S.C.E.P., Massachusetts Institute of Technology, Cambridge, MA (2005)
B.Eng. Chemical Engineering, Escola Tècnica Superior d'Enginyeria Química,
Universitat Rovira i Virgili, Tarragona, Spain (2002)

Submitted to the Department of Chemical Engineering
In partial fulfillment of the requirements for the degree of

Doctor of Philosophy in Chemical Engineering Practice

at the

MASSACHUSETTS INSTITUTE OF TECHNOLOGY

May 2007

Author:_____
Department of Chemical Engineering
May 2007

Certified by: _____
Daniel I. C. Wang
Institute Professor
Thesis Supervisor

Certified by:_____
T. Alan Hatton
Ralph Landau Professor
Thesis Supervisor

Accepted by:_____
William M. Deen
Professor of Chemical Engineering
Chairman, Committee for Graduate Students

Mechanistic Modeling of Increased Oxygen Transport Using Functionalized Magnetic Fluids in Bioreactors

by

Bernat Ollé Pocurull

Submitted to the Department of Chemical Engineering on August 28, 2006
In partial Fulfillment of the Requirements for the Degree of
Doctor of Philosophy in Chemical Engineering Practice

ABSTRACT

Absorption of gases into a liquid is of crucial importance to multiphase reactions because diffusion of a sparingly soluble gas across a gas-liquid interface generally limits the relevant reaction rates. Pertinent examples of multiphase reactions that have found application in the chemical and biochemical industries include fermentation, water treatment, and hydrogenation reactions. Gas-liquid mass transfer is of particular importance in fermentation because productivity increases in aerobic cultures are often constrained by transport of oxygen, which is only slightly soluble in water. Previous approaches to enhance oxygen transfer consisted in adding emulsified organic phases in which oxygen has a greater solubility. However, these approaches have several limitations, the most important of which is the difficult recovery of the organic phase after the fermentation.

The research presented in this thesis focuses on the use of functionalized magnetic nanoparticles to enhance gas-liquid oxygen transfer. The nanoparticles have a magnetic core and an organic coating. The magnetic core makes it possible to easily recover the fluid by passing it through a magnetic field, and the coating confers colloidal stability to the particle.

Oxygen transfer enhancement has been observed in the presence of nanoparticles coated with oleic acid and a polymerizable surfactant. In cell-free media, nanoparticles improve gas-liquid oxygen mass transfer up to 6-fold (600%) in an agitated, sparged reactor. Furthermore, they show remarkable stability in high-ionic strength media over a wide pH range. In a fermentation of *Escherichia coli*, a nanoparticle weight fraction of 0.6% increases oxygen uptake rate and cell growth by 40%.

Through a combination of experiments using both physical and chemical methods to characterize mass transfer, it has been shown that both the mass transfer coefficient (k_L) and the gas-liquid interfacial area are enhanced in the presence of nanoparticles, the latter accounting for a larger fraction of the total enhancement. This insight has been used to propose a model of the enhancement that involves two separate mechanisms: one of area enhancement and the other of k_L enhancement. It has been proposed that (i) the nanoparticles increase interfacial area by adsorbing on the gas bubble interface and stabilizing it against coalescence and (ii) the nanoparticles increase the mass transfer coefficient by causing microconvection in the surrounding fluid through Brownian motion.

The methodology developed in this thesis shows several-fold gas-liquid mass transfer enhancements and at the same time allows for easier separation over previous approaches. In addition, the modeling effort resulted in correlations that can allow for extension of this methodology from laboratory-scale to industrial scale reactions across the variable space considered

Thesis Supervisor: T. Alan Hatton
Title: Ralph Landau Professor of Chemical Engineering Practice

Thesis Supervisor: Daniel I. C. Wang
Title: Institute Professor

ACKNOWLEDGEMENTS

For some reason parents usually come *last but not least* in doctoral thesis acknowledgements but in my case they have been so instrumental in my education that any place other than first does not do them justice. They come first for devoting so much time to the upbringing of my brother Linus and me, first for understanding and embracing my choice to come to the US, and first for supporting me through it.

For some other reason, acknowledgements to the thesis advisors tend to follow a certain template of generalities, so I will try to be as specific as I possibly can with mine. I have been fortunate to be co-advised by two unique individuals, and benefited from the best of both. I thank Danny Wang for setting my priorities straight and time and again making his decisions regarding my thesis based uniquely on what was best for me. I also thank him for his straight-talking and straight-questioning that has shown me a good way in science and life: being modest, being honest, and this too, being right –or otherwise shut up. And I thank him for setting a demanding standard for my work; never during the thesis have I had the impression of even coming close to meeting this standard but it has been a worthy goal to strive for. I am sure that with years I will look through his toughness and see a man that shaped my personality in more ways than I can appreciate now.

I thank Alan Hatton above all for making the journey a fun experience. Not truly having set my heart on a specific field of research before I came to MIT, I had the privilege to choose a person to work for, rather than a field to work in. My first conversation with Alan was in late October 2002. It is hard to say what unconscious factors go into the decisions we think are rational, but I estimate that somewhere between the first and second minute in Alan's office I made up my mind to work for him. So I could have left at that point but I stayed and nodded for the following half hour instead. I cannot stress enough how essential Alan has been in making my MIT experience something exceptional. He provided me with two unique opportunities overseas for personal growth through the Practice School in Japan and in Singapore. His welcoming smile whenever I crossed his office doorstep has fueled my will to work during the hard times.

I thank the members of my thesis committee, professors Ken Smith, Greg Stephanopoulos and Bernhardt Trout, for helpful insight during the thesis, and Susan Lanza for keeping the committee meetings running smooth and giving a social life to the Wang group.

I am indebted to George Morrow III, the Dupont-MIT Alliance, and the"la Caixa" Foundation for funding, and to several graduate students, undergraduate students, and post-docs, for their contributions to my work, but to Andre Ditsch more than anyone else. Andre provided helpful advice in virtually every aspect of my thesis, but above all, was a good role model to follow. Lev Bromberg developed the synthesis procedure for the nanoparticles I used in my work. Jin Yin and Bill Perry taught me the experimental techniques for fermentation, and Brad Ciccarelli the technique for surface tension measurement. Evita Grant, as a UROP, and Tracy Holmes, as a BPEC-REU student, also contributed to this work. Fred Ngantung had the patience to listen to the miseries and triumphs of my thesis, and I was glad to listen to his in exchange.

I am grateful to Professor Bob Cohen for pioneering the PhDCEP program. I knew it was the right program for me the first time I read about it and this is what brought me to MIT. I hope the future accomplishments of the students in the program will prove Bob (and the rest of ChemE professors that believed in the program) right.

My MIT experience would not have been the same without Practice School; and Practice School would not have been the same without the company of classmate and travel mate Pete Colvin. It would not have been the same if we had not had a flat tire in a bike in the middle of the Kibi rice plains in Japan, miles from the closest village and without a patch kit. It would not have been the same without the strenuous badminton games at 40^{o}C against the Japanese employees at Mitsubishi either.

Undoubtedly the best memories I will take with me from MIT are from the friends I have made. I thank Joel Moxley for organizing course 10.24, a.k.a. *American Adolescent Studies Program*, designed to give me (*the Spaniard*) an exposure to the high points of growing up in the U.S. in the 80s and 90s. This included watching the likes of *Office Space, Caddyshack*, and the final of the Super Bowl, while eating pizza. This course has been an essential part of my integration to the United States –seriously– and I cannot be thankful enough. One day Joel will be a big shot wherever he goes, and I shall be telling this with a sigh. Gregg –with two g's– Beckham, was my first friend at MIT, the one who put his arm around my shoulder to show me how that first 10.40 problem set wasn't that hard after all. Gregg proofread my thesis and papers with laser precision. Jose Aleman was my treasured Spanish speaking connection at MIT. Joe Shuga, long-time lab mate, was a supporting comrade at work and a worthy companion for long runs around the Charles River. My favorite couple, fine-looking, eloquent Kris Wood, and beautiful and talented Jane Rempel, made sure I got out of the lab on Friday evenings and shared many great times. After I met Lusya this past year, I never again spent 40 hours in a row at MIT running a fermentation.

TABLE OF CONTENTS

LIST OF FIGURES

LIST OF TABLES

1 INTRODUCTION

1.1 Motivation

Maintaining an adequate oxygen supply to aerobic cell cultures has been a long-standing problem in fermentation technology. This problem is particularly amplified in high cell density cultures and in large scale operations, in which insufficient oxygen transfer rates limit cell growth and ultimately process productivity.

Oxygen has a much lower solubility in water than most common nutrients used in fermentation media formulation. For instance, while sugars can be dissolved to concentrations greater than 500 g/L in water, the solubility of oxygen at ambient conditions is less than 10 mg/L. This amount can be consumed in several seconds by a dense microbial broth and therefore a constant gas supply is necessary. Cells can grow at a maximum rate as long as the oxygen supply is sufficient, but when it becomes limiting, cell growth is reduced.

Many approaches have been tried to alleviate oxygen transfer limitations. In the past, research has focused on (i) influencing process conditions by designing more efficient agitation and aeration systems or by enriching air with pure oxygen, (ii) modifying the physical properties of the medium by adding organic compounds capable of solubilizing oxygen more effectively than water (iii) generating oxygen *in situ* with a chemical reaction, and (iv) introducing genetic modifications in the cells to alter oxygen metabolism. The application of most of these remedies has drawbacks and at best, the proposed solutions alleviate, but do not eliminate mass transfer limitations altogether. An incremental enhancement in oxygen transfer rates allows for an extended period of exponential cell growth but, at sufficiently high cell densities, limitations reappear. Therefore, research in new approaches to enhance oxygen mass transfer is necessary.

This thesis investigates the potential for using functionalized solutions of magnetic nanoparticles for enhancing oxygen transfer. These fluids consist of colloidal aqueous solutions of nanoparticles formed by a core of magnetite to which one or more layers of paraffin and polymer can be attached. This technology shows potential for significant mass transfer enhancement while addressing the limitations of former approaches based

on the addition of an organic phase to aqueous media. In particular it allows for the recovery of the dispersed phase after use.

1.2 Specific Aims and Method of Approach

The overall goal of this thesis is to establish the feasibility of using magnetic nanoparticles as a means to enhance solute mass transfer between a gas phase and a liquid phase, with particular emphasis on the application of oxygen transfer in fermentation. In addition, this study will attempt to provide a theoretical explanation of the physical mechanism of enhancement.

The specific aims and proposed method of approach are:

1. To characterize the capability for oxygen transfer enhancement of hydrocarbon-coated magnetic nanoparticles in cell-free systems: experiments are performed by two well-defined methods for the study of mass transfer between a gas phase and a liquid phase. These are (i) a physical method: oxygen is absorbed across the free liquid surface of a stirred beaker exposed to air, and (ii) a chemical method: oxygen is absorbed into a sodium sulfite solution and reacts with the sulfite ions; this reaction mimics oxygen consumption by cells, and is carried out in a laboratory scale bioreactor. Experiments in this model system have the advantage of allowing an accurate measurement of oxygen transfer rates while being less labor-intensive than a fermentation.

2. *To establish the potential for oxygen transfer enhancement of nanoparticles in fermentation media:* first, the biocompatibility of a typical *Escherichia coli* strain with nanoparticle solutions is verified through shake flask experiments; second, fermentations at a 5.5 L scale under an oxygen limited regime are run and oxygen transfer rates and dry cell weight are measured. This establishes the mass transfer enhancement and its connection with increased cell growth.

3. *To identify and model the physical mechanism of oxygen transfer enhancement:* since enhancement can be caused by an increase in interfacial gas-liquid area and by an increase in the oxygen flux, experiments are designed to discriminate between these two phenomena. Subsequently, attention is given to conceivable mechanisms of flux and area enhancement and an enhancement model is proposed.

1.3 Overview

This thesis is organized in six chapters; Chapter 2 reviews the literature on several topics relevant to the thesis, including fermentation technology, gas-liquid mass transfer, magnetic fluids, and nanoparticles as a means of improving transfer properties of solutions, therefore providing the basis for the discussion to follow. Chapter 3 describes in detail the chemical synthesis and characterization of nanoparticles and the experimental methods used to quantify mass transfer in cell-free model systems and in fermentation. Chapter 4 presents experimental results of enhanced mass transfer rates obtained in cell-free systems and in fermentation. In Chapter 5, a mechanism of interfacial area enhancement and a mechanism of mass transfer coefficient enhancement are presented. The main contributions of the thesis are summarized in Chapter 6.

2 LITERATURE REVIEW

This thesis studies the application of colloidal magnetic nanoparticles to a classic problem in fermentation technology, namely oxygen mass transfer. As many of the emerging applications at the interface of nanotechnology and biotechnology, this work exploits the unique properties of materials with particle size in the range of 1 to 100 nm. These include, but are not restricted to, very large surface area and interactions at length scales where wave phenomena and structural phenomena have similar features (Roco, 1999). Therefore this is a multidisciplinary problem. In order to put this thesis in context it is necessary to discuss a number of subjects ranging from classical mass transfer studies of gas-liquid absorption, hydrodynamics, and fermentation technology fundamentals to emerging disciplines that have developed due to a renewed interest in colloidal science fueled by recent advances in organometallic chemistry.

In the framework of this thesis, nanotechnology provides a tool to manipulate gas-liquid mass transfer. While this technological concept can have repercussions in virtually any process limited by mass transfer of a solute between a gas phase and a liquid phase, ranging from waste treatment to blood oxygenation and hydrogenation reactions, special emphasis is given only to its application to oxygen mass transfer in fermentation. Use of nanoparticles with the purpose of modifying the transport properties of a medium is an uncommon concept in the mainstream of research at the interface of biotechnology and nanotechnology, since most current applications are concerned with exploiting nanoparticles as investigative tools to probe ever smaller scales in biological systems and as drug delivery vehicles. However, nanoparticles have been used for over a decade to increase heat transfer properties of solutions. The term *nanofluid* (Choi, 1995) has been coined to describe a new kind of fluids used in a wide range of heat transfer applications. This thesis presents original work on the application of nanoparticles to oxygen mass transfer enhancement.

2.1 Fermentation Technology

Fermentation is defined as the anaerobic metabolism of a molecule into simpler molecules. However, the term is commonly used in microbiology to refer to the making of a product by growth, either aerobic or anaerobic, of a microorganism. This product can be the microorganism itself, a metabolite naturally generated by the microorganism,

or a foreign product that the microorganism is designed to produce through genetic engineering techniques.

Fermentation products such as cheese, wine, and beer have been produced for many centuries, but it is generally considered that fermentation technology in its modern form starts with the pioneering studies of conversion of sugar to alcohol by Louis Pasteur in the 19th century. In the 1940s, a process to produce penicillin by aerobic cell culture became an extraordinary commercial success. Spurred by this achievement, the bioprocess industry grew rapidly. Today, many fine chemicals (antibiotics, vitamins, enzymes, monoclonal antibodies) and bulk chemicals (organic acids, amino acids) are produced by fermentation processes, and the advent of recombinant DNA technology has opened the door to the development of many new products.

2.1.1 A Note on Fermentation Economics

Fermentation processes can be broadly classified into fermentation cost-intensive or recovery cost-intensive, depending on whether most of the operating cost corresponds to the fermentation step or to the downstream processing steps (Bartholomew *et al.*, 1979). Although many factors influence whether a given process falls into one of these categories, generally large-scale production of bulk chemicals is fermentation cost-intensive while production of fine chemicals such as therapeutics is recovery cost-intensive.

Better oxygen transfer permits to achieve higher cell densities in oxygen-transfer limited processes, reduces fermentation cycle time, and increases the titer of the product. Therefore, as a technology aimed at increasing oxygen mass transfer, use of magnetic nanoparticles can have a larger impact when applied to a fermentation cost-intensive process. Specifically, large scale and high-cell density fermentations are the best candidates for its application because they are the most severely limited by oxygen transfer.

Integration of fermentation and purification steps is also a critical aspect in bioprocess economics. While an increased titer of the fermentation product generally reduces the costs of the downstream processing steps, the profits can be offset when this comes at the expense of complicating the medium by adding chemicals that will be difficult to

recover. This is not the case for magnetic nanoparticles. High-Gradient Magnetic Separation (HGMS) can be used to capture nanoparticles larger than 50 nm with an efficiency above 99.9% at high flow rates (Moeser *et al.*, 2004; Ditsch *et al.*, 2005b). Furthermore, magnetic nanoparticles can be used as a replacement for traditional column chromatography for recovery and purification of proteins (Ditsch *et al.*, 2004). This potentially allows integration of fermentation and separation steps in a bioprocess.

2.1.2 Relevance of Oxygen Transfer

At high cell densities it becomes very difficult to maintain dissolved oxygen at a level that allows cells to grow at their maximum rate. When oxygen supply becomes limiting, cell viability and product formation decline; furthermore, cells start producing acetate and lactate, which inhibit cell growth. Therefore, it is highly desirable to maintain a growing culture under conditions in which oxygen limitations do not exist. If the rate of oxygen transfer to a culture is higher than the metabolic oxygen demand and no other nutrients are limiting the growth, cells can grow at their maximum rate. Under these conditions, the metabolic oxygen consumption of a culture can be expressed as:

$$OUR = \frac{\mu}{Y_{X/O_2}} X \qquad (1)$$

Where OUR is the oxygen uptake rate, μ is the growth rate of the organism, $Y_{X/O2}$ is a stoichiometric coefficient that represents the yield of biomass on oxygen, and X is the concentration of biomass. At the onset of a fermentation process, dissolved oxygen concentrations are typically high and cells can consume oxygen at a rate given by Eq. 1. If no control actions are taken to maintain high dissolved oxygen concentrations, as fermentation proceeds the oxygen levels fall to approximately zero. At some point during the fermentation, the biological demand of the culture exceeds the oxygen mass transfer rate and the culture enters an oxygen-limited regime in which the growth rate can no longer be exponential; instead, the growth slows down and becomes linear. Under these conditions, the amount of oxygen that the cells consume is expressed as

$$OUR = k_L a\left(C^* - C_{bulk}\right) \qquad (2)$$

Where $k_L a$ is a volumetric mass transfer coefficient, which is the product of a gas-liquid mass transfer coefficient and a specific interfacial area between the gas phase and the

liquid phase; C^* is the oxygen concentration at the interface and C_{bulk} is the oxygen concentration in the bulk of the liquid.

2.1.3 Strategies for Oxygen Transfer Enhancement

Numerous approaches have been tried to improve oxygen mass transfer between gas bubbles and the liquid phase. Inspection of Eq. 2 shows that oxygen uptake rates can be modified by altering the mass transfer coefficient, the specific interfacial area, or the concentration driving force. Classical engineering approaches have focused on modifying these three quantities. Alternative approaches involving generation of oxygen by a reaction or genetic engineering of the host have also been explored.

2.1.3.1 Increasing Agitation Rate and Aeration Rate

Many investigations have studied the effect of agitation and aeration on oxygen transfer and as a result, numerous empirical formulations have been proposed. Increasing the agitation rate has an effect on both the specific interfacial area – it increases it by breaking up bubbles – and the mass transfer coefficient – it reduces the thickness of the liquid boundary layer around a gas bubble (Section 2.2.2). In large scale fermentations, energy costs from power consumption are a major contributor to operating costs, and therefore, agitation rates cannot be maintained arbitrarily higher. Additionally, higher agitation rates are not an option in shear-sensitive organisms. Increasing the aeration rate enhances the interfacial area but the rate must be maintained below the flooding limit of the fermentor. In addition, various impeller types and fermentor geometric configurations have been suggested to optimize oxygen mass transfer (Hu *et al.*, 1986; Junker *et al.*, 1998).

2.1.3.2 Increasing Oxygen Partial Pressure

Increasing the partial pressure of oxygen increases the driving force for mass transfer This can be done by pressurizing the headspace of the bioreactor (Bauer *et al.*, 1974). Pressures of up to 3 bars can be used in conventional fermentors without need for mechanical modifications (Yang *et al.*, 1992), and therefore, 3-fold enhancements in *OUR* can be obtained. The driving force can also be increased by using pure oxygen or air enriched with oxygen (Flickinger *et al.*, 1977b, 1977a; Yamada *et al.*, 1978; Flickinger *et al.*, 1979); a maximum 5-fold enhancement can be obtained if pure oxygen

is used since the partial pressure of oxygen is 1 atm rather than 0.21 atm in air. Both approaches have several limitations; gas costs become significant when sparging with oxygen-enriched gas mixtures, pure oxygen is explosive and poses a safety concern, increased pressure of the carbon dioxide generated by cells is detrimental to cell growth, and recently it has been found that elevated oxygen pressure or rapid increases in oxygen levels cause oxidative stress in some organisms. Some of the mechanisms causing oxidative stress have been reviewed (Konz *et al.*, 1998).

2.1.3.3 Increasing Interfacial Area

Interfacial area can be increased by reducing the average gas bubble size. Micro-bubble dispersions (Kaster *et al.*, 1990; Bredwell *et al.*, 1998; Weber *et al.*, 2005; Zhang *et al.*, 2005), also referred to as colloidal gas aphrons (Srivastava *et al.*, 2000), are dispersions of small gas bubbles stabilized with a surfactant film that prevents bubble coalescence. Despite a reduction in the mass transfer coefficient (k_L) caused by the surfactants, smaller bubble sizes have orders-of-magnitude larger interfacial area and an extended residence time in the fermentor. Although the application of micro-bubble dispersions is attractive given the large increases in $k_L a$ that can be obtained (3 to 6-fold enhancements have been reported), no serious consideration has been given to their recovery from the fermentation broth.

2.1.3.4 Generation of Oxygen by a Chemical Reaction

Oxygen generation *via* a chemical reaction has also been used to enhance oxygen supply. Oxygen can be generated by the cleaving of hydrogen peroxide by a catalase (Schlegel, 1977; Ibrahim *et al.*, 1980; Holst *et al.*, 1982; Nies *et al.*, 1984; Pardieck *et al.*, 1992; Rosenberg *et al.*, 1992; Sonnleitner *et al.*, 1997) or by oxygen-producing algae (Adlercreutz *et al.*, 1982a; Adlercreutz *et al.*, 1982b, 1982c; Nies *et al.*, 1984). These can be attractive approaches when the organism being cultivated is shear sensitive, *e.g.* mammalian cells. The primary disadvantages are the low flux of oxygen generated by algae and the rapid deactivation of the catalases that cleave peroxides. In addition, the *in situ* generation of oxygen by hydrogen peroxide is difficult to control; if the rate of oxygen production is greater than its consumption, bubble coalescence is inevitable and defeats the original purpose.

2.1.3.5 Use of Hemoglobin

Several researchers have exploited the high affinity for binding oxygen to hemoglobin and myoglobin as a means of increasing oxygen transfer. Enhancement of oxygen transfer dependent on hemoglobin loading to the fermentation media was observed (Adlercreutz *et al.*, 1982d), but high oxygen binding affinity and deactivation of hemoglobin made this approach impractical. A bacterial heme protein was discovered in *Vitreoscilla* (Wakabayashi *et al.*, 1986) that had an amino acid sequence similar to the globin proteins of mammals. Building on this finding, an elegant approach consisting of cloning the hemoglobin gene from *Vitreoscilla* and expressing it in *Escherichia coli* was proposed (Khosla *et al.*, 1988b, 1988a). It was found that cells with the *Vistreoscilla* hemoglobin grew faster under oxygen limitations and could attain higher densities than the control strain. Subsequent studies showed that the interplay of the *Vitreoscilla* hemoglobin with the terminal oxidases was responsible for enhanced respiratory activity (Kallio *et al.*, 1996). This approach was attempted successfully in other industrially relevant organisms such as *Streptomyces* and *Saccharomyces*. A foreseeable limitation of this approach is that it does not affect the physical oxygen transfer from the gas bubbles to the liquid. A comprehensive review on the subject has been published (Frey *et al.*, 2003).

2.1.3.6 Use of Dispersed Organic Phases

Dispersion into the fermentation media of an organic phase in which oxygen has a higher solubility than in water is another approach to increase oxygen transfer; a great deal of attention has been given to the use of aqueous emulsions of hydrocarbons and perfluorocarbons to increase oxygen transfer. In the literature, these systems have often been referred to as “oil-in-water” systems, “oxygen carriers”, or “oxygen vectors”. These dispersions can be created by agitation, in which case the emulsions are unstable, or by use of surfactants, in which case the solutions remain stable without agitation. Kerosine was found to increase oxygen transfer using the sodium sulfite oxidation method (Mimura *et al.*, 1969). These findings where subsequently extended to oleic acid and toluene (Yoshida *et al.*, 1970). Subsequently the mechanism of gas transfer enhancement into oil-in-water solutions was explored and different mechanisms were identified depending on the spreading coefficient of the emulsion (Linek *et al.*, 1976). Interest quickly extended to PFCs (Mattiasson *et al.*, 1983, 1987; Lowe, 1991) because of

their high oxygen solubilities (15 to 20 times higher than water), the higher diffusivities of oxygen in PFCs as compared to water, and their remarkable biocompatibility. Spraying of a PFC through fermentation media and subsequent recycling was used in microbial systems to achieve oxygen uptake rates up to six times higher than in water (Damiano *et al.*, 1985). Emulsification of a PFC into micron-sized droplets by mechanical agitation was used to attain oxygen transfer rates 2.5-fold higher on a total liquid volume basis (per liter of water + PFC) in the presence of 40% PFC (McMillan *et al.*, 1987; Junker *et al.*, 1990; McMillan *et al.*, 1990b). An ample review of the applications of PFCs in biotechnology and biomedicine has been presented by Lowe (Lowe *et al.*, 1998). A review of the mechanisms of the mass transfer enhancement in the presence of dispersed organic phases will be presented in Section 2.2.4.

Only a few of the outlined strategies for oxygen transfer enhancement have been applied in industry with success. Traditionally, industrial focus has been placed on increasing power input, increasing aeration, and enriching the gas feed with oxygen. Judging from the number of publications to date, use of dispersed organic phases of oxygen carriers has been the most attractive alternative to these standard practices. However, its industrial application has several limitations, the most important being that PFCs and hydrocarbons cannot be easily recovered after a fermentation cycle. Other limitations include formation of foams, inefficient use of the bulk liquid (*e.g.*, 40% of the liquid phase is taken up by PFC for a 2.5-fold enhancement in oxygen transfer (McMillan, 1990)), and entrainment and evaporation of the organic phase, which in turn leads to serious environmental concerns in the case of PFCs.

Use of hydrocarbon- or PFC-coated magnetic nanoparticle dispersions offers a solution to the limitations previously listed. Recovery of the dispersed phase can be accomplished readily through HGMS (Moeser *et al.*, 2004; Ditsch *et al.*, 2005b); significant mass transfer enhancements can be obtained at particle loadings lower than 1% mass fraction (Section 4.2). In addition, the nanoparticles are non-volatile and are synthesized with benign, low-cost chemicals, which makes their application attractive from an environmental and an economic standpoint. The application of PFC-coated magnetic nanoparticles to oxygen transfer enhancement in biological processes is covered by an international patent (Olle *et al.*, 2005); a continuation-in-part of the patent also covers

hydrocarbon-coated magnetic nanoparticles. This will be discussed in more detail in Section 2.3.

2.2 Gas-Liquid Mass Transfer

Absorption of gases into a liquid or a slurry is of crucial importance to multiphase reactions, because diffusion of a sparingly soluble gas species across a thin liquid film at the gas-liquid interface generally limits the reaction rates. Many instances of multiphase reactions in 3-phase fluidized bed processes (gas-liquid-solid or liquid-liquid-solid) that have found application in the petrochemical, chemical, and biochemical industries have been listed (Kim *et al.*, 1997). Typical applications include hydrogenation and hydrodesulfurization of oil, water treatment, the Fischer-Tropsch process, coal liquefaction, methanation of CO, and fermentation.

This section introduces first the typical mass transfer steps in a fermentation process. Next, the basic film theories to model interfacial gas-liquid mass transfer are introduced. The section subsequently reviews several theoretical models that have been proposed to explain enhanced mass transfer in gas-liquid-solid or gas-liquid-liquid systems. These models are of relevance to this thesis because the underlying gas-liquid mass transfer phenomena are the same that are encountered in fermentation.

2.2.1 Mass Transfer Steps in Fermentation

Oxygenation in a fermentation process is generally achieved by sparging air while applying mechanical agitation to break up the air bubbles and maintain good mixing. The transport of oxygen from the gas bubbles to the cells has three major steps, as shown in Figure 2-1: 1) diffusion of oxygen from the bulk of the gas bubble to the gas-liquid interface; 2) diffusion through the liquid layer around the bubble; and 3) transfer by convection or turbulence to the cell. Three additional steps can be considered for a broader description, which include transport through the liquid film surrounding a cell, diffusive transport through a cellular cluster or mycelia, and transport across the cell envelope (Bailey *et al.*, 1986). Mixing inside the gas bubble is typically good and the rate at which gas molecules travel to the interface is high. The diffusivity of oxygen in the gas phase is roughly 4 orders of magnitude larger than in water and therefore step 1 seldom poses a limitation to mass transfer. Similarly, good mixing in the bulk liquid

phase is usually guaranteed by sufficient agitation and step 3 rarely limits the mass transfer process. It is widely accepted that the transfer of oxygen through the liquid film around the gas bubble (step 2) controls the overall oxygen transfer rate; therefore, the liquid film mass transfer coefficient (k_L) is a good approximation of the overall coefficient. Most of the studies presented in the literature have taken a single bubble as the representative unit of the mass transfer system and ignored bubble size distributions and effects of poor mixing in the bulk liquid phase. Another common assumption has been to neglect the curvature of the bubble; this assumption is justified because the size of a bubble is generally 2 orders of magnitude larger than the thickness of the gas-liquid interface. This latter consideration yields a 1-D mass transfer problem, with diffusion occurring only in the normal direction to the gas-liquid interface.

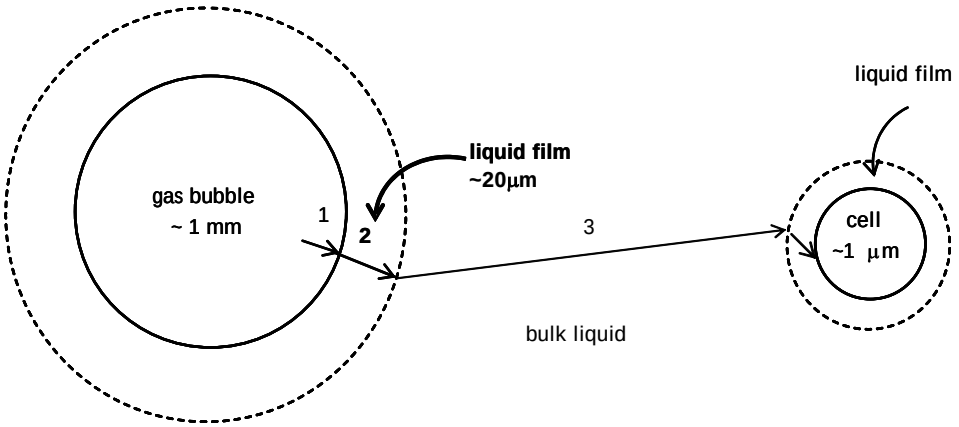

Figure 2-1. Steps in Mass Transfer from a Gas Bubble to a Cell

2.2.2 Film Theories

Several models for mass transfer at the gas-liquid interfacial region have been proposed. These models are commonly taken as a basis for modeling mass transfer in 3-phase systems. These are models that do not incorporate the hydrodynamic features of the flows at the vicinity of the gas-liquid interface.

Lewis and Whitman's *film theory* (Lewis *et al.*, 1924) assumes Fickian diffusion of a solute through a stagnant liquid film at the gas-liquid interface. Convective mass transfer is neglected and steady state diffusion assumed. This film theory predicts a dependence of the mass transfer coefficient on the diffusivity of the gas solute in the liquid phase, $D_{A,L}$, of

$$k_L = D_{A,L} / \delta \tag{3}$$

that is not consistent with experimental results. At liquid-solid boundaries, the typical relationship is given by $k_L \propto D_{A,L}^{2/3}$ and at gas-liquid boundaries, given by $k_L \propto D_{A,L}^{1/2}$. The parameter δ introduced in the expression represents the thickness of the concentration boundary layer around a gas bubble. Despite its apparent limitations, Whitman's theory has been applied to a range of complex mathematical problems for which only a simple film diffusion model yields analytical solutions.

Higbie's *penetration theory* (Higbie, 1935), assumes that turbulence brings fluid elements from the bulk to the gas-liquid interface. The elements are stagnant and the initial solute content is equal to the bulk concentration when the element first contacts the interface. Subsequently, unsteady diffusion occurs for a fixed residence time. The dependency of k_L on diffusivity and the residence time of the fluid elements is given by

$$k_L = 2\sqrt{D_{A,L} / \pi t} \tag{4}$$

Danckwerts' *surface renewal theory* (Danckwerts, 1951) proposes that not all liquid elements stay at the interface for an equal amount of time; instead, there is an age-distribution function $\psi(t) = se^{-st}$ where s is the inverse of an element's residence time at the interface (or a rate of surface renewal). The expression for k_L is

$$k_L = \sqrt{D_{A,L} s} \tag{5}$$

In both Higbie's and Danckwerts' models, the residence time at the interface determines the mass transfer rate. Therefore, this residence time must be shorter than the time scale for molecular diffusion through the liquid film. Both theories provide more accurate predictions of experimental data than Whitman's theory; however, none of the 3 models proposes physical arguments on which to calculate the value of the quantities t – given by Eq. 4 – or s – given by Eq. 5.

2.2.3 Hydrodynamic Models

Turbulence affects the rate at which liquid elements are renewed at a gas-liquid interface. Film theories fail to provide a model for the calculation of the residence time (or renewal rate) of fluid elements and therefore cannot be used to predict sets of experimental data that have been obtained at different conditions of turbulence. Several models to estimate this parameter have been proposed.

Eddy models assume that the renewal of the interface is caused by small turbulent eddies. Isotropic turbulence theory states that at high wave numbers turbulence depends only on power input per unit mass ε (which can be measured directly or calculated) and kinematic viscosity ν; the length scale and time scale characteristic of the smallest eddies at which energy dissipation occurs are given by $l = \left(\nu^3 / \varepsilon\right)^{1/4}$ and $\tau = \left(\nu / \varepsilon\right)^{1/2}$ respectively. Under the assumption that mass transfer is determined by the smallest eddies, which have smaller scales than the gas bubbles, a relation has been proposed (Lamont *et al.*, 1970)

$$k_{\mathrm{L}} = c\left(\varepsilon\nu\right)^{1/4}\left(\frac{D_{\mathrm{A,L}}}{\nu}\right)^{n} \tag{6}$$

where *c* is a constant, and the exponent *n* has a value of 1/2 for a fluid surface and 2/3 for a solid surface (the presence of surfactants can rigidify a gas-liquid interface and make it behave as a solid). Lamont proposed a value of 0.4 for the constant *c*. A value of *c* of 0.448 was reported for experiments in sodium sulfite solutions (Linek *et al.*, 2005).

Slip velocity models assume that the relative motion of a bubble in a liquid determines the surface renewal. Slip velocities are typically equated to single bubble terminal rise velocities. Bubbles are generally classified into small (bubble diameter d_{B} below 1 mm) or large (d_{B} above 2 mm) (Calderbank *et al.*, 1995). The former behave as rigid spheres, the latter have mobile interfaces. If a gas-liquid slip velocity is known for a given system, boundary layer theory can be used to estimate a mass transfer coefficient. Equations to describe mass transfer around spherical bodies have been proposed (Lochiel, 1964); for Re>>1, the Sherwood number ($Sh = k_L d_B / D_{A,L}$) is

$$Sh = 0.7\, Re^{1/2}\, Sc^{1/3} \quad \text{(immobile interface)} \tag{7a}$$

$$Sh = 1.13\left[1 - \frac{2 + 3\dfrac{\mu_G}{\mu_L}}{1 + \left(\dfrac{\rho_G \mu_G}{\rho_L \mu_L}\right)^{1/2}} \frac{1.45}{\mathrm{Re}^{1/2}}\right]^{1/2} Pe^{1/2} \quad \text{(mobile interface)} \qquad (7b)$$

where *Sc*, *Pe*, and *Re*, are the Schmidt, Peclet, and Reynolds numbers, and the subscripts *G* and *L* refer to the gas and liquid phases respectively.

While eddy models predict an increase of k_L with turbulence as a function of $\varepsilon^{1/4}$, slip velocity models predict a decrease because turbulence creates smaller bubbles, which rise at a slower velocity. The application of both types of model to extensive literature data has been reviewed (Linek *et al.*, 2005); it has been concluded that only eddy models give reliable predictions in mechanically agitated systems, which is consistent with the results of this thesis (Section 4.2.2), while in non-agitated systems both types of models are appropriate.

2.2.4 Models of Mass Transfer in the Presence of a Dispersed Phase

The presence of a dispersed phase, either liquid or solid, in which the solubility of the solute of interest is higher than in the base medium, poses an interesting theoretical mass transfer problem. Dispersions of small particles or liquid droplets have frequently been modeled by means of effective property models. Such models are appropriate when the typical dimension of a dispersed phase element is much smaller than the dimension of the domain through which mass transfer occurs. Typically, this domain is the liquid film around a gas bubble. If this requirement is satisfied, the dispersion can be considered macroscopically homogeneous in spite of its biphasic nature, and the transport and equilibrium properties of the medium, *e.g.* diffusivity and solubility, can be expressed as effective properties of the two components of the dispersion. Maxwell lead the way in the study of transport properties of 2-component mixtures by deriving a theoretical form for the effective thermal conductivity of a dilute suspension of spheres (Maxwell, 1873). An extension of Maxwell's approach that includes interactions between pairs of spheres was later presented (Jeffrey, 1973). Jeffrey's expression for the effective thermal conductivity of a dispersion can be adapted to mass transfer to obtain an analogous form for effective diffusivity of a solute *A* in a medium *L*

$$\frac{D_{\text{effective}}}{D_{\text{A,L}}} = 1 + 3\beta\phi + \phi^2\left(3\beta^2 + \frac{3\beta^3}{4} + \frac{9\beta^3}{16}\frac{\alpha+2}{2\alpha+3} + \frac{3\beta^4}{2^6} + \cdots\right) = \tag{8}$$

$$= 1 + 3\beta\phi + F(\beta)\phi^2$$

where:

$$\beta = \frac{\alpha - 1}{\alpha + 2} \tag{9}$$

$$\alpha = \frac{D_{\text{A,dispersed phase}}}{mD_{\text{A,L}}} \tag{10}$$

$$m = \frac{C_{\text{A,L}}^{\text{eq}}}{C_{\text{A,dispersed phase}}^{\text{eq}}} \tag{11}$$

The values for the coefficient F(β) are given in the original paper by Jeffrey (1973).

It has been shown that Eq. 8 underpredicts the enhancement experimentally determined in PFC-water systems (McMillan, 1990). This is because Jeffrey's analysis is based on steady state, while mass transfer from bubbles in an agitated, sparged vessel is a transient process; enhancement is largest at short times, when the dispersed phase is still not loaded with solute, and decreases with time. Different definitions of enhancement have been used in the literature; a commonly used form is the ratio of solute fluxes in the presence and absence of a dispersed phase

$$E = \frac{N_{\text{solute,with particles}}}{N_{\text{solute,base medium}}} \tag{12}$$

Since experiments are generally performed at a fixed driving force, enhancement as expressed in Eq. 12 is also the ratio of volumetric mass transfer coefficients in the presence and absence of dispersed phase. For a proper comparison with experimental results of gas absorption, it is necessary to express the solute fluxes as a function of time and integrate them over a typical exposure (or surface renewal) time.

Film theories (Section 2.2.2) have been used as the starting point for most modeling approaches for mass transfer in dispersions because the mathematical problems that arise from their use can be solved analytically. Early experimental observations of enhanced gas absorption in the presence of dispersed active carbon (Kars *et al.*, 1979; Alper *et al.*, 1980) instigated the development of film models for mass transfer in the presence of a

dispersed phase. Alper e*t al.* used carbon and quartz particles of average size 5 μm; carbon enhanced mass transfer, and quartz did not; enhancement was attributed to the highly porous structure of activated carbon. Many theoretical studies followed. Models proposed to date have been classified as homogeneous and heterogeneous (Brilman *et al.*, 2000). Homogenous models assume a homogeneous distribution of the dispersed phase in the bulk and in the film and generally do not account for concentration gradients inside the dispersed phase. Heterogeneous models account for diffusion of the solute alternately through bulk and particle phase; some have considered additional effects such as particle-particle interactions, adsorption of the dispersed phase at the gas-liquid interface, and curved geometry of the interfaces. In both types of models, it is generally argued that gas absorption enhancement occurs because the dispersed phase interacts with the solute at the gas-liquid interface by removing it from the interface and transporting it to the bulk medium. The main assumptions underlying the models presented in the literature have been summarized (Mehra, 1988). These are (i) no fluid flow in the film; (ii) diffusivity of the solute is not affected by the dispersed phase holdup; (iii) the dispersed phase does not alter the interfacial area available for mass transfer; (iv) the size of the elements of the dispersed phase is smaller than the thickness of the mass transfer film; (v) the microfilms surrounding the dispersed phase droplets or particles do not overlap; and (vi) the surface renewal frequency is unaffected by the presence of the dispersed phase. A final common element of all modeling approaches formulated thus far is that they have been developed to explain experimental data obtained in dispersed phases with particle or droplet size on the order of 1 μm to 1 mm (generally termed *microphases*.)

2.2.4.1 Homogeneous models

The central feature that distinguishes a homogenous model from a heterogeneous model is the assumption that the dispersed phase is equally distributed through the liquid film. This consideration alone simplifies the mathematical treatment of the problem significantly and in many cases allows an analytical solution. Additionally, homogeneous models assume that the dispersed phase does not directly contact the gas interface, and concentration gradients inside the dispersed phase are ignored.

A general formulation for mass transfer in the presence of a microphase using Higbie's and Danckwerts' theories has been presented (Mehra, 1988; Mehra *et al.*, 1988). The governing equations for the continuous phase and for the dispersed phase are

$$D_{\mathrm{A,L}}\frac{\partial^2 A}{\partial x^2} = (1-\phi)\frac{\partial A}{\partial t} + f\left(A, A_{\mathrm{L0}}\right) \qquad \text{(continuous phase)} \tag{13}$$

$$D_{\mathrm{p}}\frac{\partial^2 A_{\mathrm{L0}}}{\partial x^2} = \phi\frac{\partial A_{\mathrm{L0}}}{\partial t} + f\left(A, A_{\mathrm{L0}}\right) \qquad \text{(dispersed phase)} \tag{14}$$

$$f\left(A, A_{\mathrm{L0}}\right) = \phi K_0\left(A - \frac{A_{\mathrm{L0}}}{m}\right) \tag{15}$$

with initial and boundary conditions:

$$\begin{aligned} &t = 0 \quad A = A_{\mathrm{L0}} = 0 \quad all\ x \\ &t > 0 \quad A = A^*, \frac{\partial A_{\mathrm{L0}}}{\partial x} = 0 \quad at\, x = 0 \\ &A \to 0 \quad A_{\mathrm{L0}} \to 0 \quad at\, x \to \infty \end{aligned} \tag{16}$$

where A is the concentration of the solute in the continuous phase, ϕ the dispersed phase holdup, A_{L0} the concentration of solute in the dispersed phase, D_{p} the diffusivity of a dispersed phase droplet, A^* the solubility of the solute in the continuous phase, K_0 the volumetric mass transfer coefficient based on the continuous phase, and m the relative distribution coefficient for the solute between the continuous and dispersed phase. It has been shown that for spherically symmetrical droplets of size d_{p} with negligible motion relative to the continuous phase, K_0 in Eq. 15 can be estimated as $K_0 = 12 D_{\mathrm{A,L}} / d_{\mathrm{p}}^2$ (Mehra, 1988; Mehra *et al.*, 1988). From surface renewal theory, the instantaneous rate of absorption averaged over a surface renewal time is expressed as:

$$R_{\mathrm{A}} = S\int_0^{\infty} - D_{\mathrm{A,L}}\left.\frac{\partial[A]}{\partial x}\right|_{x=0} e^{-St}dt \tag{17}$$

with the surface renewal time $S = k_{\mathrm{L}}^2 / D_{\mathrm{A,L}}$. The base rate in the absence of dispersed phase can be expressed as

$$R_{\mathrm{A,base}} = \sqrt{S \cdot D_{\mathrm{A,L}}}\left[A^*\right] \tag{18}$$

Under the assumption that $D_p / D_{A,L} << \phi K_0 / S(1-\phi)m$, an analytical expression for the enhanced absorption rate in the presence of a dispersed phase is obtained

$$R_{A,enhanced} = [A^*]\sqrt{(1-\phi)D_{A,L} I_1} \tag{19}$$

where the term I_1 is

$$I_1 = \sqrt{\frac{S^2 + \left(\frac{\phi K_0}{1-\phi} + \frac{K_0}{m}\right)S}{S + \frac{K_0}{m}}} \tag{20}$$

The enhancement in the absorption rate due to the presence of the dispersed phase can be calculated as the ratio of Eq. 19 and Eq. 18. Figure 2-2 illustrates the effect of a homogeneously dispersed phase in the liquid film; droplets or particles solubilize preferentially the solute in the medium and locally deplete their surroundings. The decreased local concentrations in the surrounding medium translate into steeper concentration gradients at the interface and therefore a higher solute flux.

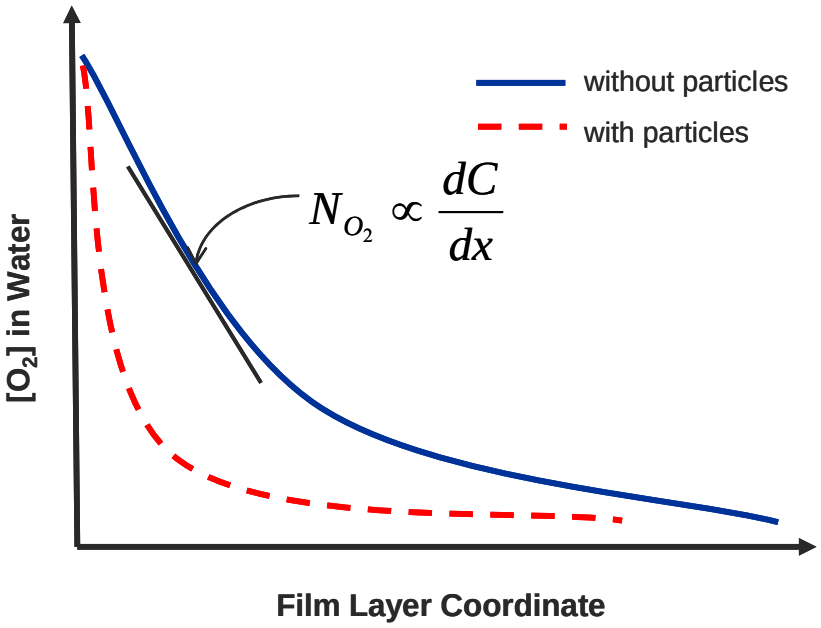

Figure 2-2. Illustration of the Effect of a Homogeneously Dispersed Phase on Mass Transfer

Using homogeneous models, reasonable predictions of enhanced mass transfer in dispersions have been obtained for cases in which the particle or droplet size is smaller

than the film thickness (Bruining *et al.*, 1986; Mehra *et al.*, 1988; Cents *et al.*, 2001). Droplets larger than the film thickness do not show enhancement, possibly because they can not penetrate into the film. A simple expression for the absorption enhancement, *E*, has been proposed (Bruining *et al.*, 1986)

$$E = \left(1 + \phi(m-1)\right)^{1/2} \tag{21}$$

where ϕ is the volume fraction of the droplet phase and *m* is the partition coefficient of oxygen between the droplet phase and the surrounding phase. Bruining makes the case that two conditions must be met to obtain an enhancement of the absorption rate: (i) the particle size must be smaller than the film thickness; (ii) an interaction between the particle and the solute is necessary because inert particles show no enhancement of mass transfer.

2.2.4.2 Heterogeneous models

Heterogeneous approaches model the solute diffusion alternately through the bulk and particle phases; in some cases, these models also account for the effect of dispersed phase droplets near the interface. Mass transfer enhancement data obtained for aqueous solutions of activated carbon particles suggest that it would be required to have higher particle holdups at the interface than in the bulk to predict theoretically the observations (Holstvoogd *et al.*, 1988); data show an initial linear increase of absorption enhancement as a function of the dispersed phase holdup, followed by a transition to a plateau at solids concentrations on the order of 1kg/m^3. Holtsvoogd *et al.* hypothesized that this change in regime corresponded to the formation of a close packing of solids at the interface. There is experimental evidence of this phenomenon; the adhesion of small metal and activated carbon particles to bubbles was investigated with a bubble pick-up method which yields an estimation of the fraction of the bubble interfacial area covered by particles (Wimmers *et al.*, 1988a, 1988b; Vinke *et al.*, 1991). The authors proposed that the concentration of particles at the gas-liquid interface could be expressed as a function of the bulk concentration through an adsorption isotherm. Subsequent work proposed a Langmuir isotherm to relate the interfacial coverage to the bulk concentration (Vinke *et al.*, 1993); a model to express the initial enhancement in gas absorption as a function of the fractional coverage of the gas-liquid interface by particles was formulated. In this model, two parameters, *k* (the adsorption constant) and ξ_{max} (the maximum possible

coverage of the interface), where determined from a fit to experimental data. This model proposes an analytical expression for the enhancement factor

$$E = 1 + \zeta \left[\frac{4D_{A,L}}{d_p k_L} \left(\frac{1 - \exp^{(-t_p/t_s)}}{t_p / t_s} \right) - 1 \right] \tag{22}$$

where ξ is the fraction of the interface covered by solids, d_p the droplet size, and t_p/t_s is the quotient of the residence time of the particle at the interface and the time it takes for the particle to saturate with solute. These two times scales can be expressed as

$$t_s = \frac{m\pi d_p^2}{24 D_{A,L}}, \quad t_p = \frac{4 D_{A,L}}{\pi k_L^2} \tag{23}$$

A version of Vinke *et al.*'s model that accounts for unsteady mass transfer of solute into the particles has been derived (Demmink *et al.*, 1998); the authors also used an expression with the form of a Langmuir isotherm but noted that the two fitted parameters initially proposed by Vinke *et al.* were dependent on the agitation conditions. Recently, a heterogenous model that accounts for the possibility of formation of several layers of solids on the gas-liquid interface has been proposed (Nagy, 2003).

Other heterogeneous models have not considered particle attachment at the interface, but rather focused on the local geometry of the interface. These models predict that the proximity to the gas-liquid interface of the closest droplet has a strong influence on the enhancement (Brilman *et al.*, 1998; Brilman *et al.*, 2000). An analytical 1-D transient model for one particle in the film with one adjustable parameter, which is valid for situations in which the dispersed phase elements and the liquid film have a comparable size was developed (Junker *et al.*, 1990; McMillan *et al.*, 1990b). Models in 2-D and 3-D that take into account the spherical shape of the dispersed phase have also been developed (Karve *et al.*, 1990); these models can only be solved with a numerical approach. Using a unit cell approach, Karve *et al.* showed that absorption enhancement is dominated by the closest particle to the interface. A mechanism of enhancement based on the enhanced solute permeability of the film, which takes into account the effects of both different diffusivity and solubility of the solute in the dispersed phase has been proposed (McMillan *et al.*, 1990b); comparison with experimental data shows good agreement at dispersed phase holdups below 0.3.

2.2.4.3 Effect of the Dispersed Phase on Interfacial Area

While the effect of a dispersed phase on the mass transfer flux of a solute has been researched in detail both experimentally and theoretically, the effects on gas-liquid interfacial area have received less attention. Most studies have been performed in stirred cells precisely to isolate flux effects by having a fixed, known interfacial area. Accordingly, mechanisms for enhanced or decreased interfacial area in the presence of a dispersed phase have not been proposed. A recent review of experimental studies on the effect of a dispersed phase on mass transfer points out that the literature contains contradictory results with regard to the effect of interfacial area and lacks systematic studies (Dumont *et al.*, 2003). Photographic methods have been used to measure bubble size distributions in the presence of emulsions (McMillan *et al.*, 1990a; Rols *et al.*, 1990). Rols *et al*. showed that the size distribution is not affected by the addition of emulsified n-dodecane, and measured a modest 15% increase of interfacial area. McMillan *et al.* showed no measurable increase in interfacial area upon dispersion of PFCs. The gas-liquid specific interfacial area in slurries of activated carbon, kieselghur, and aluminum oxide has been measured using the sodium sulfite method (Quicker *et al.*, 1984); for all materials studied, at low solid loadings, no significant changes were reported in area; at higher solid loadings, interfacial areas decreased by up to a factor of 3 for kieselguhr. The authors correlated the decrease in interfacial area with the effective viscosity of the medium. According to a recent report, carbon particles adhere to gas-liquid interfaces because of their hydrophobic nature, and promote bubble coalescence and therefore reduce interfacial area (Van Der Zon *et al.*, 2002). Bubble coalescence has been studied in solutions of alcohols and fatty acids; results show that coalescence times are proportional to the surface excess concentration of the molecular solute, and that coalescence times increase with polarity of the hydrophilic group of the solute and its chain length (Drogaris *et al.*, 1983); longer coalescence times increase interfacial area. This research is of relevance to the present thesis because the nanoparticles used in this thesis are coated with a first layer of a fatty acid and a second layer of charged, hydrophilic polymer. While nanoparticles are approximately 2 orders of magnitude larger in size than the molecular solutes used by Drogaris, they also exhibit surface active behavior (Section 4.3).

Bubble size in an agitated, sparged vessel is determined by a balance of disruptive forces and stabilizing forces (Calderbank, 1958); disruptive forces are a function of the energy dissipation rate and stabilizing forces are a function of surface tension. An expression to calculate the size of bubbles (d_B) in stirred tank reactors based on isotropic turbulence theory has been proposed (Metkin *et al.*, 1985)

$$d_B = 1.25\left(\frac{\sigma}{\rho}\right)^{3/5}\frac{1}{\varepsilon^{2/5}}\varepsilon_H^{0.37}\left(\frac{\rho}{\rho_G}\right)^{1/5} \tag{24}$$

where σ is surface tension, ρ and ρ_G are the densities of gas and liquid respectively, and ε_H is he gas holdup. The interfacial area can be expressed as a function of bubble size and gas holdup ε_H

$$a = \frac{6\varepsilon_H}{d_B} \tag{25}$$

Interfacial area exhibits a $\sigma^{-0.6}$ dependence on surface tension. Eq. 24 shows that bubble size can be altered by a dispersed phase if (i) the surface tension of the dispersion is different from that of the base fluid, (ii) the effective density of the solution is altered. Altered bubble sizes in turn affect gas holdup through the dependence of the latter on the superficial gas velocity V_S

$$\frac{\varepsilon_H}{1-\varepsilon_H} = 0.819\frac{V_s^{2/3}N^{2/5}D_I^{4/15}}{g^{1/3}}\left(\frac{\rho}{\sigma}\right)^{1/5}\left(\frac{\rho}{\rho_G}\right)^{-1/15}\frac{\rho}{\rho-\rho_G} \tag{26}$$

2.2.5 Limitations of the Available Models

The models reviewed in Section 2.2.4 are primarily based on film theories. Therefore, convective motion in the film around gas bubbles is neglected, and simple diffusive mass transfer is assumed. Clearly this has been a successful approach, judging by the body of mass transfer data in the presence of dispersions that has been correctly predicted. Since the diffusivity of a micron-sized droplet generally does not promote its capacity to enhance mass transfer (Mehra, 1988), it is not surprising that ignoring flow-enhanced particle diffusivity has a negligible impact on the accuracy of the models. In the context of microphase-enhanced mass transfer, it has been mentioned that coupling of shear fields and droplet diffusivity would yield droplet diffusivities higher than the Stokes-

Einstein value (Mehra, 1988). However, this mention is made in the context of film theory; it is apparently inconsistent to consider a shear-induced diffusivity in a stagnant film.

The dispersed phases reviewed in this section have sizes on the order of a few μm to several hundred μm. The characteristic length scale of a dispersed phase element is 2 to 3 orders of magnitude larger than that of a nanoparticle. No experimental research has been published that bridges the gap between the two length scales.

2.3 Magnetic Fluids

Magnetic fluids are colloidal dispersions of magnetic nanoparticles that have a size that can range from around 10 nm – if they are single domains – to several hundred nanometers – if they are clustered. The smallest particle sizes are preferably greater than 10 nm. Below this size, magnetic forces cannot be used to direct particle behavior because Brownian forces prevail. At the other end of the range, as particles approach 1 μm, it becomes increasingly difficult to prevent aggregation. Magnetic nanoparticles can be stabilized against unbounded aggregation by applying surface coatings. These coatings are usually surfactants (Shen *et al.*, 1998, 1999) or polymers (Moeser *et al.*, 2002a; Olle *et al.*, 2005; Ditsch *et al.*, 2005a) that provide colloidal stability to the particle and at the same time can be tailored for a specific application; some of the applications explored to date include separation of organic contaminants from water (Moeser *et al.*, 2002a), ion-exchange purifications of proteins (Ditsch *et al.*, 2004), and enhanced oxygen mass transfer. The common aspect in the applications is the exploitation of the large surface area per unit volume of the nanoparticle dispersions; mass transfer of a chemical contaminant, a protein, or a solubilized gas from a water phase to the nanoparticle phase occurs on times scales on the order of micro to nanoseconds.

2.3.1 Hydrocarbon-Coated Magnetic Nanoparticles

This thesis deals primarily with hydrocarbon-coated magnetic nanoparticles in aqueous media. Methods for preparation of magnetic particles coated with organic layers consisting of anionic surfactants with one or several polar groups and a hydrocarbon chain, such as unsaturated fatty acids and sulfonates, have been described in the literature (Meguro *et al.*, 1987); such magnetic particles are only stable in organic solvents and would aggregate in an aqueous fermentation broth. Hydrocarbon-coated particles that retain stability in aqueous media have been synthesized (Shimoiizaka, 1977) by attaching an unsaturated fatty acid to a magnetite (Fe_3O_4) core, and then adsorbing a second coating of an anionic surfactant. This approach has the disadvantage that the second layer, which provides stability in water, is physically adsorbed – and not chemically bound – to the first layer, and therefore tends to detach upon dilution or addition of ions. A synthesis method for magnetic nanoparticles coated with two layers of chemically bound oleic acid has been developed (Shen *et al.*, 2000). However, these particles retain their stability due to the ionization of carboxyl groups, and do not remain stable below pH 7.4. Typical conditions of ionic strength and pH in cell culture media place severe restrictions on particle stability. Cell culture media generally have ionic strengths on the order 1 M and a pH that can vary widely depending on the organism being grown. *Escherichia coli*, for instance, grows best at a pH around 7. Only formulations that produce particles that retain stability at high ionic strength and in a wide range of pH are suitable for application in bioprocesses.

2.3.2 Synthesis for Stability in Fermentation Media

The hydrocarbon-coated magnetic nanoparticles used in the present work are synthesized by attaching a first layer of oleic acid to an Fe_3O_4-core, to which a second layer of a polyethylene-oxide (PEO) based surfactant (Hitenol BC) is covalently attached. The outer surfactant layer contains negatively-charged sulfonate groups that confer electrostatic stabilization and long PEO chains that confer steric stabilization in aqueous media. As a result, particle stability is guaranteed at typical fermentation ionic strengths and in a wide range of pH from at least 2 to 10. The synthesis method followed is described in detail in Section 3.1.

2.3.3 Recovery and Size Control of Magnetic Nanoparticles

It has been shown that 26 nm particles with a magnetite core of 7.5 nm can only be successfully recovered at low flow velocities of up to 0.1 cm/s through an HGMS column (Moeser *et al.*, 2004). At industrially relevant column velocities above 1 cm/s, 100% recovery of the particles is not possible. Moeser *et al.* calculated that a minimum cluster size of around 50 nm is necessary for successful particle recovery. While the particles used in the present work have sizes around 20 nm, the basic synthesis method can be modified to tune the size to larger values. A general method to synthesize size-controlled nanoparticle clusters in the range of 50 to 150 nm has been developed (Ditsch *et al.*, 2005a); this method has been successfully applied in this work to obtain hydrocarbon-coated clusters of varying sizes (Section 4.1.3).

2.3.4 Advantages over Existing Technologies

Magnetic nanoparticles have a number of advantages over conventional dispersions of organic oils as previously discussed in Section 2.1.3. First, they can be separated from a fermentation broth and recovered by magnetic filtration. Second, they form colloidal dispersions with a large interfacial area. As a result, mass transfer of a solute between the surrounding liquid media and the particle can occur in a fraction of a microsecond. Third, the particles are non-volatile and therefore are not lost due to entrainment in a fermentor. Furthermore, they are synthesized with benign chemicals and could be disposed of safely if needed; therefore, their use does not pose environmental concerns. Finally, small loadings of particles, below 1% in mass fraction, are sufficient to obtain large mass transfer enhancements (Section 4.2). The loadings needed per fold-enhancement of oxygen transfer are two orders of magnitude smaller for magnetic nanoparticles than for pure hydrocarbons or PFCs. Furthermore, the nanoparticles used in this work are produced from cheap raw materials (iron chlorides, ammonia, oleic acid, and Hitenol BC), and their manufacture does not pose any challenge, since they are produced through an easily scalable laboratory process that does not require temperatures above 80^{o}C or pressurization.

2.4 Nanoparticles for Heat Transfer Enhancement

Recent research has shown that nanoparticles made of metals, metal oxides, and multi-walled carbon nanotubes greatly enhance heat transfer in liquids. It is expected that these findings will have important repercussions in the microelectronics and transportation industry (Eastman *et al.*, 2004), where cooling of devices frequently limits performance. While the anomalous magnetic, electrical, and optical properties of solid and liquid dispersions of nanosized materials have been observed previously, the discovery and exploitation of their capacity to modify heat transfer have occurred only during the last decade; during this time, research done at the Argonne National Laboratory has led the way in the development of nanoparticle-based heat transfer fluids (Choi, 1995; Lee *et al.*, 1999; Choi *et al.*, 2001; Eastman *et al.*, 2001; Keblinski *et al.*, 2002). Rather surprisingly, given the straightforward analogy of heat and mass transfer, applications of nanofluids in mass transfer have been largely ignored, perhaps because the excitement has not spread far from the mechanical engineering community where the research originally started and has stayed. To the best of the author's knowledge, only one experimental study has been published (Wen *et al.*, 2005), where it was reported that TiO_2 nanometer-sized particles *reduced* the volumetric mass transfer coefficient in a three-phase airlift reactor, and two theoretical studies were published (Ali *et al.*, 2004a; Ali *et al.*, 2004b) that predicted that the presence of nanoparticles in a falling film exposed to air would enhance mass transfer but the improvements would not be significant.

2.4.1 Experimental Studies

The first attempt at measuring increased heat transfer in nanoparticle solutions showed that a dispersion of 4% γ-Al_2O_3 in water enhanced effective thermal conductivity of the base medium by 30% (Masuda *et al.*, 1993). A decade ago, a pioneering theoretical work first proposed that nanoparticle solutions, thereafter termed *nanofluids*, could enhance the thermal conductivity of fluids and reduce pumping power in heat exchange operations (Choi, 1995). Although the author mentioned that the large surface area of nanoparticles would be beneficial to heat transfer, his initial expectation apparently was that nanoparticles of conducting materials would enhance thermal conductivity of base fluids in accordance with the predictions of effective property models; these models only take

into account the volume fraction and shape of the inclusions, but not their size or surface area (Hamilton *et al.*, 1962). Subsequently, many studies have shown that the actual enhancement that can be obtained is one order of magnitude larger than the predictions of effective property models. The dependence of the enhancement on material type, temperature, particle size, and volume fraction has been studied and will be discussed in the following section. The results obtained have established nanoparticles as a promising candidate in cooling applications and pool boiling.

2.4.1.1 Influence of Material Type

Early research concentrated on dispersions of metal oxide nanoparticles. Following Masuda *et al.*'s work, measurements of the thermal conductivity of Al_2O_3 nanoparticles and CuO nanoparticles in aqueous media were made (Lee *et al.*, 1999); the latter showed larger thermal conductivity enhancement at a given volume fraction.

Metal nanoparticles have also been the focus of research. Using ethylene glycol as a base fluid, it was shown that dispersions of copper nanoparticles provided a greater thermal conductivity enhancement than oxide nanoparticles at the same volume fraction (Eastman *et al.*, 2001).

Recently, reports have shown that carbon nanotubes can yield larger enhancements than spherical nanoparticles. Apparently this is because heat can be transferred more efficiently along high-aspect ratio fibers than across a medium of spherical nanoparticles for an equivalent distance; furthermore, carbon has a large thermal conductivity. A 2.5-fold thermal conductivity enhancement was obtained with 1% volume fraction of nanotubes which was attributed to ballistic heat transport along nanotubes (Choi *et al.*, 2001). Similar observations have been carried out by other authors (Xie *et al.*, 2003; Wen *et al.*, 2004b).

2.4.1.2 Influence of Particle Size

The thermal conductivity in aqueous media of nanoparticles of the same material (Al_2O_3) as those used by Masuda *et al.* but twice the diameter has been measured and half the enhancement in thermal conductivity has been obtained (Lee *et al.*, 1999). A lower thermal conductivity enhancement has been measured for 100 nm copper nanoparticles (Xuan *et al.*, 2000a) than for 10 nm copper nanoparticles (Eastman *et al.*, 2001); the

discrepancy has been attributed to the difference in nanoparticle size. Thermal conductivity enhancement by Al_2O_3 dispersions with varying particle size has been measured and found to be dependent on particle size and pH (Xie *et al.*, 2002b). Nanofluids containing CuO particles smaller than Al_2O_3 particles have been shown to yield larger thermal conductivity enhancement (Das *et al.*, 2003c); however this study has the limitation that the base materials of the nanoparticles being compared are different. In a subsequent paper by the same authors (Patel *et al.*, 2003), the thermal conductivities of Au and Ag nanoparticles have been compared. Despite Ag having a thermal conductivity an order of magnitude higher than Au, larger Ag nanoparticles (60-80 nm) show lower enhancement than Au (10-20 nm) particles.

2.4.1.3 Influence of Temperature

Several studies have addressed the influence of temperature in heat transfer enhancement caused by nanofluids (Lee *et al.*, 1999; Das *et al.*, 2003c; Patel *et al.*, 2003; Jang *et al.*, 2004; Kumar *et al.*, 2004). Das *et al.* observed the thermal conductivity enhancement increased from 2% to 4% over a temperature range from 21^{o}C to 51^{o}C.

2.4.1.4 Convective Heat Transfer

Early research on nanofluids concentrated on characterization of enhanced thermal conductivity. Recently, systems in which fluid flow plays a role have also been explored. Several studies have looked at forced convection. Convective heat transfer of nanofluids under laminar flow in a tube has been studied (Wen *et al.*, 2004c).; with 1.6% volume fraction of nanoparticles, a 40% enhancement in heat flux at the entrance region and a smaller (14%) enhancement in the developed region have been measured. Heat transfer in the laminar flow of graphite nanofluids with particle aspect ratios lower than one has been studied (Yang *et al.*, 2005); results show that nanoparticles increase heat transfer coefficients, but that the increase is less than the increase in the static thermal conductivity. Other studies have explored the application of nanofluids to increase the critical flux in pool boiling (Das *et al.*, 2003b, 2003a; Vassallo *et al.*, 2004; Bang *et al.*, 2005); several-fold higher critical heat fluxes in the presence of nanoparticles as compared to base fluids have been reported.

2.4.2 Modeling Studies

In most instances in the literature, the thermal performance of nanofluids has not been successfully predicted by available macroscopic theories. According to a review by (Eastman *et al.*, 2004), "*to date, … understanding how heat is transferred in nanofluids remains the greatest challenge that must be overcome in order to realize the full potential of this new class of heat transfer fluids".* The disconnection between experimental data and modeling appears to be a general trend in the nanosciences. According to a 2002 report conducted by the Basic Energy Sciences and Advanced Scientific Computing Advisory Committees to the Department of Energy (Mccurdy *et al.*, 2002), one of the fundamental challenges facing the nanosciences is to determine the essential science of transport mechanisms at the nanoscale. The report also warns that the rapid progress in experimental studies calls for a theoretical understanding, the lack of which is slowing down future advancements. The central challenge emerging from the report is that *"within 5 to 10 years, there must be robust tools for understanding … dynamics at the nanoscale, without which the scientific community will have missed many opportunities."*

This section reviews several models of enhanced heat transfer that have been proposed for nanoparticle dispersions in stationary systems and in flow systems. Special attention is given to stationary systems because the absence of flow simplifies the theoretical treatment of the heat transfer problem and makes them a good basis for further modeling efforts. It must be noted that there exists general dispute over the validity of the models that will be discussed and that the nature of the theoretical research being published is highly speculative.

2.4.2.1 Models of Stationary Nanoparticle Dispersions

The first theoretical studies of the effective thermal conductivity (and by analogy of heat and mass transfer, the effective mass diffusivity of solutes) of suspensions were undertaken over a century ago (Maxwell, 1873). A theoretical form for the effective conductivity of a suspension of spheres initially developed by Maxwell remained successful until recently for predicting the effective transport properties of suspensions of all particle sizes, down to the micrometer scale, with minor modifications proposed by other authors, *e.g.* to account for non-sphericity (Hamilton *et al.*, 1962). Following the

initial application of nanoparticle solutions to heat transfer (Choi, 1995), it became obvious that macroscopic effective property models failed dramatically at predicting the heat transfer properties of nanofluids; specially in terms of not accounting for particle size. In a comprehensive 2004 review, various heat transfer mechanisms potentially responsible for the anomalous behavior of nanofluids were examined (Eastman *et al.*, 2004). Two of them have received attention in the literature:

The formation of interfacial liquid layers around the nanoparticle has been given consideration, on the basis that liquid molecules can organize into layers in the vicinity of a solid surface (Xue *et al.*, 2003, 2004; Xue *et al.*, 2005). If the arguable assumption is made that the thermal conductivity of such layers is similar to that of the solid, it is found that, for a typical 10 nm nanoparticle, a 3 nm liquid layer shell has to be assumed (Xue *et al.*, 2005) to explain experimentally reported enhancements. It has been found by experiment and simulation that this liquid layer actually has a thickness below 1 nm. As pointed out by (Yu *et al.*, 2003, 2004), measurable increases in heat transfer can only be obtained for particle diameters below 10 nm, which excludes practically all the experimental data gathered in the literature.

Brownian motion was initially ruled out (Eastman *et al.*, 2004), (Keblinski *et al.*, 2002) as a possible mechanism of enhancement on the basis that the characteristic diffusion time of even the smallest-sized (10 nm) nanoparticles is much longer than the characteristic time for conductive heat transfer. This scaling was done using a typical diffusion coefficient for the nanoparticle estimated with the Stokes-Einstein equation; if, however, the translation velocity of each Brownian jump in a given direction – as opposed to the particle diffusion coefficient obtained from the mean squared displacement over a longer period of time – is used as a scale for the particle velocity, Brownian motion can no longer be ignored.

Several attempts have been made at estimating the increase of the thermal conductivity due to the Brownian motion of nanoparticles in the context of nanofluids. Using expressions for the increased thermal conductivity of a medium due to the rotational (Leal, 1973) and translational (Gupte *et al.*, 1995) motion of a sphere contained in it, it was estimated that Brownian motion in 10% volume fraction of 28 nm sized Al_2O_3

particles accounted for less than 0.5% of the thermal conductivity increase and therefore was not significant (Wang *et al.*, 1999).

Considering that particles would drag some of the surrounding fluid to create convection at the nanoscale, an expression was proposed for the velocity of the nanoparticle for an idealized 1-D system, as a function of its kinetic energy and imposed bulk temperature gradient (Yu, 2003). The expression showed a weak, square root dependence of velocity on temperature because it did not take into account the drag on the particle and therefore the exponential effect of temperature on the viscosity of the surrounding fluid. The expression for velocity was not incorporated into a model for enhanced thermal conductivity and therefore no comparison was made with literature data.

Brownian dynamics simulations have been used to calculate the thermal conductivity of nanofluids (Bhattacharya *et al.*, 2004). The Fluctuation Dissipation theorem was used to calculate the thermal conductivity by relation to the time-autocorrelation function of the heat flux. The model did not explicitly take into account the motion of the surrounding fluid caused by the particle displacements, and two adjustable parameters, namely a time step and a potential energy function to account for interparticle repulsions at close approach distances were used to fit simulation results to experimental data. Nonetheless, to the authors' credit, this was the first effort to account for the colloidal nature of nanofluids, a relevant aspect that had been overlooked by previous work.

A model was presented that accounted for Brownian motion of particles but instead of addressing the convective flows due to the relative motion between particle and fluid, focused on the convective heat transfer from particles to the surrounding fluid (Jang *et al.*, 2004). It was implicitly assumed that this convective heat transfer occurs in parallel mode to the bulk conduction when in fact it occurs in series; having a fast convective transfer between particles and liquid would only shift the heat transfer limiting resistance to the bulk conduction but not necessarily increase overall heat flux.

A model was proposed with two independent contributions to the thermal conductivity, namely a static term due to unequal properties of the fluid phase and the nanoparticle phase and a dynamic term due to particle motion (Kumar *et al.*, 2004). For the static term, it was explicitly assumed that there are two parallel paths for heat flow, one

through the nanoparticles and one through the surrounding liquid, which, for the reasons stated above, is a flawed assumption. For the dynamic term, Kumar *et al.* explored microconvection caused by the Brownian motion of nanoparticles as a way to explain the experimental dependence of heat transfer enhancement with temperature. A mean particle velocity was defined using kinetic theory and it was assumed that the enhancement could be expressed as a linear function of this velocity; one adjustable parameter with no clear physical significance was used to fit the model with experimental data.

A model with a static and a dynamic contribution to thermal conductivity that does not assume parallel heat transfer has been proposed (Koo *et al.*, 2004). The static term was expressed according to Maxwell's (1873) expression for the effective conductivity of a suspension; the dynamic term was expressed as a function of (i) a translational particle velocity calculated from the kinetic theory of gases; (ii) the volume of a region of influence around a creeping sphere, and (iii) two adjustable functions to account for interparticle forces and for the fact that, as particle concentration increases, the fraction of liquid that travels with the particle decreases because of interactions with other moving particles. While it seems appropriate to include electrostatic and hydrodynamic interactions in a model of nanoparticle motion, the functions that the authors proposed to account for it are not independent of each other and can only be determined by adjusting parameters to fit experimental data. Furthermore, the volume of liquid dragged by a particle was calculated with the criterion of 99% vanishing impact of the velocity disturbance, which was estimated to be roughly equal to 10^5 times the particle volume; this is a dubious claim because it assumes that each particle carries with it its whole region of influence, when only the regions immediately adjacent, one or a few diameters away from the particle are strongly affected (1 diameter away from the particle, the velocity of the fluid is 90% of the velocity of the particle, 10 diameters away is only 10%).

Prasher (Prasher *et al.*, 2005) proposed a semi-empirical heat transfer correlation to account for convection due to the motion of nanoparticles and was able to predict experimental data at different volume fractions and temperature by adjusting two parameters.

2.4.2.2 Models of Nanoparticle Dispersions in Flow Systems

Several publications have addressed the topic of heat transfer enhancement under convective flow conditions. It has been proposed that dispersion of nanoparticles under bulk fluid flow can flatten transverse temperature gradients in the fluid and thus enhance mass transfer (Xuan *et al.*, 2000a),(Xuan *et al.*, 2000b). The authors proposed a correlation to calculate the Nusselt number in the presence of nanoparticles experiencing dispersion but did not validate it with experimental results. The dispersion coefficient of the nanoparticles was calculated by using an expression obtained for flow through porous media in packed beds that contained an adjustable parameter. The expression was derived from experimental data in packed beds, where particle size is at least two orders of magnitude larger.

Possible mechanisms of nanoparticle migration (dispersion) in a solution have been studied; a flow model was proposed which includes shear-induced migration, shear-induced viscosity gradients, and nanoparticle Brownian motion (Wen *et al.*, 2004a). The authors proposed that shear and viscosity effects disturb the suspension from its equilibrium state and Brownian diffusion tends to restore uniformity. The authors did not validate their model with experimental data, but had this been done, they would have realized that since shear induced dispersion is proportional to a^2 (a being the particle diameter), and typical particles diameters are ~O(10 nm), shear effects vanish for nanoscale sized particles. Particle Peclet numbers based on reasonable flow velocities are smaller than unity and no significant enhancement is possible; therefore Wen *et al.*'s model is only useful for larger, micron-sized particles.

3 MATERIALS AND METHODS

This chapter describes, first, the methods used to synthesize, purify and characterize hydrocarbon-coated magnetic nanoparticles. Subsequently, the methods used to quantify the mass transfer enhancement in model systems and in biological systems are described. Finally, the techniques to measure the surface tension and viscosity of nanoparticle solutions are described.

3.1 Nanoparticle Synthesis and Purification

A solution of 94 g of ferric chloride hexahydrate (97% $FeCl_3 \cdot 6H_2O$, Sigma-Aldrich) and 34.4 g ferrous chloride tetrahydrate (99% $FeCl_2 \cdot 4H_2O$, Sigma-Aldrich) in 100 g of water was stirred at 80 ^oC under nitrogen sparging for 30 min in a round bottom flask. Next, 100 g of potassium oleate (40 wt% paste in water, $CH_3(CH_2)_7CH=CH(CH_2)_7COOK$, Sigma-Aldrich) was added, and the mixture was stirred for an additional 30 min. A 100 mL of an aqueous solution containing 28% ammonium hydroxide (NH_4OH, Mallinckrodt) was added to the mixture, after which the solution immediately turned black because of the formation of magnetite. The reaction continued at 80 ^oC under stirring and nitrogen sparging for 30 min, after which it is assumed that oleic acid had completely coated the magnetite aggregates. Following the coating of the magnetite aggregates, 100 g of Hitenol–BC (Daiichi Kogyo Seiyaki) and 5 g of ammonium persulfate (>98% $(NH_4)_2S_2O_8$, Sigma-Aldrich) were added to the reaction mixture. The reaction continued at 80 ^oC, under nitrogen sparging and vigorous stirring for 30 min to allow for the formation of covalent bonds between the propenyl group of Hitenol–BC and the double bond in the alkyl chain of the oleic acid. Hitenol–BC is a polyoxyethylene alkylphenyl ether ammonium sulfate that contains a reactive propenyl group; the long PEO chains and the sulfate group confer stability in water when attached to the surface of oleic-acid coated magnetite particles. The solution was cooled to room temperature and remained in the oven at 80 ^oC overnight, after which most of the residual ammonium hydroxide evaporated. The dispersion was dialyzed against distilled water (14,000 kDa MWCO dialysis membrane, Pals) in a 20 L container under mild stirring for 2 days to remove unreacted potassium oleate, Hitenol–BC, ammonium persulfate, and other salts and metal ions. Finally, the dialyzed solution was kept in the oven overnight at 80 ^oC, after which its solids contents were measured. The final solid contents were typically

between 15 to 25% in weight. This synthetic procedure yielded magnetic nanoparticles with an average number diameter between 20 and 25 nanometers (nm).

Larger particles can be obtained by varying the relative amounts of potassium oleate and iron chlorides present at nucleation, *i.e.* before formation of the magnetite cores. Nanoparticles with an average number diameter of 40 to 45 nm are obtained by (i) initially adding 33 g of potassium oleate (instead of 100 g) to the iron chloride mixture, (ii) adding ammonium hydroxide as previously described and waiting for 15 min (iii) adding the remaining 67 g of potassium oleate (iv) carrying out the rest of the synthesis steps as previously outlined. Nanoparticles with an average number diameter of 55 to 60 nm are obtained by initially adding 10 g of potassium oleate and adding the remaining 90 g after nucleation.

3.2 Nanoparticle Characterization

The size of the magnetic nanoparticles was characterized by Dynamic Light Scattering (DLS) using a Brookhaven BI-200SM instrument at a measurement angle of 90o. Samples were first passed through a 0.45 μm filter to remove dust particles before the measurements were taken. A value of the diffusion coefficient is extracted from the autocorrelation function measured by DLS, and a hydrodynamic diameter is calculated using the Stokes-Einstein equation. Number-averaged and volume-averaged size distributions are recorded. The particle sizes cited in this work correspond to number averages. All measurements were recorded in quadruplicate and reported as average values.

Zeta potential measurements were recorded using a Brookhaven ZetaPals Zeta Potential Analyzer. The built-in software uses the Smoluchowski potential model to convert electrophoretic mobility to zeta potential. Measurements were recorded in quadruplicate and reported as average values. Measurements for both DLS and zeta potential were conducted in 1000 ppm nanoparticle suspensions in fermentation media, the composition of which is described in Section 3.4.2, with an ionic strength of approximately 1 M. The pH was adjusted with acetic acid or NaOH.

3.3 Experimental Determination of $k_L a$

Mass transfer characterization experiments are made using a physical method and a chemical method. In the physical method, oxygen absorption from a gas phase to the liquid takes place after the system has been purged with an inert gas, and the change in dissolved oxygen is measured over time. In the chemical method, the rate of oxidation of sodium sulfite in a water solution as measured with a mass spectrometer allows calculation of oxygen transfer rates.

3.3.1 Physical Method: Stirred Beaker

Dynamic measurements of dissolved oxygen via surface aeration were used to determine k_L. Experiments were conducted in a cylindrical, 10.3 cm diameter beaker, filled with 500 mL of liquid, to a liquid height of approximately 6 cm. The liquid was circulated slowly by a 4.5 cm diameter, 4-bladed, axial-flow impeller (pitched-blade with each blade measuring 3 cm wide and 1.5 cm long), placed centrally in the beaker. The free surface of the liquid remained flat, *i.e.* it did not exhibit a vortex or appear broken at the agitation speeds studied (300 rpm and 500 rpm). Dissolved oxygen was measured using a dissolved oxygen polarographic sensor (YSI 5010) connected to a data acquisition meter (YSI 5100). A built-in barometer compensated for slight atmospheric pressure variations between runs. The temperature was regulated at 37±0.5 ^{o}C with a water bath and the pH of the solution was adjusted to 7.0 before the start of the experiment. Oxygen response curves were obtained by first sparging nitrogen until the dissolved oxygen concentration fell to zero and then monitoring the increase in dissolved oxygen concentration due to exposure of the liquid free surface to the room air. To ensure a constant gas-liquid interfacial area (83.3 cm^2), no air sparging was used during the second step. The relatively long duration of the experiments (~1 hour) guaranteed that the time constant of the probe did not affect the response curves. The dissolved oxygen data can be analyzed by constructing a mass balance of oxygen in the liquid phase as follows

$$\frac{dC_{O_2,bulk}}{dt} = k_L a\left(C^*_{O_2} - C_{O_2,bulk}\right) = k_L aH\left(P^*_{O_2} - P_{O_2,bulk}\right) \tag{27}$$

where k_L is the liquid-side mass transfer coefficient (it is assumed that the gas-side coefficient is much larger), a is the specific interfacial area, $P_{O_2,bulk}$ and $P^*_{O_2,}$ are the partial

pressures of oxygen in the well-mixed bulk and at saturation respectively, $C_{O_2,bulk}$ and $C^*_{O_2,}$ are the equivalent liquid phase partial pressures, H is the Henry's law constant, and t is the elapsed time. With $C_{O_2,bulk} = 0$ at t = 0, the integrated form of this expression is

$$\ln\left(C^*_{O_2,} - C_{O_2,,bulk}\right) = -k_L a t + R \tag{28}$$

where R is an integration constant. The negative slope of a plot of the left hand side of the equation against time corresponds to the value of $k_L a$.

The rationale for characterizing mass transfer by a physical method in an agitated beaker is to avoid problems associated with interfacial area and gas holdup. By conducting experiments in a system that has a fixed and known gas-liquid contact area, we obtained information on the value of k_L.

3.3.2 Chemical Method: Sodium Sulfite Oxidation

Oxygen mass transfer was characterized *via* a chemical reaction in a laboratory scale aerated and agitated fermentor by using the sodium sulfite oxidation method, which is a well-known approach in the fermentation community. The method is conducted using a sodium sulfite solution, which in the presence of Cu^{2+} catalyst, is oxidized following the reaction

$$Na_2SO_3 + \frac{1}{2}O_2 \xrightarrow{Cu^{2+}\text{or } Co^{2+}} Na_2SO_4 \tag{29}$$

3.3.2.1 Volumetric mass transfer coefficient ($k_L a$) determination

The reaction rate of the sodium sulfite oxidation is independent of the sulfite concentration. The reaction rate can be adjusted with temperature or with the catalyst concentration so that oxygen transport from the gas to the liquid, rather than the chemical reaction, is the limiting step. The reaction rate should be fast enough to guarantee a mass transfer-limited regime, but not so fast that the reaction occurs mainly in the liquid film around bubbles. The volumetric mass transfer coefficient $k_L a$ can be calculated by measuring the rate of reaction. In the present work, this is done by measuring the

effluent gas composition with a mass spectrometer (Perkin-Elmer MGA 1600) and performing a mass balance on oxygen of the gas phase through the reactor

$$OUR = \frac{F_{N_2\,in}\left[\left(\frac{C_{O_2}}{C_{N_2}}\right)_{in} - \left(\frac{C_{O_2}}{C_{N_2}}\right)_{out}\right]}{V} \tag{30}$$

where OUR is the oxygen uptake rate, $F_{N2,in}$ is the flowrate of nitrogen entering the reactor, C_{O2} and C_{N2} are the concentrations of oxygen and nitrogen entering or exiting the reactor, and V is the working volume.

The volumetric mass transfer coefficient can then be determined by rearranging Eq. 2

$$k_L a = \frac{OUR}{C^*_{O_2} - C_{O_2,bulk}} \tag{31}$$

where C^*_{O2} corresponds to the equilibrium oxygen reading for the gas outlet; by using this value, it is assumed that the tank is perfectly mixed. Alternatively, an average of the inlet and outlet gas concentrations or a mean-logarithmic value can be used for C^*_{O2}.

Experiments were performed in a 20 L (5.5 L working volume) stirred tank reactor (*Biolafitte* fermentor system, model BL 20.2). The tank was equipped with an Ingold type pH electrode, a *Biolafitte* dissolved oxygen electrode, a temperature probe, a bottom aeration system consisting of a 4-branded rotating sparger, and an agitator with 2 Rushton 4-bladed turbine impellers. A 0.67 M sodium sulfite solution was loaded into the reactor, and then a $1 \cdot 10^{-3}$M solution of copper sulfate catalyst was added. At this catalyst concentration the mass transfer is not chemically enhanced (Linek, 1966). The pH was initially adjusted around 8.0 with sulfuric acid to avoid the accelerated reaction regime typical of sodium sulfite solutions at higher pH. Temperature was maintained at 37±0.5 ^{o}C, except when specified otherwise.

3.3.2.2 Interfacial area determination

Experiments to determine the gas-liquid interfacial area were conducted with the experimental system previously described. The catalyst used was Co^{2+} instead of Cu^{2+} because the former permits operation in a regime where absorption is kinetically

enhanced (Section 4.2.2.2). Experiments were run in a 0.67 M sodium sulfite solution, at 37±0.5 ^{o}C, and at a pH of 8.5.

3.4 Cell Culture Experiments

3.4.1 Organism

Escherichia coli BL21(DE3) [pUC18]

Bacteria are a convenient choice for the purpose of this thesis because oxygen transfer is of great importance in their cultivation. *E. coli* was chosen because it is an industrially relevant, thoroughly studied organism and it has a fast growth rate compared to other bacteria (its doubling time ranges from 20 to 40 min depending on the medium). Because of its fast growth rate, *E. coli* has a specific oxygen demand higher than most organisms; this makes attaining high cell densities particularly challenging. High oxygen transfer rates are required to obtain such high cell densities and to avoid the accumulation of acetate, which is produced by *E. coli* under conditions of hypoxia and inhibits cell growth.

3.4.2 Shake Flask Studies

Shake flask experiments were conducted to test the biocompatibility of hydrocarbon-coated magnetic nanoparticles. Initially, Luria-Bertani (LB) medium was used for seed culture, with the following composition (in per Liter): 10 g NaCL, 10 g tryptone, 5 g yeast extract. *E. coli* cells were grown in 100 mL of LB medium in a 500 mL shake flask overnight at 37 ^{o}C and 220 rpm without pH control. Subsequently, the seed culture was pipetted into 500 mL shake flasks contaning chemically defined MR medium for fermentation culture. The MR medium had the following composition (/L): 13.5 g KH_2PO_4 , 4.0 g $(NH_4)_2HPO_4$, 0.7 g $MgSO_4{\cdot}7H_2O$, 0.85 g Citric acid, 10 mL of 10 g/L $FeSO_4{\cdot}7H_2O$, 10.0 mL of trace metal solution and 1.0 mL 20 g/L $CaCl_2{\cdot}2H_2O$. The trace metal solution had the following composition (in per Liter): 2.2 g $ZnSO_4{\cdot}7H_2O$, 0.5 g $MnCl_2{\cdot}4H_2O$, 1.0 g $CuSO_4{\cdot}5H_2O$, 0.1 g $Na_2MoO_4{\cdot}2H_2O$, 0.02g $Na_2B_4O_7{\cdot}10H_2O$, adjusted to pH 2.0 by HCl. Flasks contained 100 mL of MR medium with 15 g/L of glucose and 10% (v/v) of inoculated seed culture. Cultures were performed at 37 ^{o}C and 220 rpm.

The optical density at 600 nm, which provides a measure of cell growth, was measured with a UV spectrophotometer (Hewlett Packard 8452A).

3.4.3 Fermentation Experiments

Fermentations were carried out in a 20 L *Biolafitte* fermentor system, at a 5.5 L working volume. This was the same equipment used for the experimental determination of $k_L a$ through a chemical method (Section 3.3.2). The inoculation volume was 10% (v/v); the seed culture for a fermentation was grown in 5, 500 mL shake flasks, containing 100 mL of LB medium each, cultured for 9 hours at 37 ^{o}C and 220 rpm, to an OD (600 nm) of 10 units. The temperature, pH, aeration rate, and agitation in the bioreactor were controlled at 37±0.5 ^{o}C, 7.0±0.1, 5.0 slpm, and 300±5 rpm respectively. Phosphoric acid 2 M and NH_4OH:NaOH:KOH 6 M 3:1.5:1.5 were used to control the pH. The medium was the same used in the shake flask experiments (Section 3.4.2, MR medium), with the addition of 50 μg/mL of ampicillin. Fed-batch fermentations were carried out starting with a glucose concentration of 50 g/L and proceeding until this concentration decreased to zero; after this point, glucose was fed in manual injections, each 55 mL of a solution of 500 g/L glucose and 10 g/L $MgSO_4 \cdot 7H_2O$, that brought the glucose concentration in the fermentation medium up to 5 g/L. Dissolved oxygen was not controlled during the fermentation and therefore fell down to approximately zero with time; this was a deliberate strategy to bring the culture to an oxygen limited regime of growth. Under this condition, exponential growth of the cells slows down and becomes linear. Dissolved oxygen increased to values higher than zero when the glucose was consumed, and this was used as a criterion for a new glucose injection. Throughout the experiment, foaming due to extracellular products generated by *E. coli* metabolism and also due to the presence of magnetic nanoparticles, when applicable, was controlled using antifoam Q7-2243 DOW Corning and antifoam SIGMA 204. Inlet and outlet gas compositions were measured by a Perkin Elmer MGA1600 spectrometer. These data were used to calculate oxygen uptake rate history curves. Samples for measurement of optical density (600 nm), dry cell weight, glucose concentration, and ammonia concentrations were taken every hour. Optical density at 600 nm was measured with a UV spectrophotometer (Hewlett Packard 8452A); measurements were repeated 3 times and averaged. Dry cell weight measurements were carried out in triplicate; 1.5 mL samples were centrifuged at

6,000 rpm for 10 min. The supernatant was removed and stored at -20 ^{o}C for glucose and ammonia analysis. The pellet was resuspended with 0.9% NaCl solution and recentrifuged. The supernatant was discarded and samples were dried to constant weight in a 70 ^{o}C oven.

3.4.4 Cell Binding Experiments

Cell binding experiments were conducted to determine the amount of cells bound to other cells *via* interactions with nanoparticles. To measure cell binding, 4mL of *E. coli* grown on shake flasks in defined chemical media were mixed with 1 mL of nanoparticle solution for a final concentration of 0.5%w/v of nanoparticles in the mixture; pH was adjusted by HCl or NaOH. The mixture samples were left sitting for one hour before being tested for cell binding. The mixture was passed through an HGMS column that captured the magnetic nanoparticles and cells bound to the particles, while the unbound cells flowed through the magnetic column and were collected at the bottom. Cell binding was quantified by measuring the optical density at 600 nm of the feed and comparing it to that of the circulated samples with unbound cells.

3.5 Dynamic Surface Tension Measurements

Dynamic Surface Tension measurements were carried out to establish the surface activity of the nanoparticle solutions used. The apparatus used was a Kruss DSA10 instrument. Measurements were conducted by first creating a fresh interface using a pendant drop or bubble at the end of a syringe; a light source placed behind the bubble (or drop) illuminated it; an image of the drop profile was captured using a CCD camera with edge detection software, and the Young-Laplace equation was used to fit a value of interfacial tension from the resulting profile. A more complete explanation of the instrument and technique used has been presented (Faour *et al.*, 1996; Song *et al.*, 1996; Eastoe *et al.*, 2002).

Sample preparation required elimination of trace impurities present in the nanoparticle solutions. Several components used in the synthesis of the nanoparticles are surface active, especially Hitenol BC (a polymerizable surfactant) and oleic acid, and need to be washed away. A 48 hour dialysis process used to clean the particle solutions eliminated most of the unreacted free molecules of components that were not attached to

nanoparticles, but left traces in solution. Even concentrations on the ppm level of surface active compounds are enough to alter a surface tension measurement and therefore it was necessary to achieve a more thorough cleaning. This was done by means of centrifugal filtration. A 20 mL sample of dialyzed magnetic nanoparticles, 1% in weight, was loaded into a Centricon Plus-80 Millipore filter with a molecular weight cutoff of 100,000 Daltons, and centrifuged at 14,000 rpm (20,800xG) for 20 min at room temperature in a 5810 R Eppendorf Centrifuge. Particles were retained in the filter and the solution containing the impurities permeated through the filter. The surface tension of the permeated liquid was then measured. If its equilibrium value was lower than 72 mN/m (the surface tension of deionized water), the retained fraction of particles was resuspended in deionized water and the ultracentrifugation cycle was repeated. If, otherwise, the equilibrium surface tension of the permeated fraction was that of water, this was taken as an indication that the sample of particles had been completely cleaned. Typically 10 ultracentrifugation cycles were necessary for an adequate cleaning.

3.6 Viscosity Measurement

Rheological measurements were carried out in order to establish whether viscosity of nanoparticle solutions played a role in their mechanism of mass transfer enhancement. Measurements were made using a U-tube Canon-Fenske viscometer.

4 RESULTS

4.1 Particle Characterization Results

This section presents characterization data that establish that the colloidal stability of the particles used in this research is satisfactory in the range of conditions typically used in fermentation and beyond them. Additionally, it is shown that it is possible to synthesize both charged and non-charged particles and particles of different size with minor modifications to the reaction protocol presented in Section 3.1. Mass transfer characterization results presented in subsequent sections are obtained using only the particles synthesized according to the base recipe in 3.1, that is, Hitenol BC – coated nanoparticles with an approximate hydrodynamic diameter of 20 nm.

4.1.1 Zeta Potential

Stability in high ionic strength media is a crucial requirement for magnetic nanoparticles to be of use in a bioprocess. Zeta Potential, which gives a measure of the surface charge on a particle, is a good indicator of the colloidal stability of a solution of particles. Generally, the greater the charge, the better the stability.

Particles in solution tend to aggregate because of van der Waals forces acting between the bare particle surfaces; this behavior can, however, be prevented by electrostatic and steric interactions. The nanoparticles synthesized according to the protocol detailed in Section 3.1 acquire stability in aqueous media by both electrostatic and steric interactions. Their exterior coating of Hitenol BC (polyoxyethylene alkylphenyl ether ammonium sulfate) contains a sulfonate group that confers a negative charge to the particle surface. In addition, the 8-unit PEO chains in the Hitenol BC molecule can be highly solvated by water molecules, and in this form, two steric contributions are introduced; first, a repulsive osmotic contribution: as two surfaces approach, there is an increase in polymer concentration in the gap between the surfaces; second, there is an elastic contribution that accounts for the reduction in free energy on compression of the extended chains (Jeon *et al.*, 1991). As result of electrostatic and steric interactions, the nanoparticles synthesized remain colloidally stable at high ionic strength over a wide range of pH, as shown in Figure 4-1. Hitenol BC – coated particles suspended in fermentation medium (see composition in Section 3.4.2) have a Zeta Potential of

approximately -30 mV in a pH range of 1.6 to 7.5; this indicates that the sulfonate groups on the surface remain deprotonated. Figure 4-1 also shows the Zeta Potential of particles coated with Polyoxyethylene alkylphenyl ether (Noigen – RN, Dai-Ichi Kogyo Seiyaku), which do not have charged surface groups; accordingly, their Zeta Potential is approximaterly zero over the pH range studied. Despite this, they remain colloidally stable over a wide range of pH as confirmed by Dynamic Light Scattering measurements shown in Figure 4-2. The Noigen molecule has a PEO chain of 50 to 65 PEO units per 8 units of the original Hitenol BC coating, which confers stability in water. Stability in this case is obtained solely from steric interactions. Both types of particle are synthesized using the same protocol with the only difference being the exterior coating.

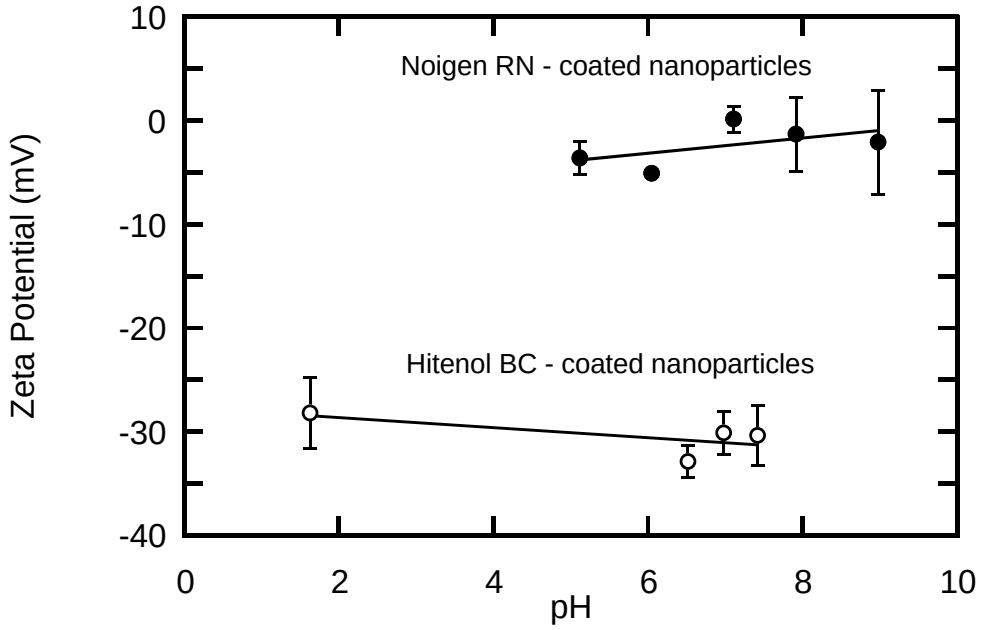

Figure 4-1. Zeta potential of Hitenol BC – and Noigen RN – coated nanoparticles as a function of pH

The results in Figures 4-1 and 4-2 show that following the synthesis procedure outlined in Section 3.1, both charged and non-charged particles stable over a wide range of pH can be synthesized. The range of pH studied covers most practical biological applications.

4.1.2 Dynamic Light Scattering

Dynamic Light Scattering (DLS) measurements yield the diffusion coefficient of particles, from which, using the Stokes Einstein equation, the hydrodynamic diameter of

the particles can be calculated. In addition to Zeta Potential measurements, hydrodynamic diameter data calculated from DLS measurements is a good indicator of the colloidal stability of a solution of particles. The hydrodynamic diameter of Hitenol BC – coated magnetic nanoparticles has an average value (number average) of 20 nm over the range of pH relevant to fermentation (around 7), as shown in Figure 4-2. The stability of the particles is still remarkable at a pH of 1.6, at which particles experience some minor aggregation to form clusters of approximately 40 nm in diameter. Also shown is the hydrodynamic diameter of Noigen RN – coated nanoparticles, which remains around 40 nm over a pH range of 5 to 9.

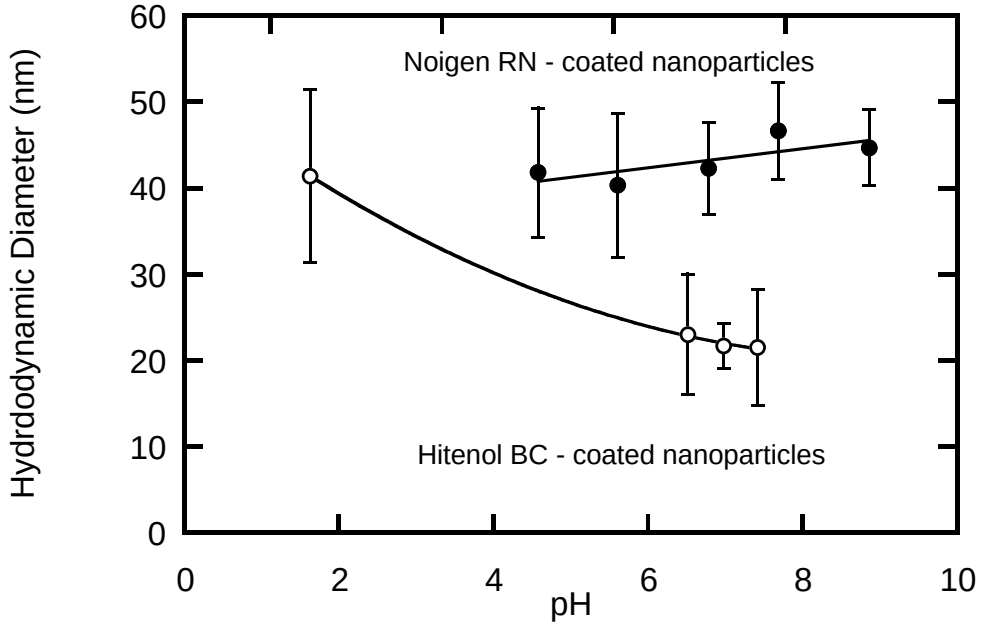

Figure 4-2. Hydrodynamic diameter of Hitenol BC – and Noigen RN – coated nanoparticles as a function of pH.

4.1.3 Synthesis of Particles of Different Size

Nanoparticles with a diameter below 50 nm are difficult to recover by HGMS (Moeser *et al.*, 2004); however, smaller particles potentially yield larger mass transfer enhancement. Flexibility to synthesize nanoparticles of different size is therefore desirable. A proof of principle that particles of size above 50 nm can be synthesized is imperative to guarantee that nanoparticles can be fully recovered.

Particle clusters of different size can be synthesized following a general method which consists of varying the ratio of attachment groups in the primary coating (COO^- in the oleic acid molecule) to iron atoms in the surface of the magnetite cores (Ditsch *et al.*, 2005a). The appropriate ratio to obtain a desired particle size can be established by trial and error. Larger particle clusters can be obtained by reducing the amount of primary coating (potassium oleate) at nucleation, *i.e.* before ammonia is added to the reaction mixture to cause nucleation of magnetite cores. Subsequently, the rest of the primary coating typically used in the synthesis of single particles can be added to stabilize the clusters. Table 4-1 shows the molar ratio of attachment groups to surface iron groups $[COO^-]/[Fe]_{surf}$ needed to obtain particle clusters of different sizes. The clusters obtained are colloidally stable over a pH range of 3 to 9 at least, according to Zeta Potential and DLS measurements (not shown).

Table 4-1. Molar ratio of attachment groups to surface iron groups needed for obtention of particle clusters of different size

Molar ratio $[COO^-]/[Fe]_{surf}$	Hydrodynamic diameter (nm) at pH 7
3.1	20 ± 3 (single particle)
1.0	42 ± 1 (cluster)
0.31	58 ± 1 (cluster)

4.2 Mass Transfer Characterization

This section presents experimental findings of enhanced mass transfer in the presence of nanoparticle dispersions. Systematic mass transfer studies are carried out using a physical method and a chemical method.

4.2.1 Physical Method: Mass Transfer in an Agitated Beaker

The rationale for characterizing mass transfer by a physical method in an agitated beaker is to avoid problems associated with interfacial area and gas holdup. By conducting experiments in a system that has a fixed, known, gas-liquid contact area, the results obtained yield information on the value of the mass transfer coefficient, k_L. Details of the experimental setup used are outlined in Section 3.3.1.

Oxygen mass transfer into an aqueous liquid phase is enhanced in the presence of nanoparticles, as shown in Figure 4-3. The time required to reach saturation is reduced by approximately 25% in the presence of a nanoparticle mass fraction of ϕ = 0.005 (0.5% w/w). Further reductions are attained at a larger particle holdup. The reduction is less significant above ϕ = 0.01 (this effect is shown more clearly in Figure 4-5). Experimental points corresponding to each reading by the dissolved oxygen probe are not shown for clarity; instead, trend lines are presented.

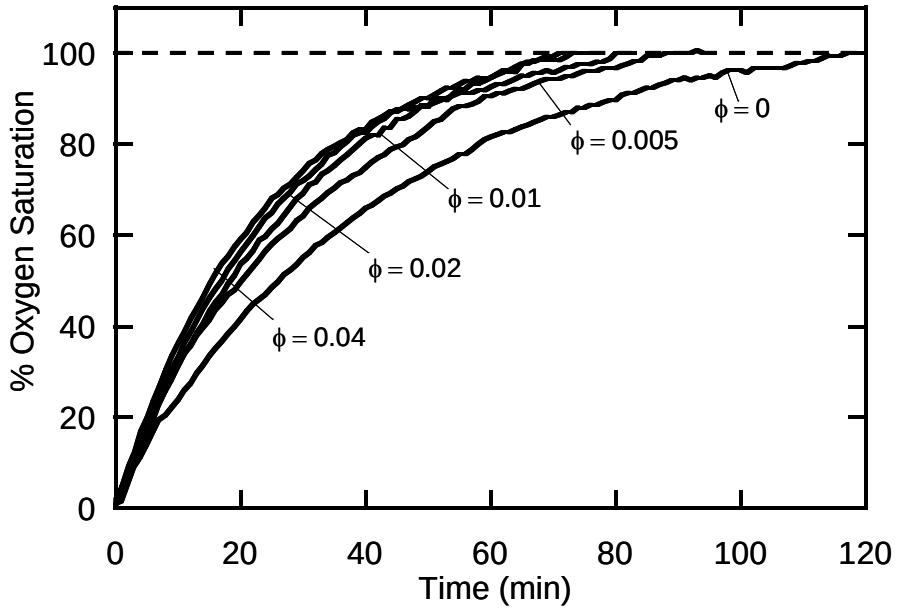

Figure 4-3. Response curves of dissolved oxygen in a stirred beaker at increasing nanoparticle holdup.

The first order curves shown in Figure 4-3 can be linearized making use of Eq. 28. The absolute value of the slope calculated from the logarithm of the driving force as a function of time corresponds to $k_L a$. The driving force is defined as the saturation concentration of oxygen (C^*) minus the concentration of oxygen in the bulk (C_{bulk}), which changes with time. Inspection of the slopes in Figure 4-4 illustrates the increase of k_L in the presence of nanoparticles. The absolute enhancement in k_L , defined as

$$E = \frac{k_{L,nanoparticles}}{k_{L,control}} \tag{32}$$

is plotted in Figure 4-5 as a function of the nanoparticle holdup for different agitation rates. It can be observed that (i) enhancement increases linearly at particle holdups

below $\phi = 0.01$, and plateaus above this value and (ii) enhancement is greater at a lower agitation rate because the ratio of k_L values in water at the two agitation speeds studied, $k_{\mathrm{L,500\,rpm}} / k_{\mathrm{L,300\,rpm}}$, is larger than the equivalent ratio of k_L values in the presence of particles. Data points are the average of 3 experiments.

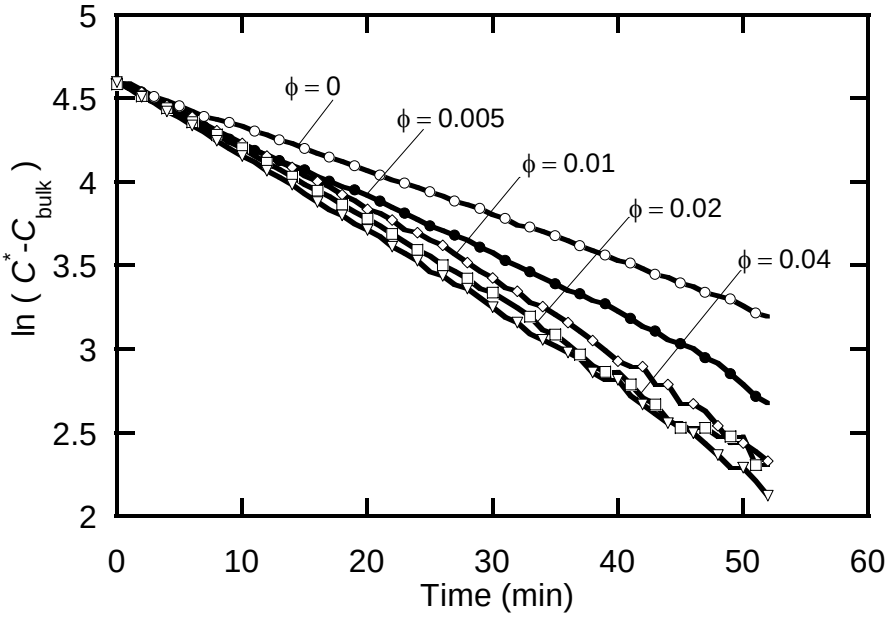

Figure 4-4. Linearized response curves of dissolved oxygen in a stirred beaker at increasing nanoparticle holdup. The absolute value of the slope corresponds to the value of $k_L a$

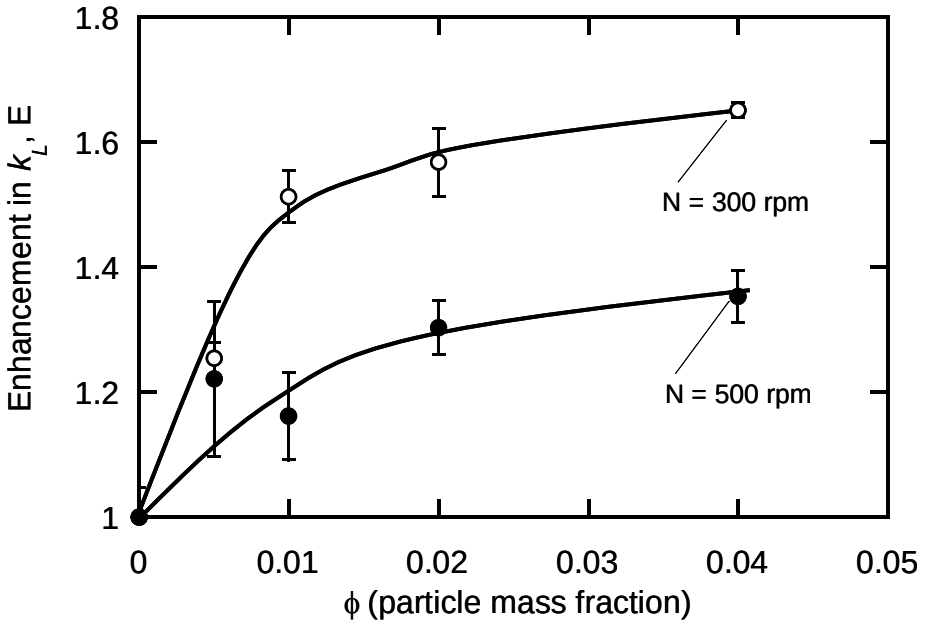

Figure 4-5. Absolute enhancement in k_L as a function of nanoparticle holdup in a stirred beaker at different agitation rates

The experimental values of k_L for the base case ($\phi = 0$) can be compared with theoretical predictions from available models to gain an understanding of the underlying mechanism of mass transfer in the absence of nanoparticles. The experimental value of k_L can be estimated from inspection of Figure 4-4. The line corresponding to the water control ($\phi = 0$) has a negative slope of $4.49 \cdot 10^{-4}$ s^{-1}. Since the specific interfacial area of the system is 16.7 m^{-1}, an experimental value of k_L of $2.69 \cdot 10^{-5}$ m/s is obtained. Film theories alone cannot be used to obtain a theoretical prediction of k_L without resorting to experimental data to estimate its hydrodynamic parameters (residence time of liquid elements at the interface or surface renewal frequency). Lamont's model (Eq. 6), based on isotropic turbulence theory, yields a prediction for k_L from easily measurable physical quantities (kinematic viscosity, diffusivity, and power input per unit volume). The power input into the beaker can be estimated as (Rushton *et al.*, 1950)

$$P_0 = \frac{N_i N_p \left(\frac{N}{60}\right)^3 D_i^5 \rho}{7.6 \cdot 10^6 g_c} \tag{33}$$

where P_0 is power input in HP, N_i is the number of impellers, N_p is the power number, D_i is the impeller diameter in cm, ρ is the liquid density in g/cm^3, and g_c has a value 980 cm/s. With the parameters listed in Table 4-2, a value of $k_L = 3.06 \cdot 10^{-4}$ m/s is estimated using Eq. 6. This value overestimates the experimental value of k_L by one order of magnitude. This suggests that energy dissipation in the beaker is nonhomogenous and therefore the basic premise of isotropic turbulence does not apply to this system.

Table 4-2. Parameters used to calculate $k_L a$ in the agitated beaker

N_i (number of impellers)	1
N_p (power number)	1 (Figure18-17 in (Perry *et al.*, 1997))
N (agitation rate)	300 rpm
D_i (impeller diameter)	4.5 cm
ν (kinematic viscosity of water at 37 ^oC)	$6.95 \cdot 10^{-7}$ m^2/s
$D_{O2,L}$ (oxygen diffusivity at 37^oC)	$3.22 \cdot 10^{-9}$ m^2/s
P_0 (calculated power input, Eq. 33)	$3.1 \cdot 10^{-5}$ HP

ε (calculated power input per unit mass)	0.023 m^2/s^3
k_L (calculated k_L, Eq. 6)	$3.06 \cdot 10^{-4}$ m/s

A hydrodynamic model of mass transfer in a stirred vessel that does not need to postulate a turbulent transport mechanism has been proposed (Olander, 1963, 1964). The mathematical treatment takes into account two regions in the stirred vessel. The first is a core region that contains the liquid swept by the agitator, which rotates like a solid body at ω_∞ rad/s. The second is an annular region between the core and the vessel walls; ω_∞ is a fraction of the agitator disk speed ($\omega_\infty/\omega_{disk}$ <1). Olander proposes the following expression for k_L

$$k_L = \nu \frac{(\alpha/3)^{1/3}}{\Gamma\left(\frac{4}{3}\right)} \frac{(A_c/A_t)^{1/3}}{(1-A_c/A_t)^{1/3}} \left(\frac{\omega_\infty}{\nu}\right)^{1/2} Sc^{-2/3} \tag{34}$$

where α is a parameter with a value of 0.94, $\Gamma(4/3)$ is the complete gamma function of 4/3, with a value of 0.893, A_c/A_t is the ratio of the interfacial area of the core region and the total interfacial area, which for the experimental setup used in the present work has a value of 0.2. The surface of the liquid rotates at ¼ th of the angular velocity of the agitator shaft (therefore $\omega_\infty/\omega_{disk}$ = 0.25), as measured experimentally. Olander's expression predicts a value of $k_L = 3.46 \cdot 10^{-5}$ m/s. This value is 30% higher than the value determined experimentally. Therefore, Olander's expression gives a reasonable description of the base mass transfer coefficient in the experimental system in the absence of nanoparticles.

The mechanism of mass transfer in the presence of nanoparticles will be discussed in more detail in chapter 5. The experimental data presented in this section show that the mass transfer coefficient k_L is altered in the presence of nanoparticles regardless of area effects.

4.2.2 Chemical Method: Sodium Sulfite Oxidation

The purpose of the experiments presented in this section is to characterize mass transfer enhancement by nanoparticles in the same equipment in which fermentations are conducted. Mass transfer data is obtained by a chemical method in a cell-free system, which is significantly less laborious than conducting fermentations.

Oxidation of sodium sulfite has frequently been used as a model system for characterization of gas-liquid absorption. A comprehensive review of the method, in which the experimental data gathered to date are systematically organized and guidelines are set for the determination of absorption characteristics of mass transfer equipment has been presented (Linek *et al.*, 1981). A convenient feature of the method is that separate determinations of the volumetric mass transfer coefficient $k_L a$ and the gas-liquid interfacial area a can be made by manipulating the relative magnitude of the rate of chemical reaction and the rate of mass transfer.

4.2.2.1 Determination of the volumetric mass transfer coefficient ($k_L a$)

The absorption flux of oxygen undergoing a pseudo-n-order reaction with sulfite ions in an aqueous phase can be expressed as (Danckwerts, 1970)

$$N \cdot a = a\left(C^*_{O_2} - C_{O_2,\text{bulk}}\right)\sqrt{\frac{2}{n+1} k_n C^{*\ n-1}_{O_2} D_{O_{2,L}} + k_L^2} \tag{35}$$

where N is the absorption rate, a the interfacial area, and n is the reaction order. The relative magnitudes of the rate of oxygen consumption by reaction and the rate of mass transfer can be compared through the Hatta number

$$Ha = \frac{\sqrt{\frac{2}{n+1} k_n C^{*\ n-1}_{O_2} D_{O_{2,L}}}}{k_L} \tag{36}$$

If the following conditions are met

$$C_{O_2,\text{bulk}} = 0 \tag{37a}$$

$$Ha < 0.3 \tag{37b}$$

$$Ha << C_{SO_3^{2-}} / \left(z C^*_{O_2}\right) \tag{37c}$$

where z is a stoichiometric coefficient (moles of sulfite reacted per mole of oxygen), then the reaction is limited by mass transfer and $k_L a$ can be obtained from oxygen absorption rates according to

$$N \cdot a = C^*_{O_2} k_L a \tag{38}$$

The left hand side of Eq. 38 corresponds to the *OUR* as defined by Eq. 30, which is experimentally measured. The concentration of oxygen at the gas-liquid interface, C_{O2}^*, can be calculated from the inlet and outlet concentrations of oxygen and nitrogen in the absorption equipment. The physical dimensions of the absorption equipment and the fluid properties used for the determination of $k_L a$ are summarized in Table 4-3.

Table 4-3. Physical dimensions and properties of the system used for the determination of $k_L a$ by the sodium sulfite method

Tank Diameter	21.7 cm
Impeller Diameter	9.8 cm
Impeller Type	2 Rushton Turbines, 4-bladed
Liquid Volume	5.5 L
Liquid Height	17 cm (approx.)
Oxygen Diffusivity (37 ^oC)	$3.22 \cdot 10^{-9}$ m^2/s
Oxygen Solubility in 0.67 M sulfite (37 ^oC)	0.124 mol/m^3
Viscosity (37 ^oC)	$6.95 \cdot 10^{-4}$ (Pa·s)
Surface Tension (37 ^oC)	70 mN/m (40 mN/m with nanoparticles)

Measurements of *OUR* at a set of operating conditions have been obtained by means of a mass spectrometer and are summarized in Table 4-4. Details of the experimental procedure followed are outlined in Section 3.3.2. Correct estimation of the value of C_{O2}^* requires accounting for the decreased solubility of oxygen in a sodium sulfite solution. The following expression has been proposed to estimate the solubility H of *pure* oxygen in a solution of sodium sulfite (Linek *et al.*, 1981)

$$H = 5.909 \cdot 10^{-6} \, exp\left(\frac{1602.1}{T} - \frac{0.9407 C_{SO_3^{2-}}}{1 + 0.1933 C_{SO_3^{2-}}} \right) \tag{39}$$

where H has units of M/atm, T has units of K, and C has units of M. Using this expression, $H = 5.89 \cdot 10^{-4}$ M/atm for a 0.67 M sodium sulfite solution at 37 ^oC. For a partial pressure of 0.21 of oxygen in air, a value of $C_{O2}^* = 1.24 \cdot 10^{-4}$ M/atm is obtained.

In the presence of $1 \cdot 10^{-3}$ M of Cu^{2+} catalyst, the rate of reaction is fast enough to maintain the dissolved oxygen levels in the bulk at zero, $C_{O_2,bulk} = 0$ (except for a brief induction time at the beginning of the experiments, during which the cuprous ions are being formed), according to the readings of a dissolved oxygen probe. Yet the chemical enhancement effect of the absorption rate caused by the catalyst is not enough to obtain a fast-reaction regime (Linek *et al.*, 1978), in which absorption rates would depend solely on reaction kinetics and not on mass transfer. Using a value of the kinetic constant k_n of 3.5 s^{-1} (Augenstein, 1967), a diffusion coefficient of oxygen at 37 ^oC of $3.2 \cdot 10^{-9}$ m^2/s, and typical values of $k_L a$ in the absorption equipment calculated from Eq. 6 and Eqs. 24 to 26, which range from $5 \cdot 10^{-4}$ m/s to $8.3 \cdot 10^{-4}$ m/s, it is found that the values of the Hatta number calculated from Eq. 36 range from 0.21 to 0.13. Additionally, the term $C_{SO_3^{2-}} / \left(z C_{O_2}^* \right)$ has a value of 2700 for a 0.67 M sodium sulfite solution. Therefore, the constraints placed by Eqs. 37a, 37b and 37c are satisfied.

The results presented in Figures 4-6 and 4-7 show that a 3 to 4 fold enhancement of $k_L a$ can be obtained at a particle mass fraction as low as $\phi = 0.0025$ (0.25% w/v). At higher particle concentrations $k_L a$ can still be further enhanced, but diminishing returns are obtained as the particle fraction approaches $\phi = 0.01$. The results illustrate that several-fold enhancement can be obtained over a broad range of operating conditions of power input per unit volume and superficial velocity which are representative of most industrially relevant conditions.

Table 4-4. Operating conditions and experimental measurements of absorption rate for the determination of k_La by the sodium sulfite method

ϕ	N (rpm)	Q (L·L-1 ·min-1)	P_G/V_L (HP/1000L)	V_s (cm·min^{-1})	OUR (mmol·L^{-1} ·h^{-1})	C_{ave}^* (atm)	k_La (mmol·L^{-1}·h^{-1}· atm^{-1})	Ha	E
0.0	300	1.0	2.8	14.5	20.6	0.208	111.8	0.20	1.0
0.0	400	1.0	6.9	14.5	37.8	0.206	186.1	0.17	1.0
0.0	500	1.0	14.7	14.5	64.4	0.204	325.4	0.14	1.0
0.0	600	1.0	25.5	14.5	96.0	0.201	499.8	0.12	1.0
0.0	288	0.5	2.8	7.2	14.1	0.205	68.7	0.20	1.0
0.0	300	1.0	2.8	14.5	20.6	0.206	99.9	0.20	1.0
0.0	320	1.5	2.8	21.7	27.3	0.207	132.2	0.20	1.0
0.0	325	2.0	2.8	28.9	30.8	0.207	148.7	0.20	1.0
0.0	350	3.63	2.8	52.5	39.4	0.208	189.2	0.20	1.0
0.0025	250	1.0	1.5	14.5	45.5	0.202	225.3		3.1
0.0025	300	1.0	2.8	14.5	73.7	0.196	375.6		3.4
0.0025	400	1.0	6.9	14.5	143.0	0.183	804.0		4.3
0.0025	500	1.0	14.7	14.5	192.3	0.174	1104.5		3.4
0.0025	288	0.5	2.8	7.2	53.4	0.190	281.0		4.1
0.0025	300	1.0	2.8	14.5	73.7	0.196	375.6		3.8
0.0025	320	1.5	2.8	21.7	107.4	0.197	546.2		4.1
0.0025	325	2.0	2.8	28.9	128.3	0.198	647.9		4.4
0.0025	350	3.63	2.8	52.5	153.2	0.202	758.0		4.0
0.005	250	1.0	1.5	14.5	48.6	0.201	241.9		3.3
0.005	300	1.0	2.8	14.5	88.1	0.194	455.2		4.1
0.005	400	1.0	6.9	14.5	149.8	0.182	822.9		4.4
0.005	500	1.0	14.7	14.5	233.3	0.167	1401.6		4.3
0.005	288	0.5	2.8	7.2	65.3	0.186	351.8		5.1
0.005	300	1.0	2.8	14.5	88.1	0.194	455.2		4.6
0.005	320	1.5	2.8	21.7	131.6	0.194	679.7		5.1
0.005	325	2.0	2.8	28.9	139.2	0.197	706.6		4.8
0.005	350	3.63	2.8	52.5	192.3	0.200	961.0		5.1
0.01	250	1.0	1.5	14.5	48.0	0.201	238.8		3.3
0.01	300	1.0	2.8	14.5	100.6	0.191	526.1		4.7
0.01	400	1.0	6.9	14.5	171.8	0.178	965.5		5.2
0.01	500	1.0	14.7	14.5	251.4	0.163	1541.7		4.7
0.01	288	0.5	2.8	7.2	73.6	0.183	403.2		5.9
0.01	300	1.0	2.8	14.5	100.6	0.191	526.1		5.3
0.01	320	1.5	2.8	21.7	177.3	0.188	943.4		7.1
0.01	325	2.0	2.8	28.9	182.6	0.193	946.5		6.4

key: ϕ = particle fraction, N = agitation rate, Q = air flow rate, P_G/V_L = Power input per unit volume calculated from the aeration number correlation (Oyama *et al.*, 1955), with P_0 (ungassed power input) calculated by Eq. 33, V_s = superficial velocity based on cross-sectional vessel area $V_s = Q \cdot V / (\pi R_T^2)$, V = tank volume, R_T = tank radius, OUR = oxygen uptake rate, $C_{ave}^* = (C_{inlet}^* + C_{outlet}^*)/2$, k_La as defined by Eq. 2, Ha as defined by Eq. 36, E defined by Eq. 32.

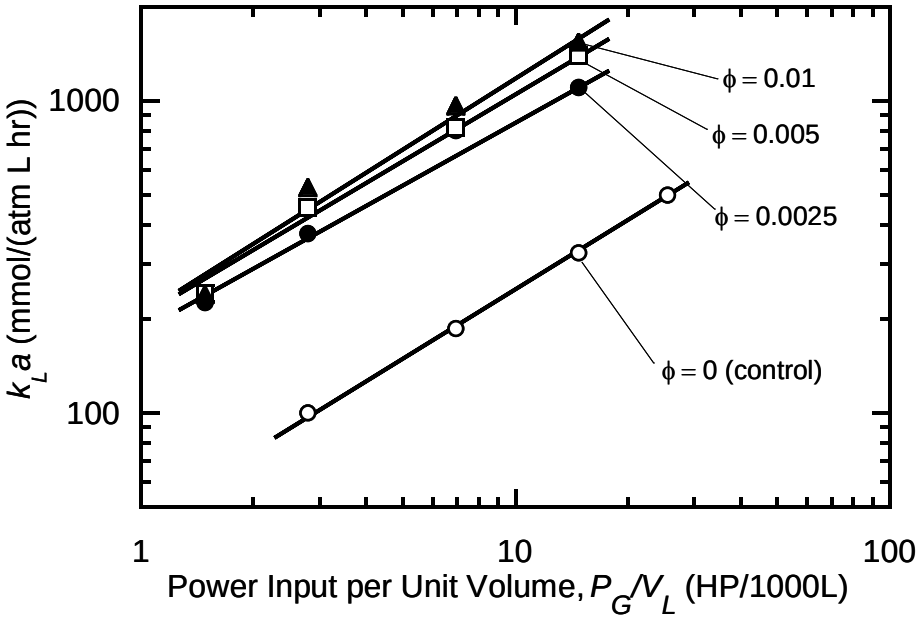

Figure 4-6. $k_L a$ measured by the sodium sulfite method as a function of power input per unit volume at several nanoparticle mass fractions. Operating conditions are T=37 °C, pH = 8.0, V_s= 14.5 cm/min

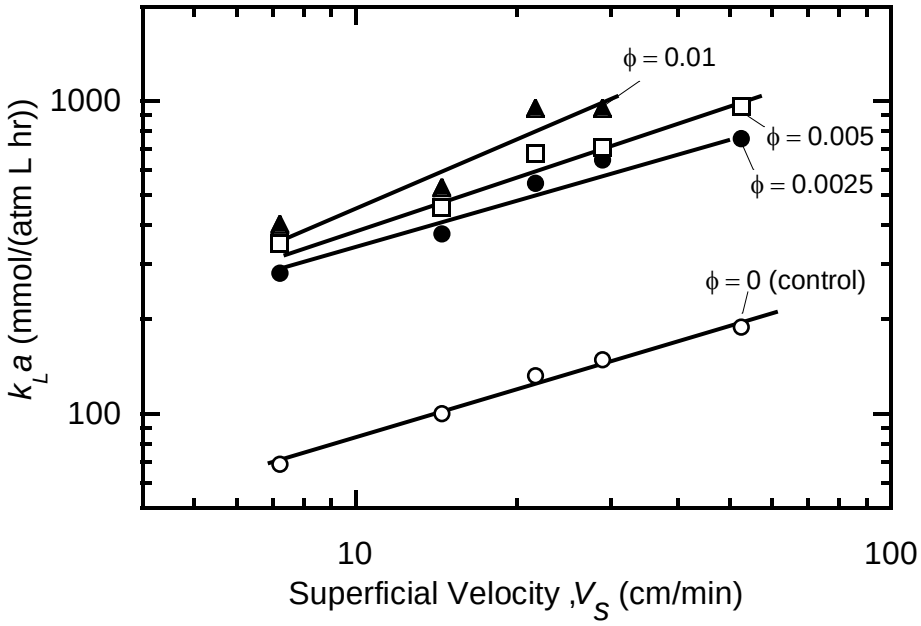

Figur

e 4-7. $k_L a$ measured by the sodium sulfite method as a function of superficial velocity at several nanoparticle mass fractions. Operating conditions are T=37 °C, pH = 8.0, P_G/V_L= 2.8 HP/1000 L

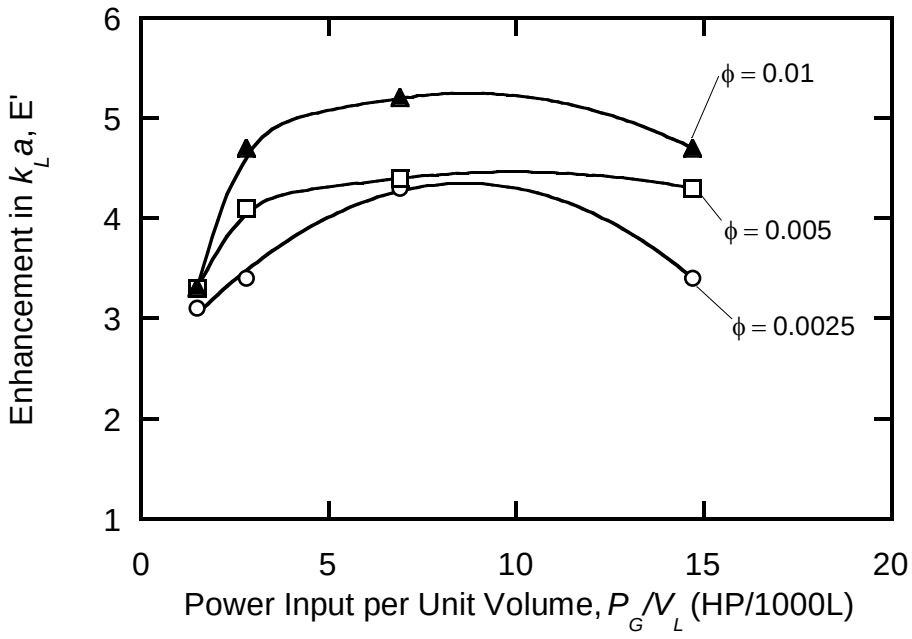

Figure 4-8. Absolute enhancement in $k_L a$ measured by the sodium sulfite method as a function of power input per unit volume at several nanoparticle holdups. Operating conditions are T=37°C, pH = 8.0, V_s= 14.5 cm/min

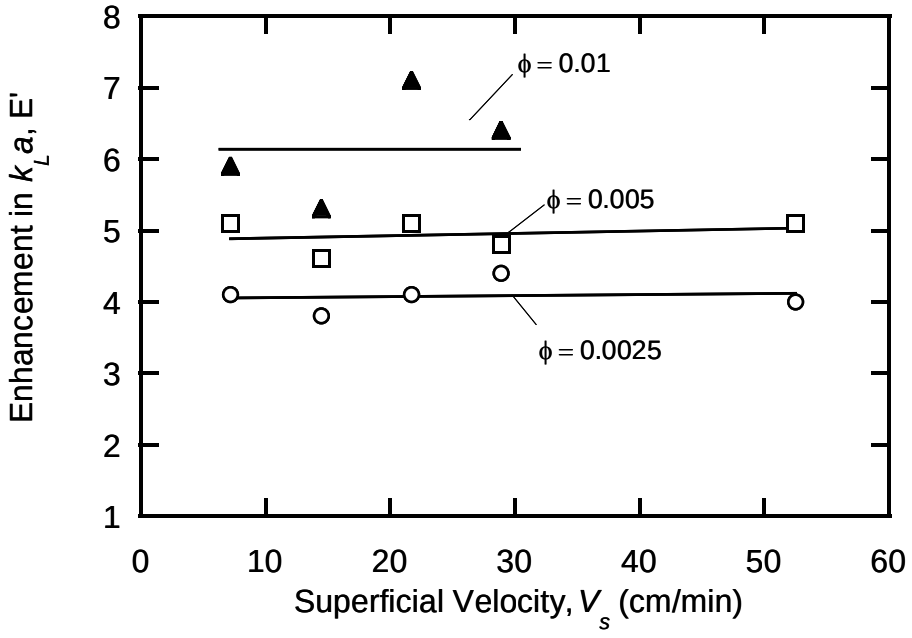

Figur

e 4-9. Absolute enhancement in $k_L a$ measured by the sodium sulfite method as a function of superficial velocity per unit volume at several nanoparticle holdups. Operating conditions are T=37°C, pH = 8.0, P_G/V_L= 2.8 HP/1000L

Figures 4-8 and 4-9 show the influence of power input per unit volume and superficial velocity on the absolute enhancement in $k_L a$ as defined by Eq. 32. It is apparent from Figure 4-8 that enhancement initially increases with power input, reaches a maximum and subsequently decreases. As shown in Figure 4-9, superficial velocity does not have noticeable effect on enhancement, possibly because the bubble rise velocity does not determine the typical exposure time of the liquid elements at the gas-liquid interface. As shown in Figure 4-11, a time scale based on isotropic turbulence prediction well k_L.

Through a non-linear least squares fit of all data presented in Table 4-4, an empirical correlation for $k_L a$ as a function of particle mass fraction, power input per unit volume, and superficial velocity is obtained

$$k_L a = a\left(1 + b\phi^c\right)\left(\frac{P_G}{V_L}\right)^d \left(V_S\right)^e \tag{40}$$

where the values of the estimated parameters are a = 12.9±5.1, b = 4.0±1.0, c = 0.34±0.09, d = 0.63±0.05, and e = 0.57±0.09 (95% confidence intervals). As shown in Figure 4-10, Eq. 40 gives a satisfactory correlation of all data. This correlation can be used for scale-up purposes but does not contain physical insight into the mechanism of mass transfer enhancement by nanoparticles.

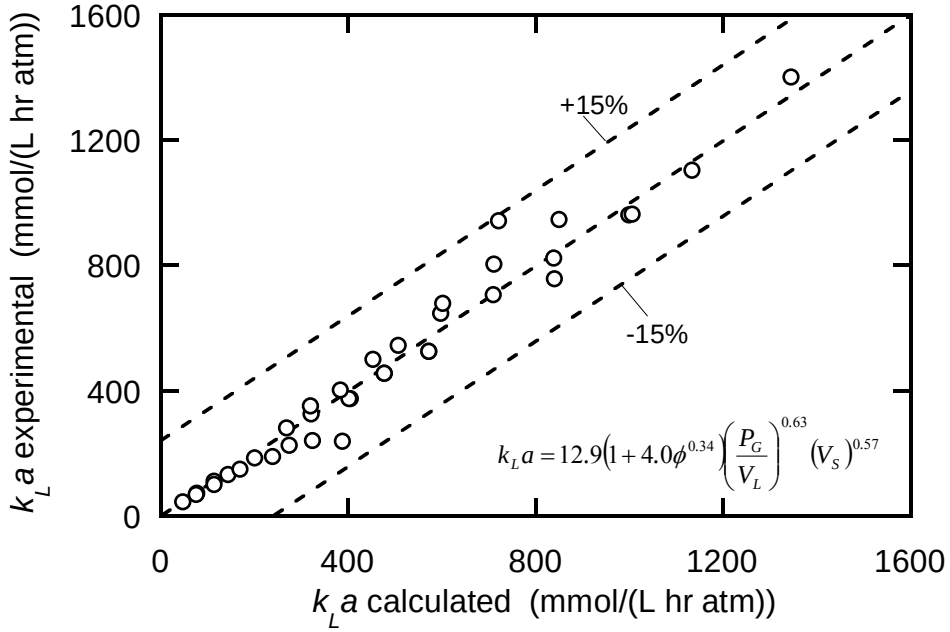

Figure 4-10. Comparison of calculated $k_L a$ values (Eq. 40) with experimental data

The first step towards understanding the mechanism of enhanced mass transfer – which will be dealt with in detail in Chapter 5 – is to identify the physical mechanism of mass transfer in the absence of nanoparticles. The experimental values of $k_L a$ for the base case (ϕ=0) can be compared with theoretical predictions using expressions for the mass transfer coefficient k_L and for the interfacial area a. A theoretical prediction of k_L has been obtained by using the Lamont model (Eq. 6), which is based on isotropic turbulence theory. A value of c = 0.448 in Eq. 6 is used, as proposed by (Linek *et al.*, 2005) for data obtained in a stirred tank system in the presence of sodium sulfite solutions. Eqs. 24, 25, and 26 are used for the estimation of the bubble diameter, interfacial area, and holdup, respectively. The product of k_L (obtained from Eq. 6) and a (obtained from Eq. 25) is plotted in Figure 4-11 and compared with experimental data. The theoretical predictions from isotropic turbulence theory agree well with experimental data. It is apparent that power input per unit volume is an appropriate quantity to correlate the mass transfer coefficient.

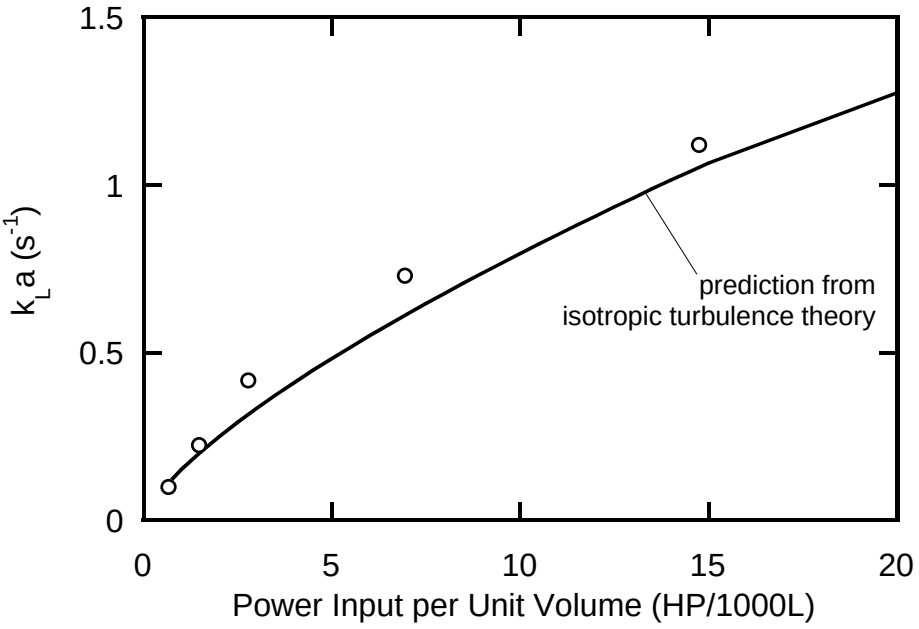

Figure 4-11. Comparison of experimental values of $k_L a$ obtained in the absence of nanoparticles with theoretical predictions of $k_L a$ obtained from isotropic turbulence theory. Theoretical values of k_L are calculated from Eq. 6 and values of a are calculated from Eq. 25

4.2.2.2 Determination of the interfacial area (*a*)

The purpose of the experiments in this section is to establish whether nanoparticles increase the gas-liquid interfacial area for mass transfer and to quantify this effect.

The reaction rate of the oxidation of sodium sulfite can be manipulated with the catalyst concentration so that it becomes several folds greater than the mass transfer rate; generally a criterion of $Ha \geq 3$ is used. The absorption rate is then greatly enhanced by the reaction and the effect of the hydrodynamic conditions can be ignored. Under these conditions, the absorption rate depends only on the interfacial area and reaction kinetics. Eq. 35 reduces to

$$N \cdot a = a C^*_{O_2} \sqrt{\frac{2}{n+1} k_n C^{*\,n-1}_{O_2} D_{O_{2,L}}} \tag{41}$$

The appropriate experimental conditions for determination of the interfacial area can be predicted if information on the kinetic constant of the reaction is available. Adoption of literature data on kinetic constants for the sulfite oxidation is discouraged (Linek *et al.*, 1981) because the literature data show significant differences between measurements made in equivalent conditions by different authors. Alternatively, an appropriate range of catalyst concentrations that permit operation in a regime where absorption is kinetically enhanced can be selected. This is done by performing absorption experiments at increasing catalyst concentration, as shown in Figure 4-12. For this purpose, Co^{2+} is used instead of Cu^{2+} because it is not possible to attain an enhanced absorption regime with Cu^{2+} (Linek *et al.*, 1981); instead, low Co^{2+} concentrations generally suffice. It is found that above a concentration of Co^{2+} of $1 \cdot 10^{-5}$ M, the absorption rate increases with catalyst concentration. This observation is equally valid in the presence of nanoparticles at mass fractions of $\phi = 0.0025$ and $\phi = 0.005$. Inspection of Figure 4-12 reveals that nanoparticles increase the gas-liquid interfacial area; it also reveals that doubling the nanoparticle mass fraction, from $\phi = 0.0025$ to $\phi = 0.005$, does not have a significant effect on the interfacial area. These considerations are made under the assumption that the reaction rate is not altered in the presence of nanoparticles.

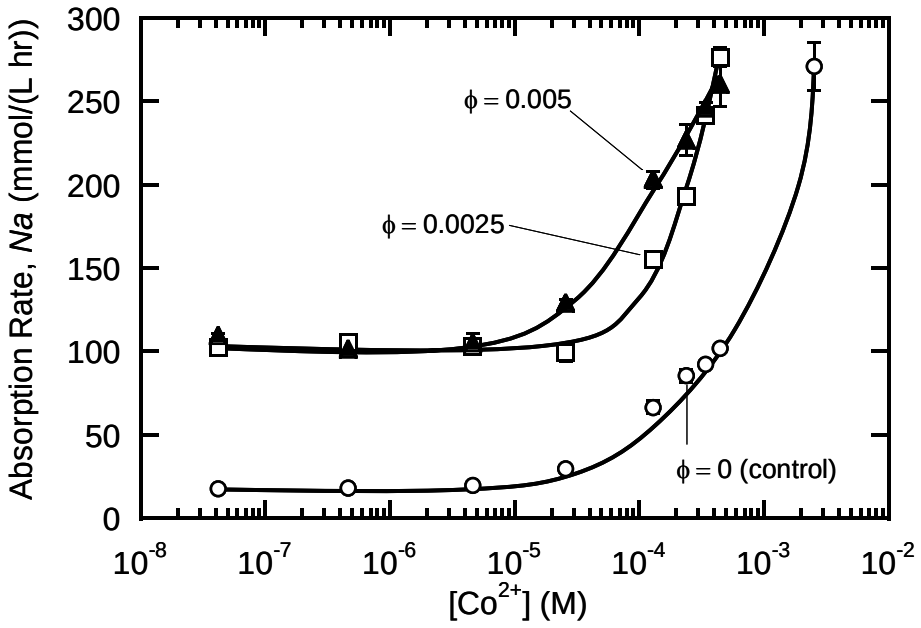

Figure 4-12. Absorption rate as a function of cobalt ion concentration at pH=8.5, T=37 °C, P_G/V_L=2.8 HP/1000 L, V_s = 14.5 cm/min, and $[SO_3^{2-}]$ = 0.67 M. Above $[Co]^{2+} = 10^{-4}$ M, the absorption rate is enhanced by the chemical reaction

The interfacial area enhancement can be quantified using Eq. 41, even if an accurate measure of the kinetic constant is not available. Rearranging Eq. 41 and taking a ratio in the presence and absence of particles, the following expression for the area enhancement is obtained

$$E_{\text{area}} = \frac{a_{\text{nanoparticles}}}{a_{\text{control}}} = \frac{(N \cdot a)_{\text{nanoparticles}}}{(N \cdot a)_{\text{control}}} \frac{\left(C_{O_2}^* \sqrt{C_{O_2}^{*\,n-1}} \right)_{\text{control}}}{\left(C_{O_2}^* \sqrt{C_{O_2}^{*\,n-1}} \right)_{\text{nanoparticles}}} \tag{42}$$

where the values of the kinetic constants and the diffusion coefficient initially present in Eq. 41 cancel. The C_{O2}^* terms do not cancel because the average value of the oxygen solubility depends on the oxygen partial pressure in the gas phase, which is not constant during the bubble residence time in the absorption equipment; instead, it decreases as the oxygen in the bubble is depleted. Inlet and outlet values of oxygen concentration in the gas phase are measured by a mass spectrometer and the corresponding concentrations in the liquid phase are determined using Henry's law and Eq. 39. The concentration of oxygen at the gas-liquid interface, C_{O2}^*, is calculated as the average of the inlet and outlet

saturation concentrations of oxygen in the liquid phase. There is agreement in the literature that the sodium sulfite oxidation under heterogeneous conditions has (i) order zero with respect to the sulfite concentration at high concentrations of sulfite (typically above 0.3 M) and (ii) order two with respect to dissolved oxygen at oxygen concentrations below $3.6 \cdot 10^{-4}$M (Reith *et al.*, 1973; Laurent *et al.*, 1974; Sathyamurthy *et al.*, 1979; Ogawa *et al.*, 1982). Therefore, *n* in Eq. 42 has a value of 2.

Table 4-5 summarizes the values of area enhancement corresponding to experimental data collected above a catalyst concentration of 10^{-4} M in Figure 4-11 (below this catalyst concentration, the mass transfer is not enhanced by the chemical reaction and Eq. 42 does not yield the true ratio of interfacial areas).

Table 4-5. Calculated values of interfacial area enhancement as a function of Co^{2+} concentration at pH = 8.5, T = 37 ^{o}C, P_G/V_L=2.8 HP/1000 L, V_S = 14.5 cm/min, and $[SO_3^{2-}]$ = 0.67 M

ϕ (mass fraction)	$[Co]^{2+}$ (M)	*OUR* ($mmol \cdot L^{-1} \cdot h^{-1}$)	C_{O2}^{*} average (mol/m^3)	E_{area} (Eq. 42)
0.0	$1.30 \cdot 10^{-4}$	66.3	0.116	1.0
0.0	$2.40 \cdot 10^{-4}$	85.5	0.114	1.0
0.0	$3.40 \cdot 10^{-4}$	92.2	0.114	1.0
0.0	$4.46 \cdot 10^{-4}$	101.9	0.113	1.0
0.0	$2.55 \cdot 10^{-3}$	271.0	0.094	1.0
0.0025	$1.30 \cdot 10^{-4}$	155.4	0.107	2.7
0.0025	$2.40 \cdot 10^{-4}$	192.8	0.102	2.7
0.0025	$3.40 \cdot 10^{-4}$	241.3	0.097	3.3
0.0025	$4.46 \cdot 10^{-4}$	276.5	0.093	3.6
0.005	$1.30 \cdot 10^{-4}$	203.0	0.101	3.8
0.005	$2.40 \cdot 10^{-4}$	226.6	0.099	3.3
0.005	$3.40 \cdot 10^{-4}$	245.8	0.097	3.4
0.005	$4.46 \cdot 10^{-4}$	260.3	0.095	3.3

The average value of area enhancement in the presence of ϕ = 0.0025 mass fraction of nanoparticles at P_G/V_L = 2.8 HP/1000 L and V_S = 14.5 cm/min is 3.1±0.5 (average of the 4 values in column 5, for ϕ = 0.0025, Table 4-5). For ϕ = 0.005, this value is 3.4±0.2. At equivalent conditions of power input and superficial velocity, the corresponding enhancement in k_La (Table 4-4) is 3.4 for ϕ = 0.0025 and 4.1 for ϕ = 0.005. Therefore,

for this particular experimental condition, most of the enhancement in $k_L a$ is due to an increase in the interfacial area. As will be shown in Section 4-3, the nanoparticles used in this work reduce the surface tension, σ, of an aqueous solution to approximately 40 mN/m; which is 30 mN/m below the value for pure water (70 mN/m at 37 ^{o}C). According to Eqs. 24 and 25, the gas-liquid interfacial area in an agitated, sparged absorption vessel exhibits a $\sigma^{-0.6}$ dependence. Therefore, a lower surface tension yields a higher interfacial area. Using the values of surface tension in the presence and in the absence of particles previously mentioned, Eqs. 24 to 26 can be used to predict a theoretical area enhancement factor of 1.46. This factor is lower than the experimental values in Table 4-5. This suggests that the mechanism by which nanoparticles increase gas-liquid interfacial area is more complex than merely surface tension reduction. It is possible that nanoparticles also affect interfacial area by preventing bubble coalescence.

A quantitative analysis of the relative contribution of area effects to the total enhancement in $k_L a$ can only be made by performing interfacial area measurements for the range of conditions presented in Table 4-4. Estimations of area enhancement have been made as described previously for a nanoparticle mass fraction of $\phi = 0.0025$ and the results are summarized in Table 4-6.

Table 4-6 Calculated values of interfacial area enhancement as a function of power input and superficial velocity at pH = 8.5, T = 37 °C, $[Co^{2+}] = 2.40 \cdot 10^{-4}$ M, and $[SO_3^{2-}] = 0.67$ M

ϕ	N (rpm)	Q ($L \cdot L^{-1} \cdot min^{-1}$)	P_G/V_L (HP/1000L)	V_s (cm·min-1)	OUR ($mmol \cdot L^{-1} \cdot h^{-1}$)	C_{O2}^* average (mol/m^3)	E_{area} (Eq. 42)
0	250	1.0	1.5	14.5	57.9	0.117	1.0
0	300	1.0	2.8	14.5	85.5	0.114	1.0
0	400	1.0	6.9	14.5	103.3	0.112	1.0
0	500	1.0	14.7	14.5	125.0	0.111	1.0
0	288	0.5	2.8	7.2	54.2	0.118	1.0
0	300	1.0	2.8	14.5	85.5	0.114	1.0
0	320	1.5	2.8	21.7	113.0	0.111	1.0
0	325	2.0	2.8	28.9	115.3	0.111	1.0
0.0025	250	1.0	1.5	14.5	130.6	0.202	2.5
0.0025	300	1.0	2.8	14.5	192.8	0.196	2.7
0.0025	400	1.0	6.9	14.5	300.4	0.183	4.0
0.0025	500	1.0	14.7	14.5	315.5	0.174	3.5
0.0025	288	0.5	2.8	7.2	122.7	0.190	2.5
0.0025	300	1.0	2.8	14.5	192.8	0.196	2.7
0.0025	320	1.5	2.8	21.7	312.9	0.197	3.9
0.0025	325	2.0	2.8	28.9	330.0	0.198	4.1

The data in column 8 of Table 4-6 are presented graphically in Figure 4-13. The shapes of the interfacial area enhancement curve and the k_La enhancement curve as a function of power input (Figure 4-13a) for $\phi = 0.0025$ closely resemble each other; this indicates that the k_La enhancement trend – an initial increase at low power input followed by a decrease above approximately 8 HP/1000 L – is caused primarily by a change in interfacial area rather than a change in k_L. Figure 4-13a further shows that (i) enhancement in k_L also contributes to total enhancement and (ii) enhancement in k_L decreases with power input; therefore, the higher, the base mass transfer coefficient, the lower the enhancement in k_L. Both these observations are consistent with the data presented in Section 4.2.1. Enhancement data as a function of superficial velocity, shown in Figure 4-13b, do not show as clear a pattern; while the k_La enhancement remains approximately constant as a function of superficial velocity, area enhancement increases above a superficial velocity of 20 cm/min.

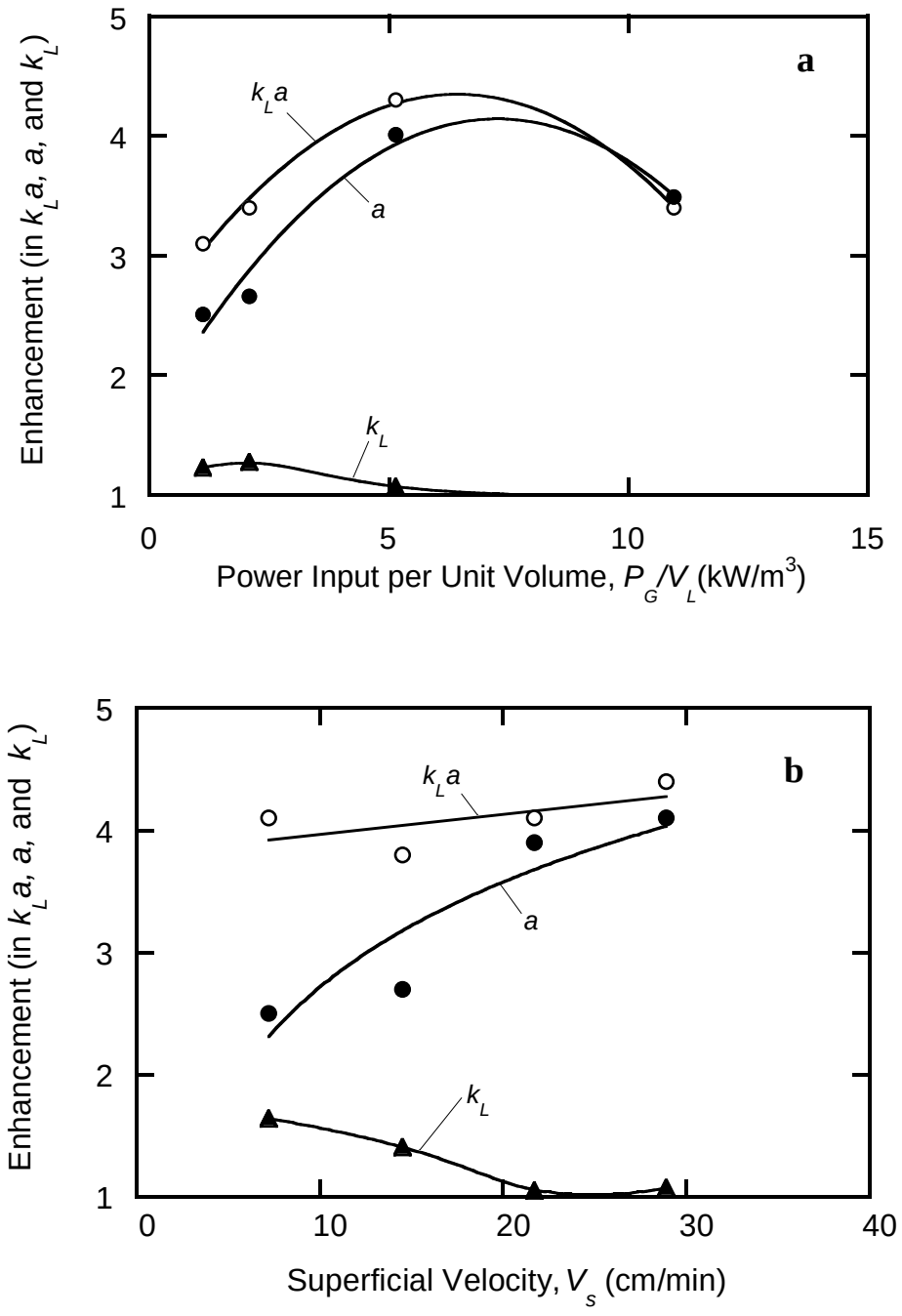

Figur
e 4-13. Enhancement in $k_L a$, a, and k_L for ϕ = 0.0025, pH=8.0, T=37 ^{o}C as a function of (a) power input per unit volume at Vs= 14.5 cm/min, and (b) superficial velocity at P_G/V_L= 2.1 kW/m^3. The enhancement in k_L is calculated as $E_{k_L} = E_{k_L a} / E_a$

The considerations in this section have been made without using kinetic data describing the catalyzed sodium sulfite oxidation. Calculation of the gas-liquid interfacial area is only possible if kinetic data are used. While the goal of this section has been to determine interfacial area enhancement rather than interfacial area, an approximate

estimate of the latter can be made to verify that the experimental values are on the order of theoretical predictions. A value of k_n^0 of $1.3 \cdot 10^3$ $m^3/(mol \cdot s)$ at 20 °C and $[CoSO_4] = 3.56 \cdot 10^{-4}$ M can be calculated from published data (Laurent *et al.*, 1974). This value can be used to calculate k_n at the experimental conditions of the present work (37 °C and $[CoSO_4] = 2.4 \cdot 10^{-4}$ M) using the following expression (Linek *et al.*, 1981)

$$k_n = k_n^0 \frac{[CoSO_4]}{[CoSO_4]^0} \exp^{\left\{\frac{-E_n}{R}\left(\frac{1}{T}-\frac{1}{T^0}\right)\right\}} \tag{43}$$

Taking the activation energy of the reaction E_n to be 53.4 kJ/mol (Linek *et al.*, 1971), a value of k_n of $2.94 \cdot 10^3$ $m^3/(mol \cdot s)$ is calculated. The oxygen uptake rate measured at P_G/V_L = 2.8 HP/1000 L, V_s = 14.5 cm/min, and $\phi = 0$ (Table 4-6), its corresponding value of C_{O2}^*, and the estimation obtained for k_n are used in Eq. 41 to obtain an estimate of the interfacial area of 245 m^{-1}. This value is 18% lower than the prediction of 297 m^{-1} that can be obtained using Eqs. 24, 25, and 26.

4.2.2.3 Effect of Temperature on Enhancement

This section investigates the effect of temperature on the mass transfer coefficient in aqueous solutions of two types of nanoparticles: (i) 20 nm particles synthesized as described in Section 3.1 and (ii) 80 nm clusters of magnetite cores coated with random copolymers of ethylene oxide (EO) and propylene oxide (PO) repeat units, the synthesis method of which has been described elsewhere (Moeser *et al.*, 2002b; Ditsch *et al.*, 2005a). Experiments are performed following the procedure outlined in Section 3.3.2.1. A range of temperatures from 20 °C to 80 °C is explored. Oxygen uptake rates measured at P_G/V_L = 2.8 HP/1000 L, V_s = 14.5 cm/min, and a mass fraction $\phi = 0.0025$ for both types of particles are shown in Figure 4-14; measurements for a water control are shown for comparison. Oxygen uptake rates for water remain approximately constant in the temperature range studied. Although diffusivity of oxygen increases with temperature, its solubility in water decreases and the overall effect is to maintain the oxygen uptake rates in water roughly constant. The solubility of oxygen in hydrocarbons also decreases with temperature; however, as opposed to the data for the water control, the oxygen uptake rates for both types of particles show a strong positive dependence on temperature.

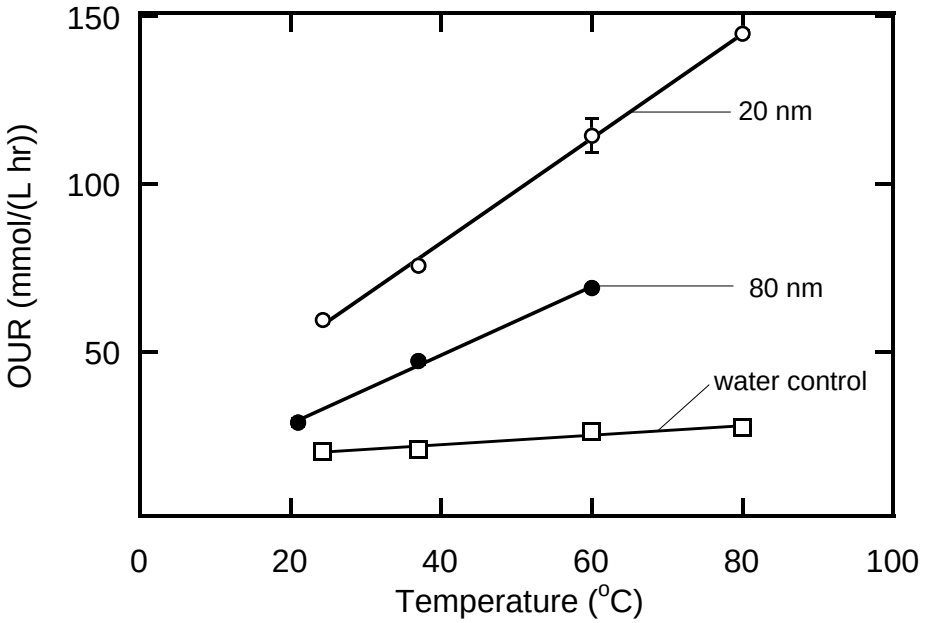

Figure 4-14. Oxygen uptake rate as a function of temperature for 80 nm – PPO–PEO–coated particles, 20 nm – oleic acid–coated particles, and a water control

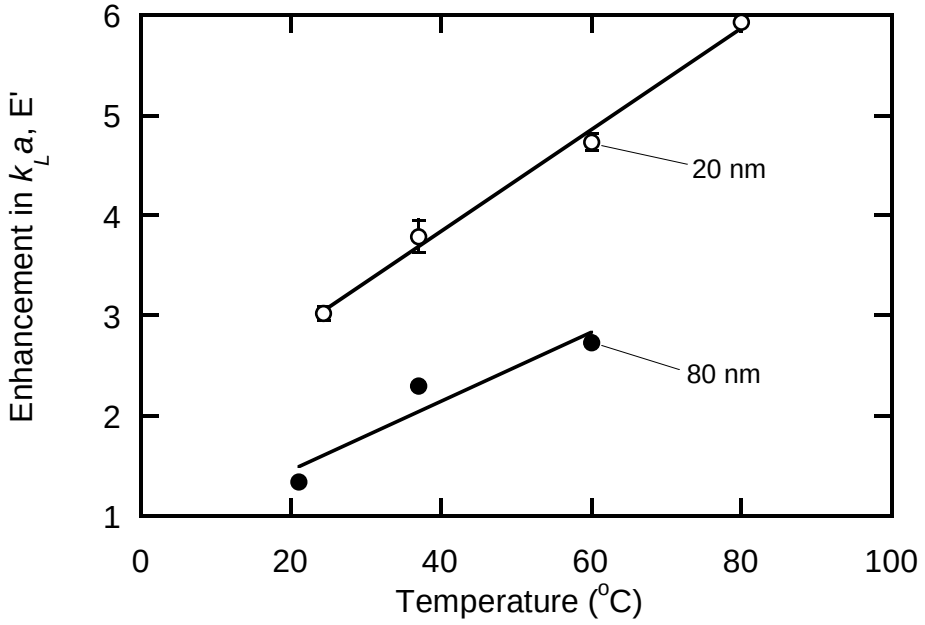

Figure 4-15. Enhancement in $k_L a$ as a function temperature for 80 nm–PPO–PEO–coated particles and 20 nm – oleic acid–coated particles.

Enhancement in $k_L a$ as a function of temperature is shown in Figure 4-15. A strong temperature dependence is evident for both types of particles; a 3 to 6 fold enhancement

of $k_L a$ takes place from 25 ^oC to 80 ^oC in the presence of $\phi = 0.0025$ oleic acid–coated particles, whereas a 1.3 to 2.7 fold enhancement of $k_L a$ takes place from 20 ^oC to 60 ^oC in the presence of $\phi = 0.0025$ PPO–PEO–coated particles.

The enhancement trends as a function of temperature are not a product of the different solubility (or temperature dependence of solubility) of oxygen in water, oleic acid, and PPO–PEO copolymers. Although the solubility of oxygen in oleic acid is 4 times higher than in water, a solution with mass fraction $\phi = 0.0025$ of oleic acid–coated nanoparticles contains approximately a mass fraction of oleic acid $\phi_{oleic} = 0.2 \cdot 0.0025 = 5 \cdot 10^{-4}$, which can account for only $5 \cdot 10^{-4} \cdot 4 = 0.002$ (0.2%) of the total amount of oxygen solubilized in the media; PPO–PEO copolymers are not reportedly known as oxygen carriers.

Figures 4-14 and 4-15 show that both nanoparticles coated with oleic acid and Hitenol BC (20 nm) and PPO–PEO–coated nanoparticles (80 nm) enhance mass transfer.

4.3 Surface Tension Measurements

This section investigates the equilibrium surface tension of aqueous solutions of nanoparticles. The experiments test the hypothesis that the nanoparticles used in the present work can accumulate at a gas-liquid interface.

A concentrated solution of nanoparticles (~5% w/v) is thoroughly stripped of free surfactant by following the method described in Section 3.5. Subsequently, the equilibrium surface tension of purified samples is measured, starting at 4% w/v and successively diluting the samples up to 10 million times. The equilibrium surface tension of the samples exhibits a decrease from 71.9 mN/m at $\phi = 5 \cdot 10^{-9}$ to 45.8 mN/m at $\phi = 4 \cdot 10^{-5}$, as shown in Figure 4-16. Beyond a nanoparticle mass fraction of $\phi = 4 \cdot 10^{-5}$, the change in surface tension becomes less pronounced. The data inside the box marked with a discontinuous line can be studied making use of the Gibbs adsorption isotherm, which relates the surface coverage Γ of the gas-liquid interface to the rate of change of the surface tension with the natural logarithm of concentration $\partial\gamma/\partial\ln(c)$

$$\Gamma = -\frac{1}{RT}\frac{\partial\gamma}{\partial(\ln c)} \tag{44}$$

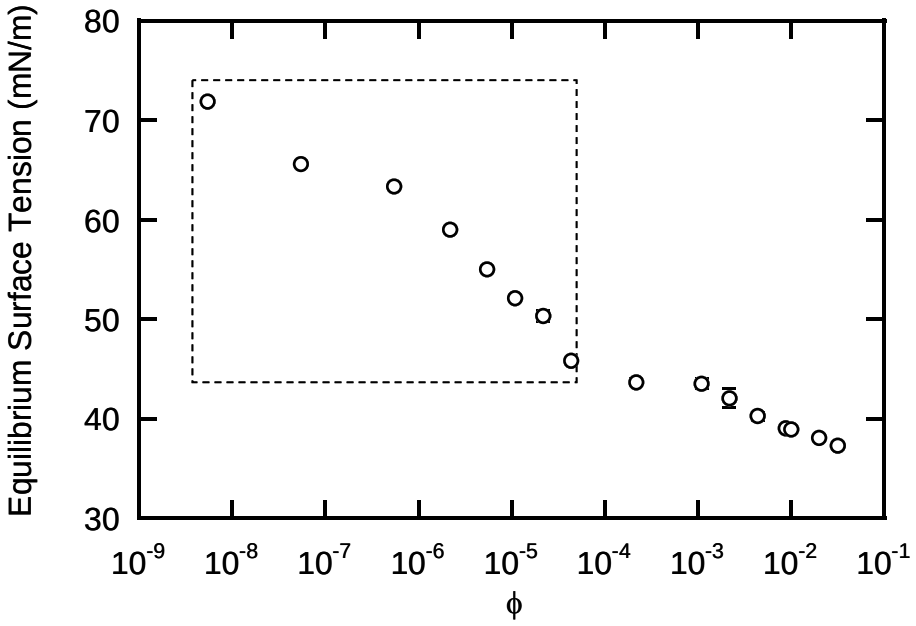

Figure 4-16: Equilibrium surface tension of aqueous solutions of oleic acid–coated nanoparticles as a function of nanoparticle mass fraction.

Values of Γ are computed from the slopes between consecutive points in the marked box in Figure 4-16. The values of Γ conform well to a Langmuir isotherm, as shown in Figure 4-17. A Langmuir isotherm has the form

$$\frac{\Gamma}{\Gamma_{max}} = \frac{K_a\phi}{1+K_a\phi} \tag{45}$$

where Γ_{max} is the maximum surface coverage of the interface and K_a is the equilibrium adsorption constant. This expression can be rearranged in the form

$$\frac{\phi}{\Gamma} = \frac{1}{\Gamma_{max}K_a} + \frac{\phi}{\Gamma_{max}} \tag{46}$$

Therefore, a plot of ϕ/Γ as a function of ϕ has a slope of $1/\Gamma_{max}$ and crosses the y axis at $1/(\Gamma_{max}\cdot K_a)$. The values of Γ_{max} and K_a estimated from the data in Figure 4-16 are $1.98\cdot10^{-10}$ mol/cm^2 and $1.38\cdot10^{6}$ mL/g, respectively.

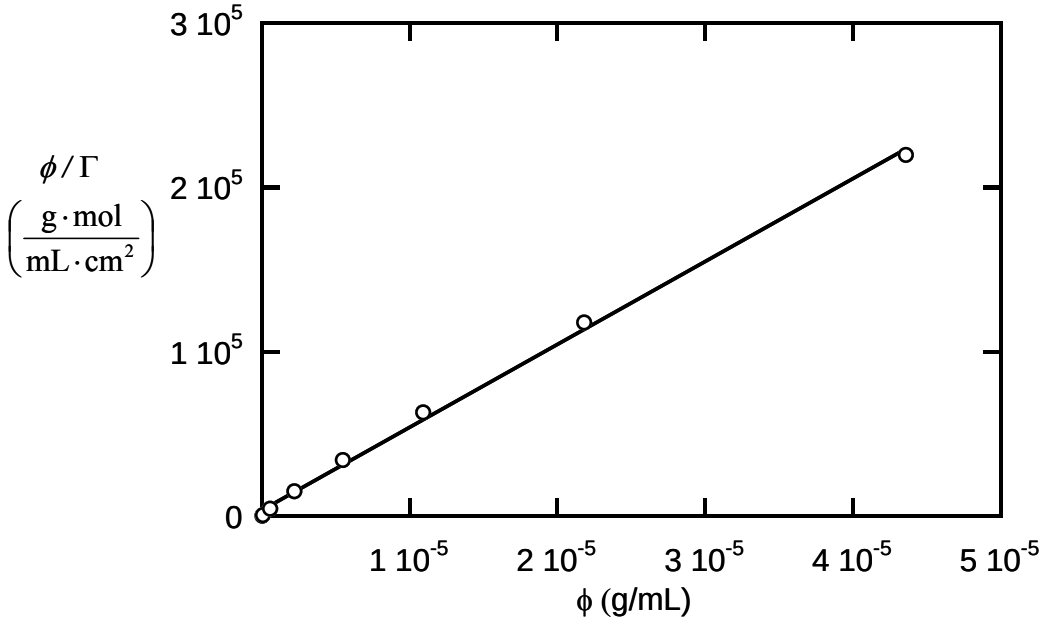

Figure 4-17: Fit of calculated surface coverage data to a Langmuir isotherm

The molecule used for the exterior coating of the nanoparticles, Hitenol BC, is a polymerizable surfactant. It is likely that the surface activity of the nanoparticles is bestowed by this exterior coating. Alternatively, it is possible that certain regions of the oleic acid–coated magnetite cores are not completely coated by Hitenol BC during the synthesis process and that some hydrophobic chains of oleic acid remain exposed to the surrounding water; a nanoparticle with hydrophobic regions and charged regions on its surface could behave as a surfactant.

4.4 Viscosity Measurements

This section presents the investigation of the dependence of the viscosity of oleic acid–coated nanoparticles on nanoparticle volume fraction. The results obtained are used to establish that viscosity does not play a role in the mechanism of mass transfer enhancement by nanoparticles. Measurements are made following the procedure outlined in Section 3.6.

Abnormal increases in viscosity in the presence of nanoparticles have been reported for alumina in water and titania in water in the range of 1 to 10% volume fraction (Pak *et al.*,

1998; Wang *et al.*, 1999); values of viscosity measured by the previous authors are several fold larger than the predictions of typical viscosity models such as the Einstein model.

In the present work, viscosity in the range of nanoparticle volume fractions (ϕ_V) of 0 to 0.65 has been studied. This corresponds to a range of nanoparticle mass fractions (ϕ) of 0 to 0.25 (Appendix 8.1). Viscosity in the range of volume fractions explored in Section 4.2 (ϕ_V from 0 to 0.026, or ϕ from 0 to 0.01) has approximately the same value as the viscosity of water, as shown in Figure 4-18. In addition Figure 4-18 shows that the viscosity is only significantly increased beyond that of the base fluid (water) above a nanoparticle volume fraction of 0.1 (ϕ = 0.04). The experimental values are lower than the predictions of the Einstein model. This finding indicates that the viscosity increase by nanoparticles is not responsible for the leveling of the k_L enhancement curve as a function of particle mass fraction reported in Figure 4-5 (Section 4.2.1).

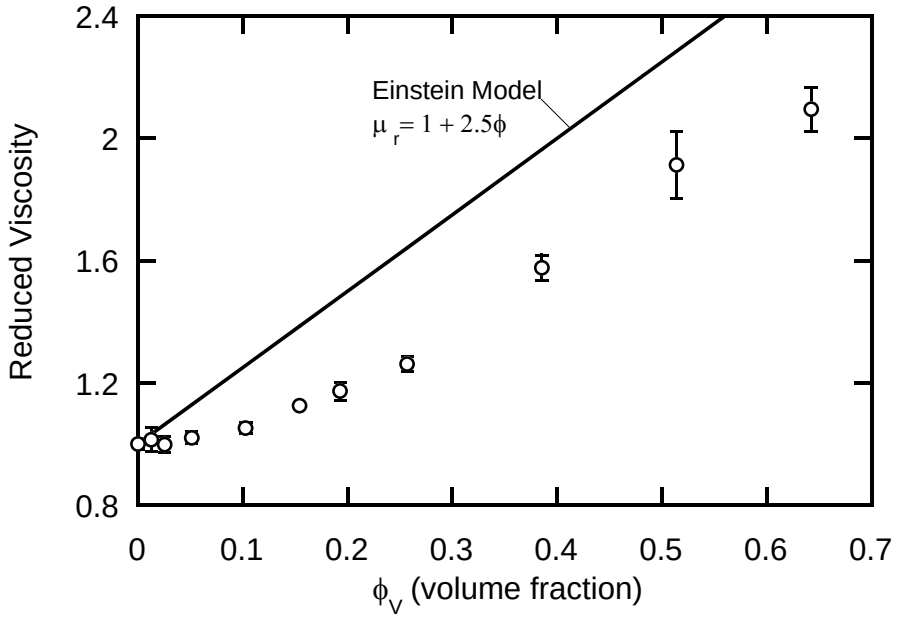

Figure 4-18: Reduced viscosity of oleic acid–coated nanoparticles as a function of volume fraction at 37 °C

4.5 Biocompatibility Studies

Shake flask tests are conducted to determine the biocompatibility of nanoparticles with the host organism chosen. Shake flask cultures of *E. coli* are performed in an aqueous control and at nanoparticle mass fractions of 0.005, 0.01, and 0.02. *E. coli* grows well in the presence of nanoparticles, as shown in Figures 4-19 and 4-20; this is evinced by optical density and glucose concentration measurements, which are both indicative of cell growth. A slightly prolonged lag phase in shake flask culture is typical of studies conducted in the presence of dispersed PFC emulsions (McMillan, 1990); this phenomenon is not observed when *E. coli* is grown in the presence of nanoparticles. Results closely similar to those shown in Figure 4-19 and 4-20 are obtained when *E. coli* is grown in the presence of Noigen RN – coated nanoparticles (not shown).

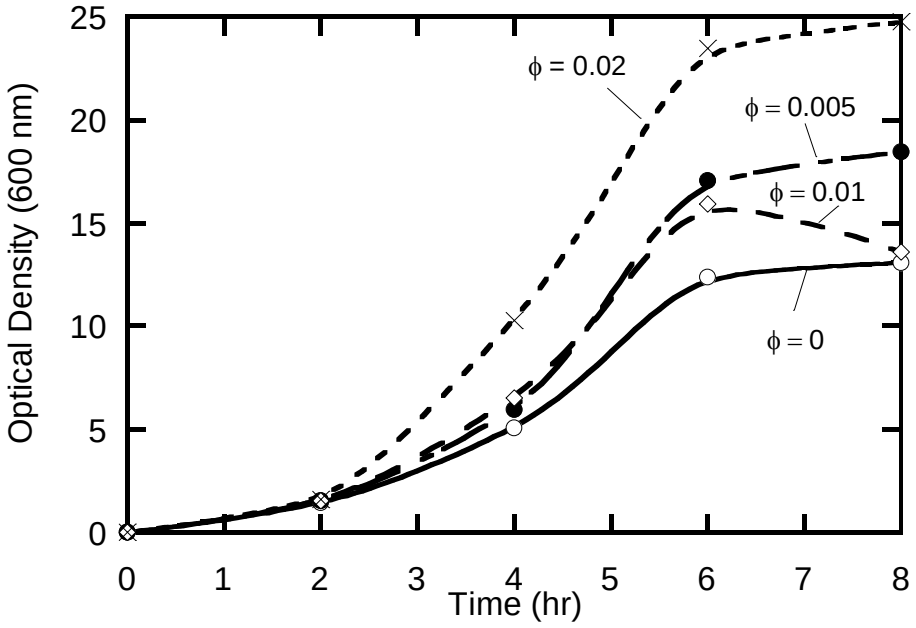

Figure 4-19. Optical density at 600 nm of *E. coli* grown in a shake flask as a function of culture time at increasing concentrations of oleic acid–coated nanoparticles

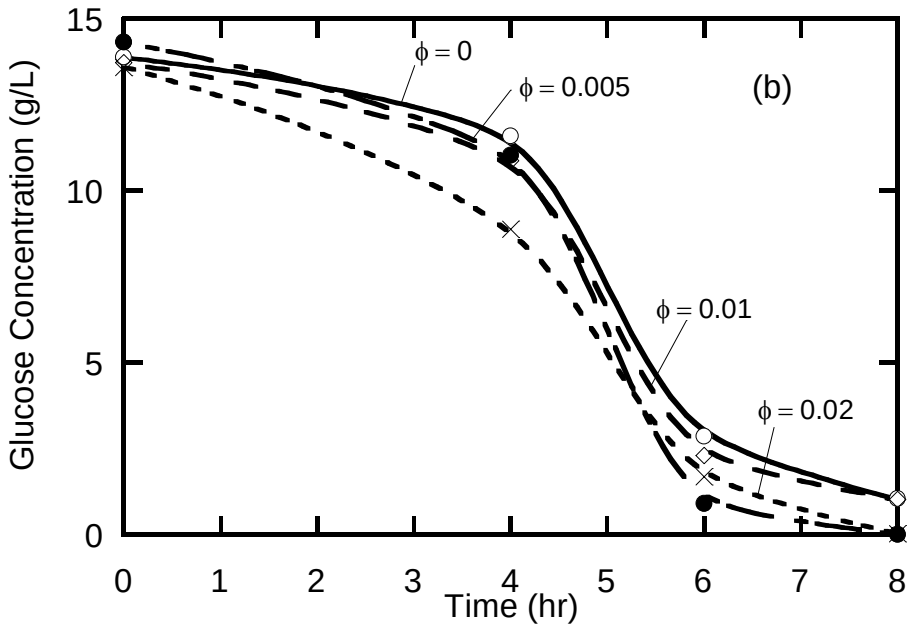

Figure 4-20. Glucose consumption by *E. coli* grown in a shake flask as a function of culture time at increasing concentrations of oleic acid–coated nanoparticles

4.6 Fermentations

Fermentations in the presence of nanoparticles are conducted to characterize the enhancement of oxygen mass transfer in biological media and to quantify the enhancement of cell growth. The results are compared to a control run conducted in the absence of nanoparticles. The results presented in this section show that oleic acid–coated nanoparticles enhance oxygen transfer rates and that this enhancement translates to corresponding increased cell concentration. The mass transfer enhancements measured are lower than those measured by a chemical method in Section 4.2.2 at equivalent conditions of power input per unit volume and superficial velocity (2.8 HP/1000 L and 14.5 cm/min); possible causes of this discrepancy are discussed. Experiments are conducted as outlined in Section 3.4.3.

The results presented in Figures 4-21 and 4-22 confirm the capacity of oleic acid–coated nanoparticles for enhancing oxygen mass transfer and consequently improving cell growth. Figures 4.21a and 4.21b show, respectively, the dissolved oxygen profiles and oxygen uptake rate profiles for 3 fermentations conducted at mass fractions of oleic acid–coated nanoparticles of $\phi = 0$, $\phi = 0.0057$, and $\phi = 0.02$. Since no control action is taken

to regulate the dissolved oxygen concentration in the bioreactor, oxygen levels decrease to zero as cells proliferate. For the control run, dissolved oxygen falls to zero at 6 hours; this happens at 8 hours for $\phi = 0.0057$ and approximately 9 hours for $\phi = 0.02$. The extended period during which dissolved oxygen concentrations remain above zero in the presence of nanoparticles is evidence that greater mass transfer rates are maintained as compared to the control run. Figure 4.21b shows that beyond the time at which dissolved oxygen levels fall to zero, greater oxygen uptake rates are maintained in the presence of nanoparticles; before this time, cell growth is not limited by oxygen mass transfer and therefore no differences are manifest between the runs. The average integrated values of the oxygen uptake rate under oxygen transfer–limited growth, defined as

$$OUR_{\text{average}} = \frac{1}{t_{\text{final}} - t\big|_{\text{DO}=0}} \int_{t\big|_{\text{DO}=0}}^{t_{\text{final}}} OUR(t)dt \qquad (47)$$

are 1.3 greater than the control for $\phi = 0.0057$ and 1.4 greater for $\phi = 0.02$. Since the dissolved oxygen concentration in the medium is zero under the conditions defined in Eq. 47, according to Eq. 2, the values of $k_L a$ are respectively 1.3 and 1.4 times greater than in the control as well.

Higher cell growth rates are maintained in the presence of nanoparticles when the cultures grow under an oxygen transfer–limited regime, *e.g.*, after 6 hours in the control run, or after 8 hours for $\phi = 0.0057$. This is supported by the optical density and dry cell weight profiles shown in Figure 4-22. The enhancement in optical density or dry cell weight in the presence of nanoparticles has a value of 1.5 immediately after oxygen limitations are encountered; it has a value of 1.3 near the end of the fermentations. Since nanoparticles contribute to the optical density of a sample, data in Figure 4-22a have been normalized by substracting the background optical density due to nanoparticles from each data point; base values of optical density are measured for samples containing $\phi = 0.0057$ and $\phi = 0.02$ and devoid of cells. Similarly, dry cell weight data in Figure 4-22b has been normalized by substracting from each data point the corresponding weight of nanoparticles as measured in a sample devoid of cells. Optical density values are linearly related to dry cell weight values (not shown); this supports the use of optical density measurements for quantifying cell growth in opaque solutions of nanoparticles.

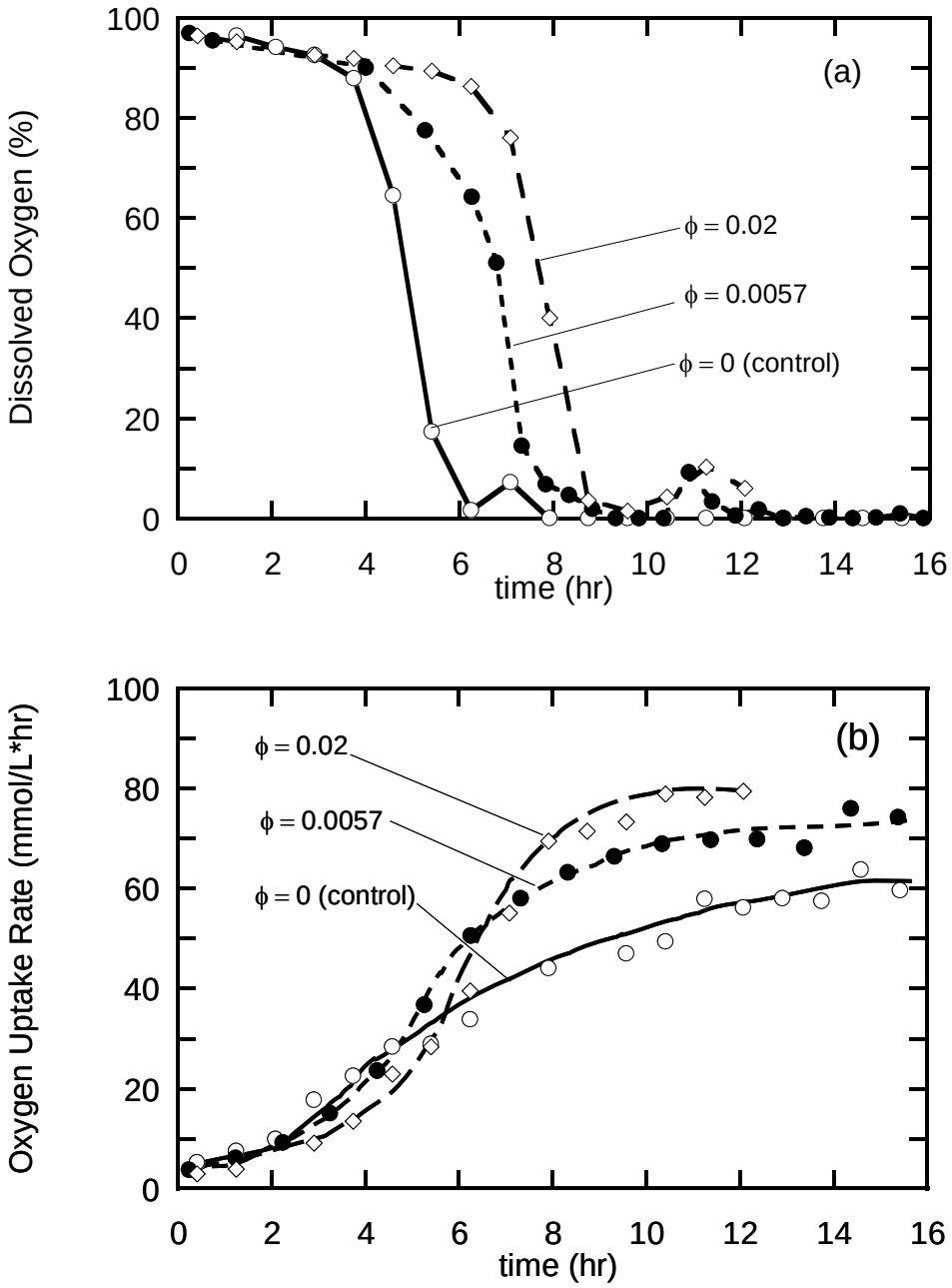

Figure 4-21 (a) Dissolved oxygen profiles and (b) Oxygen uptake rate profiles during fed–batch fermentations conducted at mass fractions ϕ = 0, ϕ = 0.0057, and ϕ = 0.02 of oleic acid–coated nanoparticles

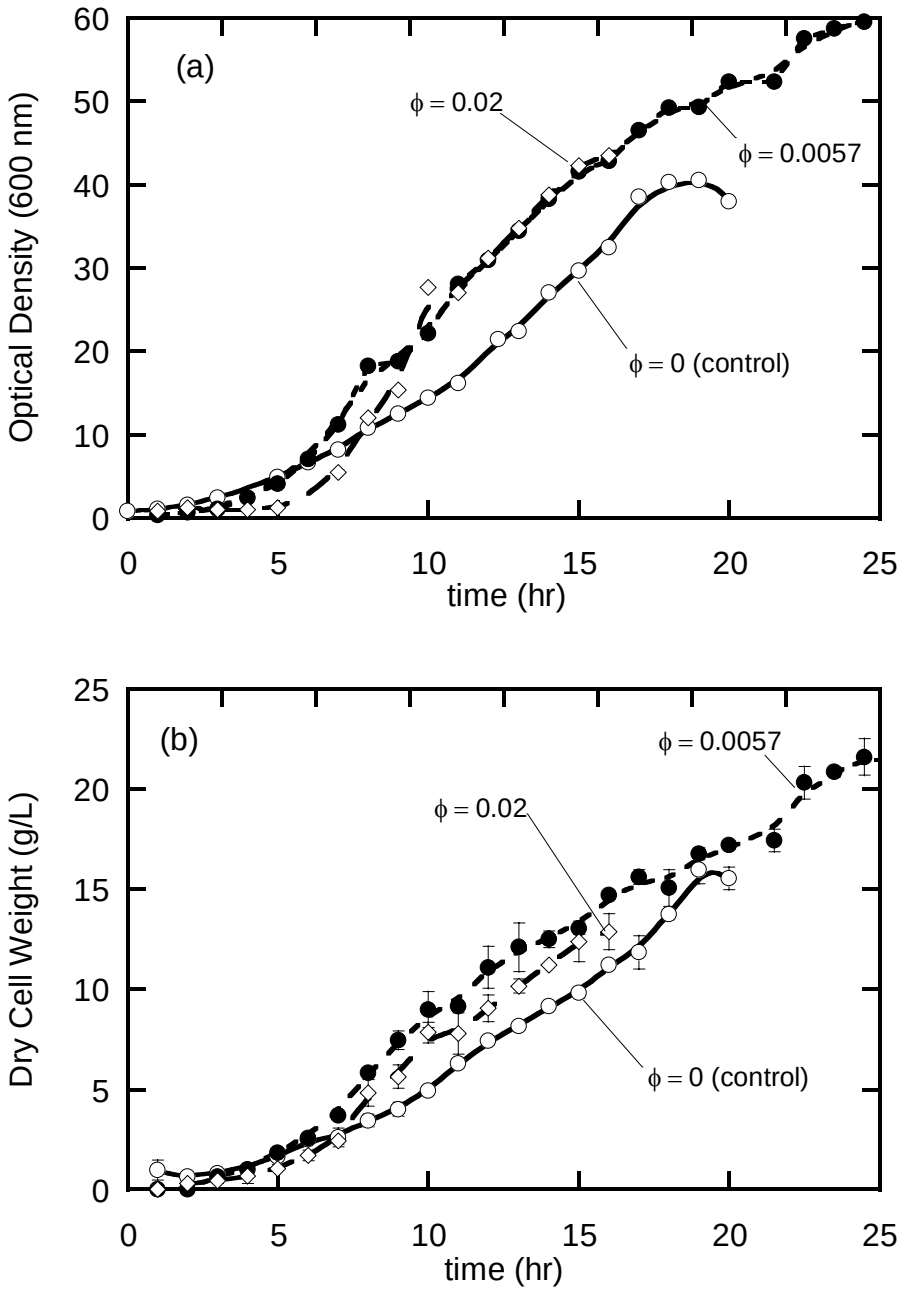

Figure 4-22 (a) Optical density at 600 nm and (b) Dry cell weight during fed-batch fermentations conducted at mass fractions ϕ = 0, ϕ = 0.0057, and ϕ = 0.02 of oleic acid–coated nanoparticles

The increase in cell growth does not occur as a result of an alteration of the *E. coli* metabolism by nanoparticles; it is instead a sole consequence of the greater oxygen transfer rates. Although *E. coli* can metabolize oleic acid, glucose will always be the most readily utilized carbon source if both nutrients are available. Furthermore, only traces of free molecules of oleic acid are expected to be present in the nanoparticle

solutions; the oleic acid incorporated in the nanoparticles is chemically attached to the magnetite cores and therefore cannot be consumed by cells. These observations are supported by Figure 4-23, which shows that the specific oxygen uptake rates (the amount of oxygen consumed per g of cell and per unit time) are the same with and without nanoparticles. Therefore, in the presence of nanoparticles, each cell has the same oxygen consumption rate on average, although there are more cells per unit volume.

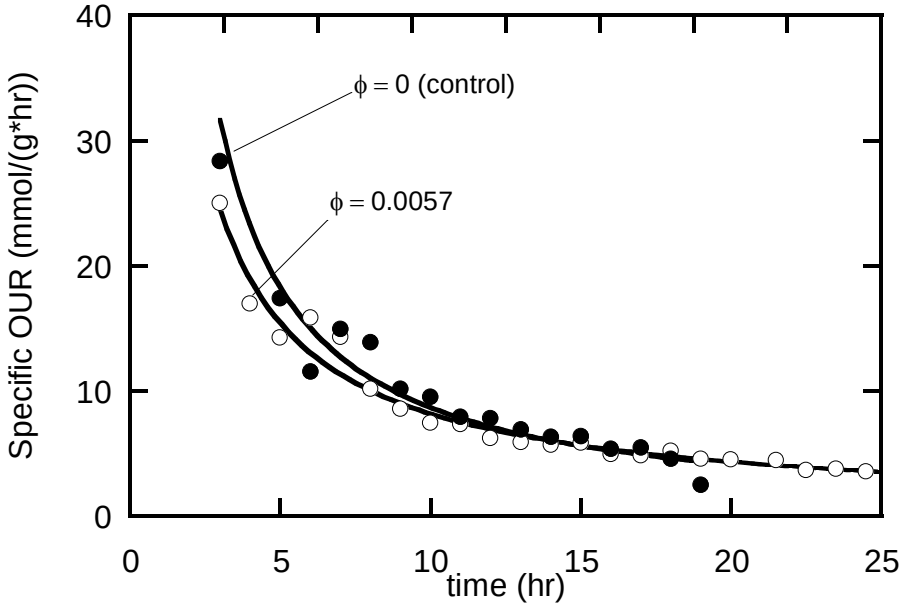

Figure 4-23 Specific oxygen uptake rates during fed-batch fermentations conducted at mass fractions $\phi = 0$ and $\phi = 0.0057$ of oleic acid–coated nanoparticles

In summary, the results presented in this section show that:

The enhancement in mass transfer obtained in fermentations is smaller than that measured by the sodium sulfite method (Section 4.1.2). Several reasons for this difference can be speculated:

- The coalescing behavior of aqueous solutions of sodium sulfite may be different from that of fermentation medium due to different salt concentrations and different viscosities. The mechanism by which nanoparticles enhance interfacial depends most likely on the coalescing behavior of the media (Section 5).

- The reaction rate of the sulfite oxidation could be altered in the presence of nanoparticles. The reaction of dissolved oxygen with SO_3^{2-} is catalytically sensitive

to traces of heavy metal ions (Linek et al., 1978); these could be present in the nanoparticle solutions in the form of Fe^{2+} and Fe^{3+}.

- Nanoparticles adhere to the surface of bacteria and cause them to cluster; this could create an additional diffusional resistance to oxygen mass transfer. The phenomenon of nanoparticle to cell attachment is studied in the following section.

A 40% increase in oxygen uptake rate and dry cell weight of *E. coli* can be obtained using a nanoparticle mass fraction of 0.57% in a fed-batch fermentation. It is expected that the increases in the oxygen transfer coefficient and in the cell concentration reported in this section would translate to corresponding increased concentration of products synthesized by the host organism, such as primary and secondary metabolites.

The oxygen transfer rate in a biological medium has been increased in a conventional agitated and aerated fermentor without any mechanical modification.

4.7 Cell Binding Experiments

This section first tests the hypothesis that oleic acid-coated nanoparticles attach to *E. coli*; the hypothesis is confirmed and the phenomenon of nanoparticle to cell attachment is quantified. It is shown that both charged and non-charged nanoparticles attach to cells to a similar extent. This suggests that the mechanism of attachment involves hydrophobic interactions. Experiments are performed as outlined in Section 3.4.4.

Attachment of charged nanoparticles to *Pichia pastoris* as a function of pH has been reported (Ditsch, 2004) and hypothesized to be mediated by a protein on the surface of the cell. The two types of nanoparticle described in Section 4.1 are used to test attachment to *E. coli*. Oleic acid–coated nanoparticles with an exterior coating of Hitenol BC (8 PEO units) are stabilized by electrostatic and steric effects. Oleic acid-coated nanoparticles with an exterior coating of Noigen RN (60 PEO units) are stabilized by steric effects only. Results in Figure 4-24 show the fraction of bound cells that are retained in a HGMS column as a function of pH; magnetic nanoparticles attach to these cells and cause them to be retained in the metal mesh of the HGMS column. Higher cell

concentrations result in an increased percentage of bound cells. The percentage of cells attached shows a minimum at a pH around 6 to 7 and increases at lower and higher pH.

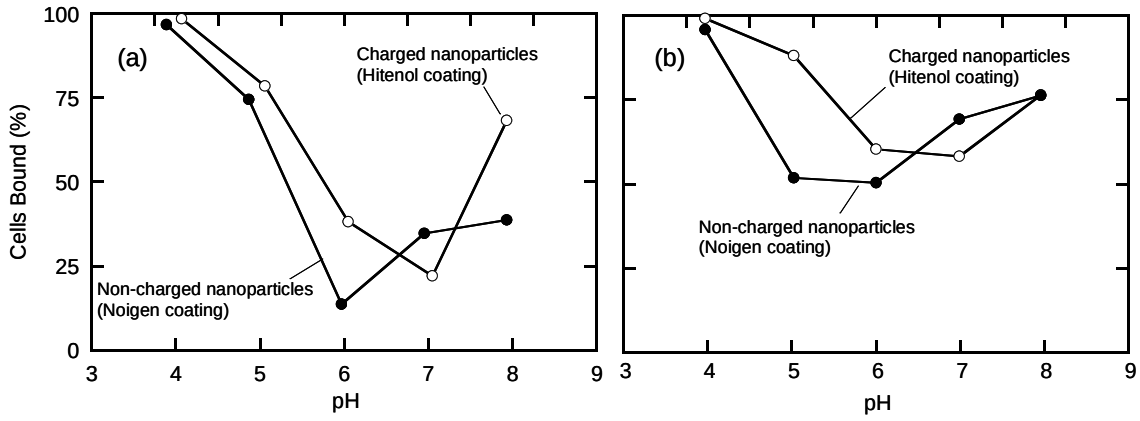

Figure 4-24 Nanoparticle-to-cell binding at $\phi = 0.005$ as a function of pH for (a) 1.05 g/L *E. coli,* (b) 5.18 g/L *E.coli.*

The binding patterns are similar for both charged and non-charged particles. At least in the case of Noigen RN–oleic acid–coated nanoparticles, electrostatic interactions are not responsible for the attachment. It can be speculated that the attachment process is mediated by hydrophobic interactions. There could be regions on the nanoparticle surface not covered by PEO, where the first coating of oleic acid would expose the hydrophobic chains.

According to the literature, adhesion of proteins (free proteins or proteins on the surface of a cell) to flat surfaces can be prevented by PEO chains of a minimum length between 35 and 100 EO units (Nagaoka *et al.*, 1983), although shorter PEO chains can also efficiently reject proteins provided that the chain density is high (Prime *et al.*, 1993). In the present study, nanoparticles coated with molecules that contain 8 PEO-unit chains and 60 PEO-unit chains both showed strong binding to cells; this observation suggests that the packing of the PEO chains on the surface of nanoparticles is imperfect or otherwise that the observations by Nagaoka *et al*. and Prime *et al.* do not apply to highly curved surfaces like nanoparticles.

5 MODELING

The experimental data presented in Section 4.2 suggest the existence of two separate mechanisms of mass transfer enhancement in the presence of nanoparticles. According to the data, enhancement can take place by an increase in gas-liquid interfacial area or by an increase in the mass transfer coefficient.

This section is organized in three parts. First, a mechanism by which nanoparticles enhance interfacial area is presented. This mechanism hypothesizes that nanoparticles accumulated at the gas-liquid interface stabilize gas bubbles against coalescence, therefore maintaining smaller bubble sizes and greater interfacial areas. Second, a mechanism by which nanoparticles enhance the mass transfer coefficient is proposed. This mechanism hypothesizes that random motion of the nanoparticles generates microconvection in the surrounding fluid. Third, predictions of the two models are compared to the experimental data.

5.1 Mechanism of Gas-Liquid Interfacial Area Enhancement

This section first reviews recent literature that shows that colloidal particles can act as surfactants by adsorbing at the gas-liquid interface and preventing gas bubble coalescence. The finding that colloidal particles can adsorb to an interface is in agreement with the results presented in Section 4.3. Second, it is shown that the energy necessary to remove a nanoparticle from the air-water interface is sufficiently large to assume that the adsorption is irreversible. Third, a scaling analysis is used to justify that nanoparticles can adsorb to a bubble interface on a shorter time scale than the typical time scale for collisions between bubbles, and therefore collisions take place between bubbles that are already protected with a layer of colloid. Fourth, an expression to predict the interfacial area enhancement as a function of the agitation conditions is proposed. Finally, the experimental mass transfer enhancement as a function of temperature is discussed qualitatively.

5.1.1 Literature Review: Colloidal Particles at Interfaces

5.1.1.1 Particle-Stabilized Emulsions and Foams

A number of studies have demonstrated the ability of fine solid particles to stabilize emulsions and foams. As early as 1903, a publication reported the formation of a layer of

fine solid particles around air bubbles in water (Ramsden, 1903). Subsequent research established that particles could act as emulsifiers (Pickering, 1907) and identified the importance of the contact angle, θ, that the particle makes with an oil-water interface in determining the type of emulsion, *i.e.* oil/water or water/oil (Finkle *et al.*, 1923). After these initial studies, no work was published in this field until recently, when interest in the study of particles as stabilizers was revived in the areas of food science (Gibbs *et al.*, 1999; Rousseau, 2000) and biomedicine (Schutt *et al.*, 2003). Lately, work by Binks and collaborators, has established the role of particles in emulsion stabilization processes (Binks *et al.*, 2001; Binks, 2002; Arditty *et al.*, 2003; Aveyard *et al.*, 2003; Du *et al.*, 2003; Binks *et al.*, 2005a; Binks *et al.*, 2005b). Fine solid particles have also been shown to stabilize aqueous foams (Pugh, 1996); hydrophilic particles enhance foam stability by accumulating at the plateau borders of the foam films and delaying the process of film drainage. A review of the foam stabilizing properties of proteins and nanoparticles has been presented (Murray *et al.*, 2004).

This set of observations is consistent with experimental measurements of this thesis and with previous work (Olle *et al.*, 2005). In this thesis, it was observed that nanoparticles coated with oleic acid and Hitenol BC increased slightly the foam height in a sparged beaker; such foaming could be eliminated by the addition of small amounts of antifoaming agents. In Olle *et al*.'s patent, Yin conducted fermentations in the presence of nanoparticles coated with perfluorocarbons (Zonyl® FSA, Dupont), and observed greatly enhanced foaming in a sparged, agitated system. The severe foaming was very difficult to reduce, even with continuous addition of antifoaming agents.

5.1.1.2 Particles Compared to Surfactants

The research mentioned previously suggests that particles can act as surfactant molecules by accumulating at interfaces between fluids. However, significant differences exist between the two. First, while surfactant molecules can assemble to form micelles in the bulk of a solution, particles – if properly stabilized in water – do not form assemblies. Second, while the key parameter in determining at what phase is a surfactant preferentially located is the hydrophile-lipophile balance number, the corresponding parameter for spherical particles is the contact angle between the particle and the interface (Binks, 2002). This angle is smaller than 90^{o} for hydrophilic particles, *e.g.*,

metal oxides (Binks, 2002) (the particle would lie preferentially on the water side of an air-water interface) and bigger than 90° for hydrophobic particles (the particle would lie preferentially on the air side). Third, as will be discussed in detail in the following section, the energy of adsorption of nanoparticles to an interface is on the order of 1000 kT, while for surfactants it is typically on the order of 1 to 10 kT (where 1 kT is the thermal energy). As a result, once they have been adsorbed to an interface, nanoparticles do not detach (Binks, 2002). In contrast, surfactant adsorption is a reversible process.

5.1.1.3 Strong Interfacial Adsorption of Particles

When a spherical particle of radius R, initially immersed in the water phase, adsorbs at the air-water interface, the following areas are created or destroyed: a fraction of the interface between the particle and the water is lost ($S_{p\text{-}w}$), and replaced by a new interface between the particle and air ($S_{p\text{-}a}$); furthermore, an area at the air-water interface ($S_{a\text{-}w}$), which is a function of θ, as illustrated in Figure 5-1, is eliminated by the presence of the particle. The energy of adsorption of the particle to the interface is a function of the interfacial tension γ_{aw}, R, and θ, and can be expressed as (Binks, 2002; Dong *et al.*, 2003; Wang *et al.*, 2005)

$$E = \pi R^2 \gamma_{aw} (1 + \cos\theta)^2 \tag{48}$$

With γ_{aw} = 72 mN/m, R = 10 nm, and assuming θ = 90°, an upper bound of E = 5500 kT is found. For angles greater or smaller than 90°, the value of E decreases. The energy necessary to remove a nanoparticle once it has attached to an air-water interface is therefore sufficiently large to assume that the adsorption is irreversible.

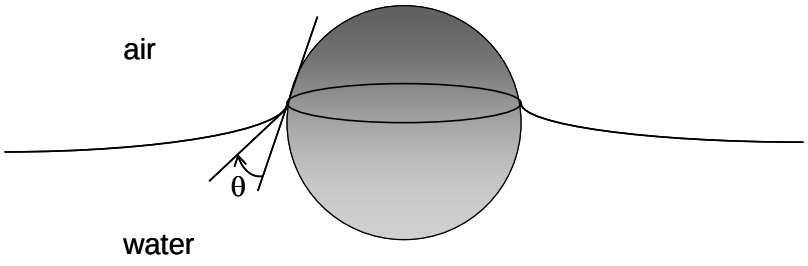

Figure 5-1 Illustration of the 3-phase contact angle θ between a spherical nanoparticle and an air-water interface

Irreversible adsorption of particles to an air-water interface has been demonstrated by a Langmuir apparatus (Aveyard *et al.*, 2000). Partially hydrophobic silica nanoparticles with a diameter of 20 nm were shown to stabilize air bubbles (Dickinson *et al.*, 2004); a sharp increase in stability occurred when 2 M NaCl was added to the aqueous phase. The authors rationalized that the increased stability was a result of the screening of electrostatic repulsions between the particles attached at the interface, which would in turn allow a closer packing of particles and a change in the contact angle θ. The lack of a reliable method to measure θ for particles in the nanometer range is a limitation that pervades the research reviewed in this section.

5.1.1.4 Coalescence Prevention

Coalescence is a two-step process. First, two air bubbles have to approach and collide. Second, the intervening aqueous film has to drain to a critical thickness, which is typically on the order of 50 nm (Tobin *et al.*, 1999), to the point of rupture, which allows the two drops to merge. If a layer of nanoparticles surrounds the bubble, particles must be forced out of the interface for coalescence to occur. According to the previous estimation of the energy of adsorption, there is a large energy barrier that prevents this from happening.

Prevention of coalescence by addition of surfactants has been widely studied. Similarly, block copolymers have been shown to reduce coalescence in polymer blends, Nanoparticles have been shown to reduce coalescence in air-water systems, oil-water systems, and polymer blends. In all three cases, the mechanisms by which coalescence is suppressed are not well understood.

It has been proposed that copolymers reduce coalescence by reducing interfacial tension (Vilgis *et al.*, 1990), by inducing repulsive interactions between droplets (Milner *et al.*, 1996; Lyu *et al.*, 2002), and by creating concentration gradients along the interfaces that result in Marangoni stresses, which in turn stabilize droplets (Van Puyvelde *et al.*, 2002). Coalescence suppression is more effective with larger amounts of compatibilizer and at larger molecular weights of the block copolymer (Van Hemelrijck *et al.*, 2005). Recently, a review on coalescence reduction by copolymers has been presented (Van Puyvelde *et al.*, 2001). Addition of diblock copolymers to a polymer blend results in

smaller particle sizes and a narrower particle size distribution (Sundararaj *et al.*, 1995). Sundararaj *et al*. showed that there exists a critical shear rate in polymer systems where a minimum drop size is achieved. They reasoned that at higher shear rates the droplets have higher approach velocities and their coalescence probability increases. Nanoparticles have also been shown to suppress coalescence. Silica particles reduce coalescence of polymer blends (Vermant *et al.*, 2004), oil-water emulsions (Arditty *et al.*, 2003), and air bubbles in water (Du *et al.*, 2003)

5.1.2 Proposed Mechanism of Interfacial Area Enhancement by Nanoparticles

5.1.2.1 Outline

Nanoparticles can increase interfacial area by (i) inhibiting coalescence and (ii) facilitating bubble break-up by reducing surface tension. As previously shown in Section 4.2.2.2, facilitated bubble breakage due to a lower interfacial tension can account for an area enhancement factor of only 1.5, and therefore cannot be the sole mechanism responsible for interfacial area enhancement. This section shows that nanoparticles stabilize gas bubbles by adsorbing on their interface on a time scale smaller than the typical collision time between two bubbles. This yields a stabilized dispersion in which bubble size is determined by breakage processes, whereas in the absence of nanoparticles bubble size is dominated by coalescence processes and an unstable dispersion exists.

5.1.2.2 Scaling analysis

According to Kolmogorov's theory, the mean size of bubbles in an isotropic turbulent flow is determined by the size of the smallest eddies. An expression to calculate the size of bubbles in stirred tank reactors based on a balance of disruptive forces (which are a function of turbulence intensity) and stabilizing forces (which are a function of surface tension) due to Metkin *et al.* was used in Section 4.2.2 to predict $k_L a$ as a function of power input. As shown in Figure 4-11, a model that incorporates Eqs. 24 to 26 predicts accurately the experimental data *in the absence* of nanoparticles.

The average bubble size predicted from the simultaneous solution of Eqs. 24 and 26 is shown in Figure 5-2. It can be observed that the bubble diameter initially decreases rapidly with increasing power input and subsequently the decrease is slower. The

asymptote at increasing power inputs shows that the smallest average bubble diameter that can be obtained with the experimental equipment used is approximately 300 μm.

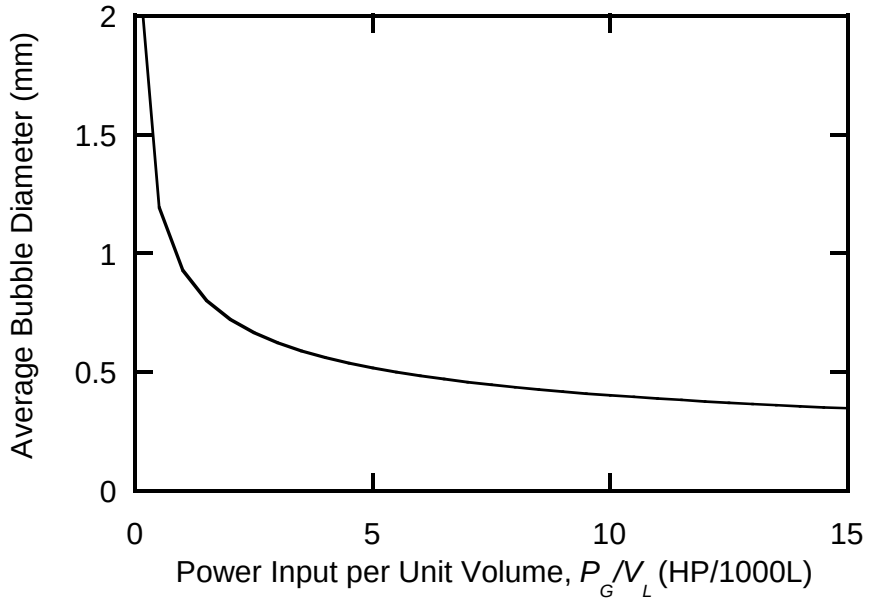

Figure 5-2 Average bubble diameter calculated with Eqs. 24 and 26.

The theoretical expressions for the average bubble diameter based on Kolmogorov's isotropic turbulence theory (Metkin *et al.*, 1985; Kawase *et al.*, 1987; Kawase *et al.*, 1988) predict a dependence with surface tension with an exponent of 3/5. With typical values of surface tension of 72 mN/m for an air-water interface and 39 mN/m for an air-water interface in the presence nanoparticles (Figure 4-16), interfacial area is predicted to increase by approximately 50% in the presence of nanoparticles.

$$\frac{d_{\text{B,control}}}{d_{\text{B,nanoparticles}}} \propto \frac{a_{\text{B,nanoparticles}}}{a_{\text{B,control}}} \propto \left(\frac{\sigma_{\text{air-water}}}{\sigma_{\text{air-water+nanoparticles}}} \right)^{3/5} \sim 1.46 \qquad (49)$$

Considering that experimental measures of area enhancement in the presence of nanoparticles were on the order of 4-fold (Figure 4-13), the prediction of Eq. 49 is quite inaccurate. This is not surprising since the ratio in Eq. 49 only considers bubble breakage processes, which are affected by surface tension, but does not incorporate coalescence processes.

To establish whether the processes of bubble breakage and coalescence occur in the hydrodynamic flow studied, several characteristic times can be estimated (Tcholakova *et al.*, 2003)

The *average residence time,* t_R, is the time that an air bubble spends in the agitated tank. Experiments are performed at a working volume of 5.5 L at typical gas flow rates of 1 vvm (5.5 L/min). Therefore, it can be estimated that $t_R \sim 1$ min.

The *deformation time* characterizes the process of bubble breakage and deformation and is given by the expression (Levich, 1962)

$$t_D = \frac{\eta_D}{5\rho_C^{1/3}\varepsilon_m^{2/3}d_B^{2/3}} \tag{50}$$

with typical values of η_D (viscosity of the bubble, air) = 1.7×10^{-5} N·s/m^3, ρ_c (density of the continuous phase, water) = 1000 kg/m^3, ε_M (power input per unit mass) = 2 m^2/s^3, and d_B (bubble diameter) = 1 mm, a value of $t_D \sim 0.2$ μs is obtained. Since t_D is much smaller than t_R, bubbles have enough time to deform and break while they rise in the fermentor. Furthermore, the lifetime of the eddies of size ~ d_B, given by

$$t_C = \frac{\rho_C^{1/3}}{\varepsilon_m^{1/3}}d_B^{2/3} \tag{51}$$

takes on values of 2 to 10 ms in the range of ε_M studied, which is four to five orders of magnitude larger than t_D; this is a sufficiently long time for the air bubbles to deform and break. The lifetime of turbulent eddies is also a measure of the characteristic duration of one collision between bubbles.

The process of bubble coalescence is characterized by the ratio of the mean *collision time*, t_C, to the *drainage time*, t_{DR}, which characterizes the drainage of the liquid film between two bubbles. The drainage time (for which there is no theoretical expression at present) is, in turn, affected by the presence of surface active agents in the medium. The characteristic time for adsorption of the nanoparticles to the bubble interface in turbulent regime can be estimated using an expression for surfactant adsorption (Levich, 1962)

$$t_A = \frac{10\Gamma \eta_c^{1/2}}{C_s \varepsilon_m^{1/2} d_B} \tag{52}$$

where C_S is the particle concentration in % weight (~0.25 to 1) and Γ is the surface concentration corresponding to a monolayer coverage, which is estimated at Γ = 2.7 mg/m^2 assuming that a surface monolayer of particles forms and that this monolayer has a packing density of 0.9 ($(1/6)\pi\sqrt{3} \approx 0.906$). A range of values for t_A from 1.85 to 18.5 μs is obtained. Since $t_A << t_C$, (the process of nanoparticle adsorption to the bubble interface is much faster than the process of bubble collision), collisions take place between bubbles that have had sufficient time to get coated with nanoparticles.

5.1.2.3 Effect of agitation on interfacial area enhancement

Experimental data for gas-liquid dispersions is usually characterized using the Sauter mean diameter (d_{32}) of bubbles; d_{32} is the quotient of the third and second momentum of the probability density function of the bubble sizes

$$d_{32} = \frac{\int_{d_{min}}^{d_{max}} d_B^3 p(d_B) \mathrm{d}d_B}{\int_{d_{min}}^{d_{max}} d_B^2 p(d_B) \mathrm{d}d_B} = \frac{\sum_{i=1}^{k} n_i d_{B_i}^3}{\sum_{i=1}^{k} n_i d_{B_i}^2} \tag{53}$$

where n_i is the number of bubbles of size i.

According to Eq. 53, d_{32} is related to the maximum and minimum stable bubble sizes in the dispersion, d_{max} and d_{min}. The maximum stable drop size can be estimated from the balance of the turbulent and surface tension forces acting on a bubble. It has been postulated (Hinze, 1955) that a drop breaks when the ratio of the inertial and surface tension forces acting on it, given by the Weber number,

$$We = \frac{\rho_C N^2 D_i^3}{\sigma} \tag{54}$$

reaches a critical value. The maximum stable drop size, d_{max} , above which a drop breaks, is a function of the agitation speed, N (Hinze, 1955; Calderbank, 1958; Shinnar, 1961)

$$\frac{d_{max}}{D_i} = C_1 We^{-3/5} = C_1' N^{-1.2} \tag{55}$$

where the constants C_1 and C_1' are characteristic of the geometry of the impeller type and size.

The minimum bubble size that can remain stable against coalescence can be estimated from the condition that the turbulent energy on a pair of bubbles is insufficient to prevent their adhesion (Shinnar *et al.*, 1960)

$$\frac{d_{min}}{D_i} = C_2 We^{-3/8} = C_2' N^{-0.75} \tag{56}$$

where C_2 and C_2' are constants.

According to Eqs. 55 and 56, both d_{max} and d_{min} decrease with the agitation speed, but d_{max} decreases faster. In a dispersion maintained by agitation, a dynamic equilibrium will be established between breakage and coalescence, such that any bubble larger than d_{max} will break up, and any bubble smaller than d_{min} will coalesce (Liu *et al.*, 1999).

Given that d_{32} can be measured experimentally (by optical microscopy or laser diffraction) while neither d_{max} or d_{min} can be measured accurately, some authors have attempted to establish whether models with the functional form of Eqs. 55 and 56 also describe the change of d_{32} as a function of agitation. It has been shown experimentally (Shinnar, 1961; Sprow, 1967) that for systems where the bubble size is dominated by the breakage process, data for d_{32} are well represented by Eq. 55 ($d_{32} \sim d_{max}$), while for systems where the bubble size is dominated by coalescence processes, data for d_{32} are well represented by Eq. 56 ($d_{32} \sim d_{min}$). An example of the former would be a dilute dispersion of air in water, while an example of the latter would be a concentrated dispersion.

The values of the d_{32} corresponding to the experiments shown in Figure 4-13 can be calculated from the experimental values of interfacial area by using Eq. 25 and from calculated values of gas phase holdup obtained using Eq. 26. Figure 5-3 presents a log-log plot of the average bubble size as a function of agitation speed. The values of the slopes for the control and for an experiment at $\phi = 0.0025$ are -0.78 and -0.39. These are in reasonable agreement with the exponent values of -0.75 and -1.20 in Eqs. 55 and 56. The exponent of -0.78 indicates that, in the absence of nanoparticles, an unstable dispersion dominated by coalescence is obtained. In contrast, the exponent of -1.39 in the presence of nanoparticles indicates that a fully stabilized dispersion dominated by breakage is obtained. Therefore, in the presence of nanoparticles bubbles are stable against coalescence.

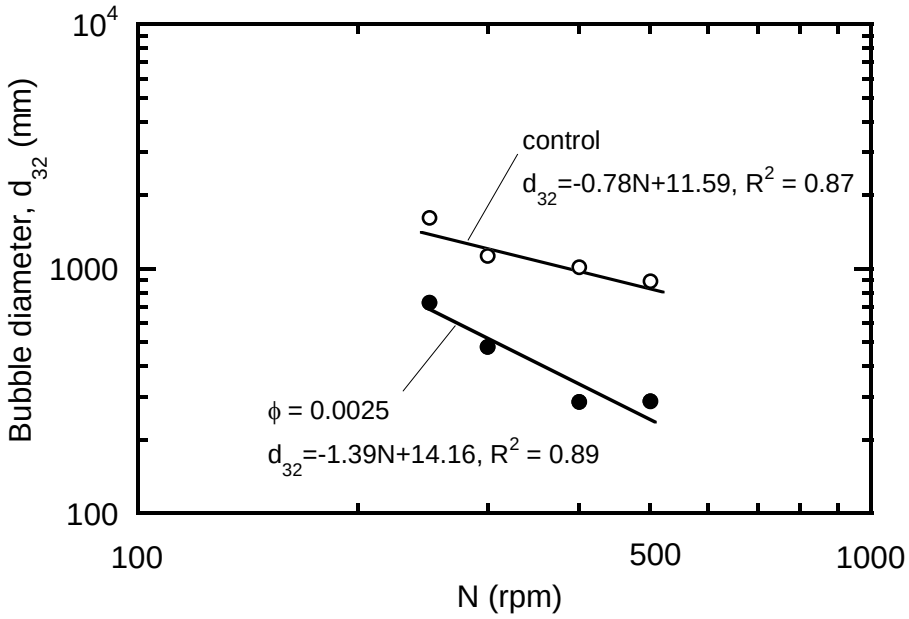

Figure 5-3 Average bubble diameter as a function of agitation speed. Operating conditions are T=37°C, pH = 8.0, Vs= 14.5 cm/min

Similar results have been published in the literature for stabilization of liquid-liquid dispersions in suspension polymerization (Jahanzad *et al.*, 2005). Jahanzhad *et al.* found that the exponent for the droplet size as a function of agitation speed changed from -0.74 to -1.24 upon addition of poly(vinyl alcohol), which acts as a stabilizing agent.

In view of the results shown in Figure 5-3 and the preceding analysis, it is proposed that the following equations can be used to predict the interfacial area for experiments in the absence and presence of nanoparticles

$$a_{\text{control}} = \frac{6\varepsilon_{\text{H,control}}}{d_{\text{B}}} = \frac{6\varepsilon_{\text{H,control}}}{e^{11.59}N^{-0.78}} \tag{57a}$$

$$a_{nanoparticles} = \frac{6\varepsilon_{\text{H,np}}}{d_{\text{B}}} = \frac{6\varepsilon_{\text{H,np}}}{e^{14.16}N^{-1.39}} \tag{57b}$$

Therefore, the interfacial area enhancement can be calculated as

$$E_{\text{area}} = \frac{a_{\text{nanoparticles}}}{a_{\text{control}}} = \frac{\varepsilon_{\text{H,np}}e^{11.59}N^{-0.78}}{\varepsilon_{\text{H,control}}e^{14.16}N^{-1.39}} = 0.077N^{0.61}\frac{\varepsilon_{\text{H,np}}}{\varepsilon_{\text{H,control}}} \tag{58}$$

It must be noted that the values of the pre-exponential parameters C_1' and C_2' ($e^{11.59}$ and $e^{14.16}$) are dependent on the geometry of the equipment and should not be used to predict interfacial area in different equipment, whereas the values of the exponents (-0.78 and -1.39) should be applicable to other experimental systems as long as conditions of isotropic turbulence exist.

It is also proposed that Eq. 57b can apply to nanoparticle fractions above $\phi = 0.0025$. While no experiments measuring interfacial area enhancement as a function of agitation speed above this mass fraction have been conducted, data in Figure 4-12 suggest that increasing the nanoparticle fraction from $\phi = 0.0025$ to $\phi = 0.005$ does not yield a significant interfacial area increase. Underlying this claim is the assumption that, at a nanoparticle fraction of $\phi = 0.0025$, the gas bubble interfaces are already saturated with nanoparticles and further addition of nanoparticles does not alter the nature of interface.

5.1.2.4 Effect of temperature on interfacial area enhancement

It has been shown in Section 4.2.2.3 that mass transfer enhancement by nanoparticles depends strongly on temperature. According to the mechanism of interfacial area enhancement presented in the previous section, an increase in temperature causes the average bubble diameter to increase because viscosity is reduced and the film drainage

process between bubbles becomes faster, which in turn increases the coalescence efficiency. This phenomenon has been demonstrated experimentally elsewhere (Lazrak *et al.*, 1998). While the acceleration of the film drainage process should be the same in the control and in the presence of nanoparticles, in the latter case the final coalescence event between bubbles is still prevented by the layer of nanoparticles adhered to the bubble interface. Consequently, a more pronounced temperature effect on the average bubble diameter can be expected in the control experiments. This can explain qualitatively the increase in mass transfer enhancement as a function of temperature in the presence of nanoparticles presented in Figure 4-15.

5.2 Mechanism of Mass Transfer Coefficient Enhancement

This section first reviews effective property models of enhanced mass transfer in the presence of dispersions and it is demonstrated that its application is unsuitable to nanoparticle dispersions. Second, several potential mechanisms of enhancing the mass transfer coefficient are discussed based on scaling analysis. Third, it is proposed that microconvection caused by nanoparticle random motion causes the enhancement of the mass transfer coefficient. An empirical expression that relates enhancement to the nanoparticle mass fraction is proposed. Fourth, the effect of nanoparticles on gas-liquid interfacial mobility is discussed. Finally, an expression to predict the mass transfer coefficient enhancement as a function of nanoparticle volume fraction and agitation conditions is proposed.

5.2.1 Limitations of Effective Property Models

Effective property models (Section 2.2.4) have been successfully used to predict enhancement of mass transfer in multiphase reactions in the presence of a dispersed microphase (Mehra, 1988). These models are appropriate when the typical dimension of a dispersed phase element is much smaller than the dimension of the domain through which mass transfer occurs (the liquid film around a gas bubble). A 20 nm particle is typically 100 to 1000 times smaller than the thickness of the liquid boundary layer around a gas bubble. A dispersion of nanoparticles is therefore macroscopically homogeneous in spite of its biphasic nature, and the diffusivity and solubility of oxygen

in the medium can be expressed as effective properties of the two components of the dispersion. However, the effective property models presented in Section 2.2.4 fail to predict accurately the experimental values of k_L enhancement obtained in an agitated beaker (Section 4.2.1), as shown in Figure 5-4.

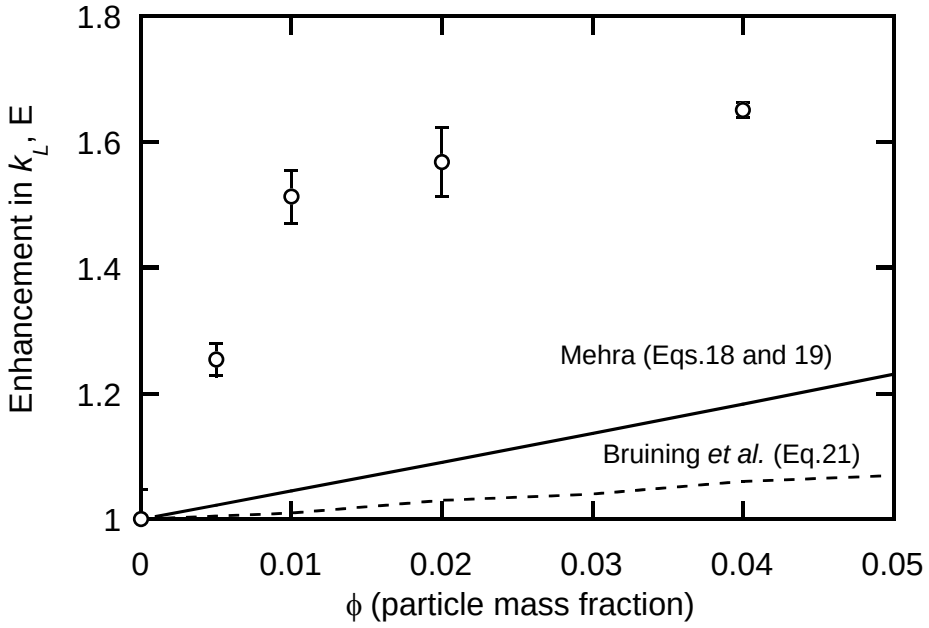

Figure 5-4 Comparison of k_L enhancement data obtained in a stirred beaker at 300 rpm with predictions from models by Mehra (Eqs. 18 and 19, with S = 2 sec^{-1}, m = 4) and Bruining *et al.* (Eq. 21).

As discussed in Section 2.4.1, a number of studies have shown that the *heat* transfer enhancement in nanoparticle dispersions is likewise largely underpredicted by effective property models, such as the Maxwell-Garnett theory. Some authors have hypothesized that Brownian motion by the nanoparticles is responsible for the large experimental enhancements reported (Bhattacharya *et al.*, 2004; Jang *et al.*, 2004; Koo *et al.*, 2004; Kumar *et al.*, 2004; Prasher *et al.*, 2005) but there is no agreement in the literature. Furthermore, mounting experimental evidence indicates that heat transfer enhancement does not only depend on the size and volume fraction of particles, but also on surface properties of the particles (which are a function of pH, ionic strength of the medium, and nanoparticle composition) (Xie *et al.*, 2002a; Patel *et al.*, 2003; Lee *et al.*, 2006) and

temperature (Das *et al.*, 2003c). In view of this, it is likely that interparticle forces (electrostatic repulsions and Van der Waals attractions) play a significant role.

5.2.2 Potential Mechanisms of Mass Transfer Coefficient Enhancement

5.2.2.1 Nanoparticle dispersion

Some authors have proposed that convective heat transfer enhancement is caused by nanoparticle dispersion and have fitted an empirical dispersion coefficient to experimental data (Pak *et al.*, 1998; Xuan *et al.*, 2000b; Xuan *et al.*, 2003). However, it has been shown through order-of-magnitude estimates of the various terms of the energy equation that heat transfer associated with nanoparticle dispersion is negligible compared to heat conduction and convection (Buongiorno, 2006)

5.2.2.2 Nanoparticle Brownian motion

Random motion of nanoparticles acting as oxygen carriers can contribute to an increase in mass transfer in excess of the bulk diffusive flow of oxygen. The characteristic time that describes oxygen diffusion across the length of one nanoparticle is

$$t_{\mathrm{D}} = \frac{d_{\mathrm{p}}^2}{2D_{\mathrm{O}_2}} \tag{59}$$

With d_{P} = 20 nm (particle diameter) and D_{O2} =3.22·10^{-9} m^2/s at 37 $^{\mathrm{o}}$C, t_{D} = 6·10^{-8} s. The effect of Brownian motion on the effective diffusivity can be estimated by comparing this time to the time required for a particle to travel its diameter by mean displacements, which can be obtained from the Stokes-Einstein equation

$$t_{\mathrm{B}} = \frac{3\pi\mu d_{\mathrm{p}}^3}{2k_{\mathrm{B}}T} \tag{60}$$

with μ = 6.95·10^{-4} kg/(m·s), T=37 $^{\mathrm{o}}$C, and k = 1.381 x 10^{-23} J/K (Boltzmann's constant), t_{D} = 6.1·10^{-6} s. Since $t_{\mathrm{B}} >> t_{\mathrm{D}}$, the contribution of the Brownian motion of the particle to mass transfer is negligible compared to the bulk diffusive flow of oxygen.

5.2.2.3 Thermophoresis

Nanoparticles can diffuse due to a temperature gradient, with a thermophoretic velocity given by

$$V_T = -\beta \frac{\mu}{\rho} \cdot \frac{\nabla T}{T} \tag{61}$$

where β is a proportionality factor of order $1 \cdot 10^{-3}$. In the mass transfer experiments conducted in a stirred beaker, the liquid and gas phases are in thermal equilibrium and therefore $V_T \sim 0$. In the experiments conducted in a fermentor, the gas phase is at most 10 ^oC cooler than the liquid phase, and therefore $V_T \sim 1 \cdot 10^{-11}$ m/s. Therefore, in both systems thermophoresis does not contribute to enhanced mass transfer.

5.2.2.4 Microconvection caused by nanoparticles

On the nanoparticle diameter length scale, an enhancement of oxygen mass transfer can be expected if the time it takes for the particle, and therefore, *the fluid surrounding this particle*, to travel its own diameter is smaller than t_D. This time scale can be estimated as

$$t_C \sim \frac{d_p}{v_{thermal}} \tag{62}$$

The velocity scale $v_{thermal}$ can be obtained by application of kinetic theory to liquids. A nanoparticle of radius d_p immersed in a medium, receiving continuous collisions from surrounding water molecules, experiences a mean square displacement after a time t that can be expressed as (Einstein, 1906)

$$\left\langle x^2 \right\rangle = \frac{k_B T}{3\pi\mu a} \cdot t \tag{63}$$

Since a particle has a kinetic energy equal to $3k_BT/2$ (corresponding to the three degrees of freedom, $k_BT/2$ each), the instantaneous velocity of a particle of mass M is

$$v_{thermal} = \sqrt{\frac{3k_BT}{M}} \tag{64}$$

For a 20 nm oleic acid-coated nanoparticle at 300 K, $v_{\text{thermal}} \sim 1$ m/s. This value is similar to proposed values of thermal velocity for aqueous suspensions of polysterene spheres (Pusey, 1991; Nagele, 1996). In comparison, a typical thermal velocity for a water molecule would be 1000 m/sec. With $v_{\text{thermal}} = 1$ m/s, a value of $t_C = 2 \cdot 10^{-8}$ s is obtained. The ratio t_D / t_C is a Peclet number based on the particle size

$$Pe_p = \frac{v_{\text{thermal}} \cdot d_p}{D_{O_2}} \tag{65}$$

which expresses the relative importance of convection in the fluid surrounding a nanoparticle to bulk diffusion. This number has an approximate value of 3 for a 20 nm particle at $T = 37\ ^{o}$C. Therefore, scaling considerations indicate that the convective flow of oxygen in the immediacy of the nanoparticle caused by the relative motion between the particle and the surrounding fluid has the same order of magnitude as the diffusive flow of oxygen.

5.2.3 Proposed Mechanism of Mass Transfer Coefficient Enhancement

5.2.3.1 Microconvection Concept

Keller (Keller, 1971), while studying blood flow, was the first to suggest that suspended particles (blood cells) could be the source of small eddies that could enhance conduction of heat and diffusion of molecular species, but presented no rigorous calculation. A precise derivation of this effect was presented later for a dilute suspension of neutrally buoyant spherical particles under simple shear flow at small particle Peclet numbers (Leal, 1973). Both Keller's experiments and Leal's derivation focused on large particles where Brownian effects are negligible.

Several investigations have proposed the application of a similar mechanism to the prediction of enhanced heat transfer by nanofluids (Jang *et al.*, 2004; Koo *et al.*, 2004; Prasher *et al.*, 2005). Brownian effects are no longer negligible in nanofluids.

The Reynolds number based on the velocity scale given in Eq. 64 can be expressed as

$$\text{Re} = \frac{\rho d_p v_{\text{thermal}}}{\mu} \tag{66}$$

and it has an approximate value of 0.03. This is sufficiently small for the velocity field to be well represented by Stokes flow around a sphere (Taylor, 1932). The radial and angular velocity components for Stokes flow past a stationary sphere in an unbounded medium can be expressed, with r as the distance from the sphere's center, as:

$$v_r = U\cos\theta\left[-\frac{d_p^3}{2r^3}+\frac{3d_p}{2r}+1\right]$$
$$v_\theta = U\sin\theta\left[-\frac{d_p^3}{4r^3}-\frac{3d_p}{4r}-1\right] \qquad (67)$$

The radial component of the velocity has approximately 70% of its maximum value at a distance of 1 sphere radius, d_p, from the particle surface, and around 15% at 10 radii away. Therefore, the hydrodynamic boundary layer extends further than 10 diameters from the particle.

5.2.3.2 Empirical Fit

Given the multiplicity of scales of the phenomena involved, a theoretical formulation is not attempted. Instead, experimental data are fitted with an empirical expression. According to Figure 4-5, the enhancement in the mass transfer coefficient increases linearly with the mass fraction of nanoparticles up to $\phi \sim 0.01$. Above $\phi \sim 0.01$, the mass transfer enhancement plateaus quite rapidly. The following empirical expression is proposed to describe the enhancement of the mass transfer coefficient below $\phi \sim 0.01$

$$k_{L,np} = k_{L,control}\left(1+C\phi\right) \qquad for\ \phi < 0.01 \qquad (68)$$

where C is an adjustable parameter with a value of 51.4 for experiments performed at 300 rpm in an agitated beaker. It is plausible that at low concentrations of nanoparticles ($\phi << 0.01$) the shells of perturbed fluid around a particle do not overlap significantly. The flattening of the enhancement curve at $\phi > 0.01$ could be an indication that significant overlap between the shells of perturbed fluid exists at this concentration of nanoparticles because the interparticle distances are smaller on average (and therefore most fluid around the particles is mobilized). The mean surface-to-surface distance

between nanoparticles is a function of the dispersed phase *volume fraction*[1]. As shown in Figure 5-5, for a nanoparticle volume fraction of 0.026 of 20 nm sized oleic acid-coated nanoparticles (corresponding approximately to a mass fraction of 0.01), the typical surface-to-surface distance is roughly 35 nm, just 1.75 times the particle diameter.

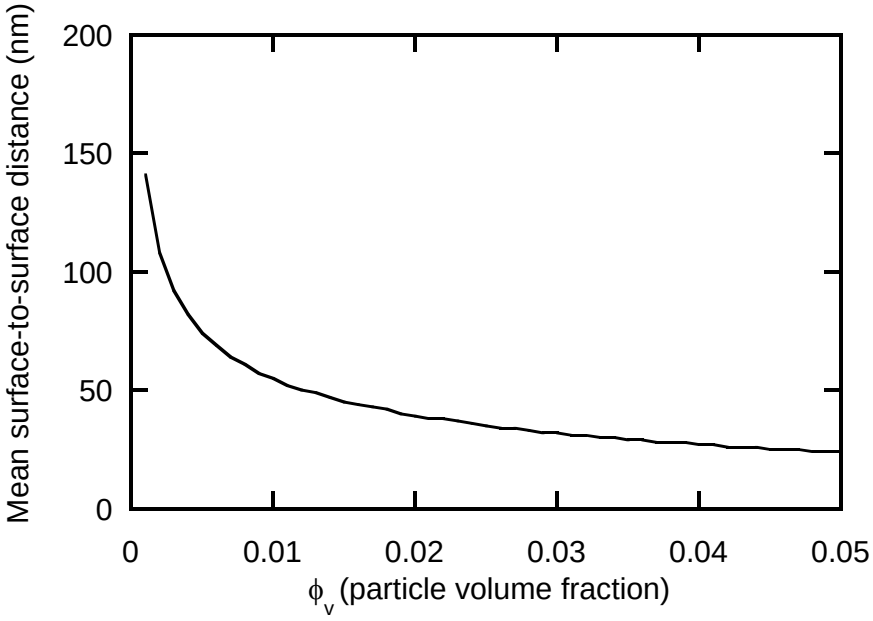

Figure 5-5: Mean surface-to-surface distance between nanoparticles as a function of volume fraction

An investigation published recently has claimed that mass diffusion of a dye is faster in a nanofluid than in water (Krishnamurthy *et al.*, 2006). The authors visualized a dye diffusing in a well, and reported a mass diffusion enhancement above 10-fold at a volume fraction of Al_2O_3 nanoparticles of 0.5%. However, to make their nanoparticle solutions stable, Krishnamurthy *et al.* used Tween 80 surfactant, which must have accumulated at the gas-liquid interface. Since there cannot be a static system in the presence of surface tension gradients, Marangoni flows are likely to have developed. It is therefore likely that this work reported erroneous mass transfer enhancements.

[1] The relationship between volume fraction and mass fraction for oleic-acid coated nanoparticles is $\phi_{volume} = 2.57\phi_{mass,}$ see Appendix 7.1 for detailed calculation.

5.2.4 Retardation of Gas-Liquid Surface Mobility by Nanoparticle Adsorption

The presence of surfactants is known to alter the interfacial mobility of gas bubbles and retard its motion. It is likewise expected that the nanoparticles researched in this thesis immobilize the gas-liquid interface. This would have a detrimental effect on the mass transfer coefficient, which would partly counteract the enhancement reported in the previous section. This detrimental effect can be ignored in the study of the experiments in a stirred beaker that lead to Eq. 68, on grounds that the free liquid surface rotates at a constant speed and is not immobilized.

Immobilization of the gas-liquid interface of bubbles is certain to occur in the experiments conducted in an aerated and agitated fermentor (Section 4.2.2). It is generally accepted that contaminants such as surfactants adsorbed on the interface of a bubble are dragged by the surrounding liquid towards the rear of the bubble, where they build up. This generates a surface tension gradient that opposes the surface flow and increases the drag, which leads to immobilization of the interface and reduction of mass transfer effectiveness (Levich, 1962). The mass transfer coefficient of a bubble is a function of the interface mobility. If a bubble is rigid, its mass transfer coefficient can be expressed as (Frossling, 1938)

$$k_{\mathrm{L,rigid}} = c\sqrt{\frac{v_{\mathrm{rise}}}{d_{\mathrm{B}}}}D^{2/3}\nu^{-1/6} \tag{69}$$

where v_{rise} is the relative velocity between the bubble and the liquid and C is a constant that takes experimental values between 0.42 and 0.95. The mass transfer coefficient for bubbles that have a mobile interface can be expressed as (Bird *et al.*, 1960)

$$k_{\mathrm{L,mobile}} = 1.13\sqrt{\frac{v_{\mathrm{rise}}}{d_{\mathrm{B}}}}D^{1/2} \tag{70}$$

The rise velocity of a bubble with a mobile interface can be calculated as (Clift *et al.*, 1978)

$$v_{\text{rise,mobile}} = \sqrt{\left(\frac{2.14\sigma}{\rho d_{\text{B}}}\right) + 0.505 g d_{\text{B}}} \tag{71}$$

which is an expression valid for bubbles larger than 1.3 mm. In the experimental system used, average bubble diameters calculated from interfacial area measurements for the control experiments are in a range that spans above and below 1.3 mm. Bubbles are larger than 1.3 mm at power inputs below 2.5 HP/1000L. Above this value of power input, bubbles are smaller than 1.3 mm and behave as rigid. The rise velocity of a bubble with a rigid interface can be calculated as (Ng *et al.*, 1999)

$$v_{\text{rise,rigid}} = 5450 \Delta\rho d_{\text{B}}^2 \left(\frac{7}{6}\text{Re}^{0.15} + 0.02\,\text{Re}\right)^{-1} \tag{72}$$

where $\Delta\rho$ is the density difference between the gas phase and the liquid phase.

Average bubble sizes calculated from interfacial area measurements in the presence of nanoparticles are smaller than 1.3 mm in the entire range of power input conditions studied.

Eqs. 68 and 69 apply to bubbles in free rise. Turbulence, however, reduces the mean bubble rise velocity by up to 50% (Alves *et al.*, 2003). It has been assumed that turbulence reduces bubble rise velocity by a factor equal for rigid and mobile bubbles.

Using Eqs. 69 to 72 together with Eqs. 57a, 57b, and 68, the following expression for the mass transfer coefficient enhancement is proposed

$$E_{k_{\text{L}}} = \frac{k_{\text{L,np}}}{k_{\text{L,control}}} = (1 + C\phi) C' \frac{\sqrt{\dfrac{v_{\text{rise,np}}\left(d_{\text{B,np}}\right)}{d_{\text{B,np}}\left(N, \varepsilon_{\text{H,np}}\right)}}}{\sqrt{\dfrac{v_{\text{rise,control}}\left(d_{\text{B,control}}\right)}{d_{\text{B,control}}\left(N, \varepsilon_{\text{H,control}}\right)}}} \qquad \textit{for } \phi < 0.01 \tag{73}$$

where the bubble diameters $d_{\text{B,np}}$ and $d_{\text{B,control}}$ are functions of the gas holdup and agitation conditions, as given by Eqs. 57a and 57b. The bubble rise velocity in the presence of nanoparticles, v_{rise}, is given by Eq. 71 at agitation conditions in which $d_{\text{B,control}}$ is larger

than 1.3 mm and by Eq. 72 otherwise. The value of *C*' can be adjusted from experiments.

5.3 Comparison of Model Predictions with Experimental Data

Model predictions of $E_{k_L a}$ have been obtained multiplying Eqs. 73 and 58 ($= E_{k_L} E_a$) and are shown in Figures 5-6 and 5-7. Figure 5-6 shows model predictions assuming that the bubbles are rigid in both the control and in the presence of nanoparticles. Figure 5-7 shows predictions assuming that the bubbles are mobile in the control and rigid in the presence of nanoparticles. It would be appropriate to assume that the bubbles in the control are mobile below 2.5 HP/1000L and rigid above, but that would generate a discontinuous line. A more complete model could also account for the fact that, at any given power input, a size distribution of bubbles exists, some of which are mobile (larger than 1.3 mm) and some of which are rigid. The additional complexity that this would introduce is not justified given that the present model already has two adjustable parameters.

The predictions of the model capture the initial rapid increase of $E_{k_L a}$ as a function of power input and the subsequent flattening at large values of power input. Separate predictions of E_{k_L} and $E_{k_L a}$ are shown in Figure 5-8 for experiments conducted at $\phi = 0.0025$, which is the only experimental data set for which separate measurements of interfacial area and volumetric mass transfer coefficient were made. Figure 5-9 presents a step-by-step flowchart of the calculations leading to the model predictions (solid lines) in Figures 5-6, 5-7 and 5-8.

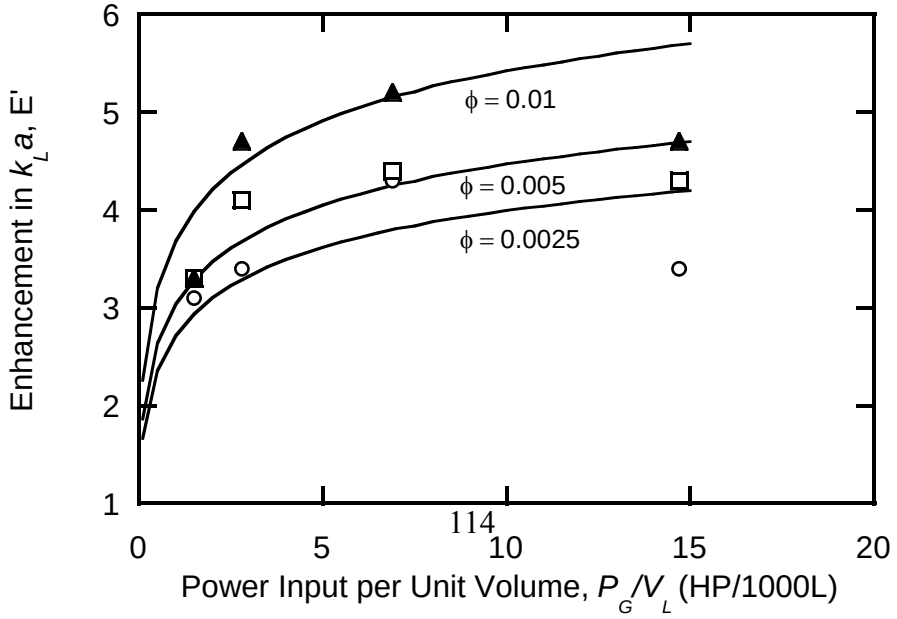

Figure 5-6: Comparison of model predictions (solid lines, calculated as $E_{k_La} = E_{k_L} E_a$ (Eqs. 73, 58), with *C* = 54.1, *C*' = 0.9) with experimental data of k_La enhancement. Bubbles are rigid for both the control and in the presence of nanoparticles

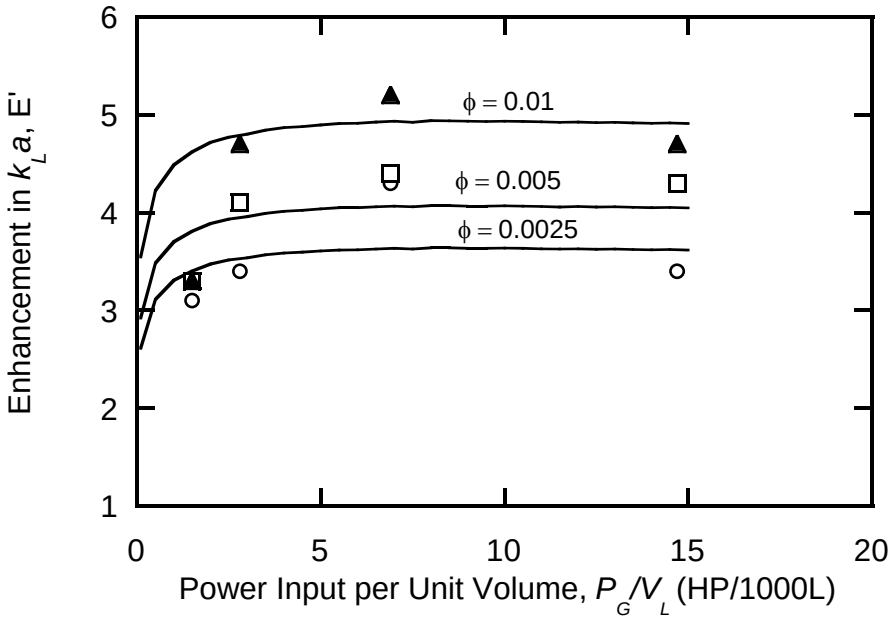

Figure 5-7: Comparison of model predictions (solid lines, calculated as $E_{k_La} = E_{k_L} E_a$ (Eqs. 73, 58), with *C* = 54.1, *C*' = 0.9) with experimental data of k_La enhancement. Bubbles are mobile for the control and rigid in the presence of nanoparticles

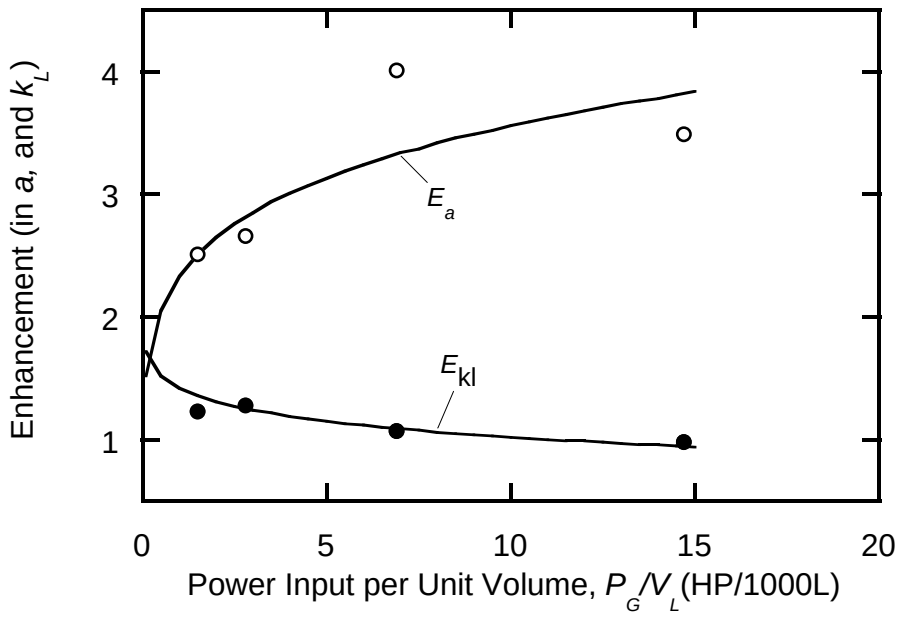

Figure 5-8: Comparison of model predictions (*C* = 54.1, *C'* = 0.9) with experimental data of *a* and k_L enhancement. Values of E_a (open circles) are calculated from experimental measures of *a*. Values of E_{k_L} (closed circles) are calculated as $E_{k_L} = E_{k_L a} / E_a$ from measures of $k_L a$ and *a*. Model predictions (solid lines) are calculated using Eqs. 72 and 57 and assuming mobile bubbles in the control and rigid bubbles in the presence of nanoparticles.

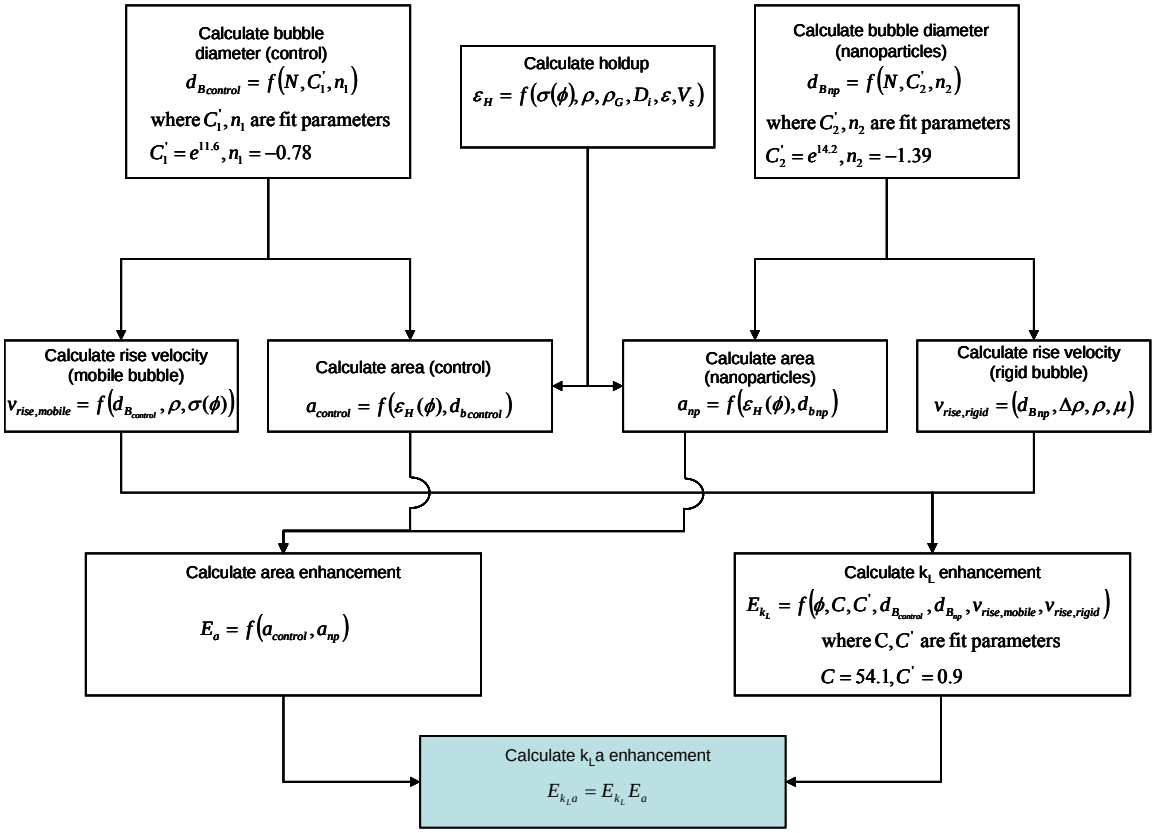

Experimental Parameters

ε = power input
N = agitation speed
V_s = superficial velocity
ϕ = nanoparticle mass fraction
D_i = impeller diameter

Physical Properties

ρ = liquid density
ρ_G = gas density
$\Delta\rho$ = density difference between gas and liquid phases
μ = liquid viscosity
σ = surface tension

Calculated Magnitudes

ε_H = holdup
d_B = bubble diameter
a = specific interfacial area
k_L = mass transfer coefficient
$k_L a$ = volumetric mass transfer coefficient
E_a = area enhancement
$E_{k_L} = k_L$ enhancement
$E_{k_L a} = k_L a$ enhancement

Adjustable parameters

$C, C', C_1', n_1, C_2', n_2$

Figure 5-9: Step-by-step flowchart for the calculation of E_{k_L} , E_a , and $E_{k_L a}$

5.4 Discussion

5.4.1 Critique of the Area Enhancement Model

The mechanism of interfacial area enhancement by prevention of coalescence is consistent with the interfacial area measurements presented in Section 4.3. This mechanism is also consistent with data generated using PFC-coated magnetic nanoparticles (Olle *et al.*, 2005). Yin conducted *E. coli* fermentations in the presence of magnetic nanoparticles coated with Zonyl® FSA fluoropolymers and reported several-fold oxygen uptake rate enhancements (data included in Olle *et al.*'s patent, 2005). The surface tension of these fluoropolymers is 18 mN/m, lower than the surface tension of the nanoparticles used in this thesis (40 mN/m). The lower surface tension of PFC-coated nanoparticles could bestow stronger surface adsorption, a more severe reduction of coalescence, and a greater mass transfer enhancement. Furthermore, Yin observed severe foaming, which would be consistent with a drastic reduction of coalescence.

However, the model has several limitations:

First, while it hypothesizes that coalescence reduction is what causes the enhancement of interfacial area, no direct measurement of the coalescence rate has been made. The equipment necessary for performing such measurements was not available. Nevertheless, there appears to be enough evidence of this phenomenon in the literature (reviewed in Section 5.1.1) to justify the claim. Furthermore, a theoretical estimate of the adsorption energy of nanoparticles at an interface (Section 5.1.1.3), together with surface tension measurements of nanoparticle solutions (Section 4.3) both substantiate the claim that particles prevent coalescence (by accumulating and strongly adsorbing at the interface).

Second, the model assumes that the interfacial area enhancement is not a function of nanoparticle concentration above $\phi = 0.0025$. This claim is made on grounds that data in Figure 4-12 suggest that increasing the nanoparticle fraction from $\phi = 0.0025$ to $\phi = 0.005$ does not yield a significant interfacial area increase. However, these data are not entirely conclusive, and experiments at $\phi > 0.0025$ covering a range of agitation conditions would be needed to confirm the claim.

Relatively little is known about the exact behavior of nanoparticles at interfaces. Most research to date has been experimental and a theoretical formulation of nanoparticles at interfaces is missing. Conversely, the behavior of surfactants at interfaces has been investigated in depth and modeled in detail. All equations used in Section 5.1 assume that the behavior of nanoparticles is the same as that of surfactants, which is most likely an incomplete picture.

5.4.2 Critique of the k_L Enhancement Model

The parameter C in the empirical equation proposed to describe the enhancement in k_L as a function of nanoparticle fraction (Eq. 68) has been fit from data obtained in a stirred beaker and thereafter used to predict k_L enhancement in an agitated, aerated fermentor. Although the determined parameter appears to fit reasonably well to the data obtained in the agitated, aerated system, such an approach is only justified if the parameter relates to an effective property of the medium that is independent of the experimental setup (*i.e.* effective oxygen diffusivity).

Recent publications indicate that heat transfer enhancement in nanofluids does not only depend on the size and volume fraction of nanoparticles, but also on their surface properties. It appears that a comprehensive model attempting to describe transfer properties would have to include electrostatic repulsions and attractions between particles and solvent structuring. Such a model would involve a broad range of length and time scales and would most likely require molecular dynamics or Stokesian dynamics simulations.

5.4.3 Relationship to Fermentation Experiments

The mechanism presented describes the experimental trends in mass transfer enhancement as a function of nanoparticle concentration and agitation conditions. Given the colloidal nature of the system studied, other variables such as electrolyte concentration, pH, and temperature are necessarily relevant as well. However, they have not been included for simplicity.

Different electrolyte concentrations could explain why the mass transfer enhancements measured using the sodium sulfite technique are significantly larger than those measured in fermentation experiments. It is plausible that high electrolyte concentrations screen

the repulsions between negatively charged nanoparticles adsorbed at the bubble interfaces, thereby facilitating a more compact packing. This, in turn, would reduce coalescence further. It has been observed elsewhere that addition of electrolytes increases bubble stability in surfactant solutions (Ghosh, 2004); Ghosh *et al*. found that NaCl reduced coalescence in the presence of sodium dodecyl sulfate, and LiCl eliminated it altogether. The authors hypothesized that the electrolytes screened the repulsions between the head groups of the surfactants adsorbed at the bubble interfaces, thus increasing the packing of surfactant molecules and reducing coalescence. It has also been shown that partially hydrophobic silica nanoparticles of 20 nm in size can stabilize air bubbles, and a sharp increase in stability occurrs when 2 M NaCl is added to the aqueous phase (Dickinson *et al.*, 2004). The sodium sulfite solutions used in this thesis have concentrations of Na^+ on the order of 1.4 M. This concentration of positively charged ions is notably higher than that in the fermentation medium used, which is approximately 0.2 M of K^+ (the concentration of other cations is negligible).

Finally, all fermentation experiments have been performed in duplicate, and additional experiments were conducted to verify the generality of the mass transfer enhancement results: (i) experiments were performed in fermentors at a smaller scale (1 and 1.5 L), and (ii) experiments were performed with cultures of *Pichia pastoris* (Lorenzo-Gonzalez, 2005). In all cases, the mass transfer enhancements obtained were on the order of 40 to 60%.

6 CONCLUSIONS

6.1 Experimental Section

1. Oxygen transfer enhancement has been observed in the presence of colloidal dispersions of magnetite (Fe_3O_4) nanoparticles coated with oleic acid and a polymerizable surfactant. These fluids improve gas-liquid oxygen mass transfer up to 6 fold (600%) in an agitated, sparged reactor and show remarkable stability in high-ionic strength media over a wide pH range. These results are relevant to a wide range of processes limited by the mass transfer of a solute between a gas phase and a liquid phase, including fermentation, hydrogenation reactions, and waste treatment.

2. Through a combination of experiments using physical and chemical methods to characterize mass transfer, it has been shown that

    a. Both the mass transfer coefficient (k_L) and the gas-liquid interfacial area (a) are enhanced in the presence of nanoparticles, the latter accounting for a larger fraction of the total enhancement.

    b. The enhancement in k_L measured by physical and chemical methods is similar and ranges from 20% to 60% approximately.

    c. The enhancement in k_L increases linearly below a nanoparticle mass fraction of 1% and subsequently plateaus.

    d. The enhancement in $k_L a$ shows a strong temperature dependence.

    e. Both particles coated with oleic-acid, which has a higher solubility for oxygen than water, and particles coated with polymers not known as oxygen carriers enhance mass transfer in an agitated, aerated system. Therefore, the oleic acid coating is not essential to obtain mass transfer enhancement.

3. The equilibrium surface tension of an air-water interface is reduced from 72 mN/m to less than 40 mN/m at mass volume fractions of nanoparticles above 0.1%.

4. A 40% increase in oxygen uptake rate and dry cell weight of *E. coli* can be obtained using a nanoparticle mass fraction of 0.6% in a fed-batch fermentation. It is expected that the reported increases in the oxygen transfer coefficient and in the cell concentration would translate to corresponding increased concentration of products synthesized by the host organism, such as primary and secondary metabolites. The oxygen transfer rate has been increased in a conventional agitated and aerated fermentor without any mechanical modification.

6.2 Modeling Section

1. Colloidal particles can adsorb to a gas-liquid interface. The energy necessary to remove a nanoparticle from the air-water interface is sufficiently large to assume that this adsorption is irreversible.

2. Nanoparticles can increase interfacial area by (i) inhibiting coalescence and (ii) facilitating bubble break-up by reducing surface tension. Increased bubble breakage can account for an area enhancement factor of only 1.5, and therefore cannot be the sole area enhancement mechanism. Nanoparticles stabilize gas bubbles by adsorbing on their interface and creating a stabilized dispersion in which bubble size is determined by breakage processes. In contrast, in the absence of nanoparticles, bubble size is dominated by coalescence processes and an unstable dispersion exists.

3. Effective property models of enhanced mass or heat transfer in the presence of dispersions are unsuitable to predict the transport properties of nanoparticle dispersions.

4. It has been proposed that the mass transfer coefficient is enhanced by the random motion of the nanoparticles, which causes convection in the surrounding fluid. An empirical expression that relates enhancement to the nanoparticle mass fraction, gas-liquid interfacial mobility, and agitation conditions has been presented.

5. The anomalous transfer properties of nanofluids have perplexed researchers for almost a decade and, to date, no model has been presented that has been widely

accepted as a complete description of the physical mechanisms underlying their performance. It is not at all clear that one mechanism can explain the body of data that has been generated already in the field, either. In addition, the different experimental measures of thermal properties presented in the literature have been made in systems with broadly different hydrodynamic conditions, from stagnant systems to free and forced convection systems.

6.3 Recommendations for Future Research

Assuming the mechanisms of area and k_L enhancement proposed in Section 5 are correct, the mass transfer enhancements realized should not be restricted to oxygen mass transfer. Instead, it should be possible to generalize them to many other gas-liquid systems. Many gas-liquid reactions in three-phase fluidized-bed reactors could be accelerated. Some examples include hydrogenation and hydrodesulfurization of residual oils, hydrogenation of unsaturated fats, slurry methanation of CO, waste water treatment, the Fischer-Tropsch process, coal liquefaction, and synthesis gas fermentations.

Synthesis gas fermentations, through which biomass can be converted to bio-based products that replace petroleum-based products, are an appealing target for use of magnetic nanoparticles. Gas-liquid mass transfer is a bottleneck that has prevented the commercialization of syngas fermentation products. The mass transfer limitations are a consequence of the low solubilities of H_2 and CO – the major syngas components – in aqueous media. Since the solubilities of these two gases in water are even lower than the solubility of oxygen, the mass transfer limitations are more accentuated than in aerobic fermentations.

Mass transfer limited reactions that require high temperatures can be another attractive target for use of magnetic nanoparticles since, as shown in Figure 4-14, the enhancement of mass transfer is more pronounced at high temperatures. Many hydrogenation reactions require high temperatures and would therefore be appropriate targets. For instance, production of high trans fatty acids from hydrogenated oils requires temperatures from 100 ^{o}C to 200 ^{o}C.

A systematic study of the effect of electrolyte concentration and type on $k_L a$ enhancement would shed light on the observed differences between the enhancements measured using the sodium sulfite technique and those measured in fermentation. Such knowledge could be used to target applications in which mass transfer processes occur in media where magnetic nanoparticles can be most effective.

Recovery of the nanoparticles is of crucial importance to the success of the method presented in this thesis. Nanoparticles with a diameter below 50 nm are difficult to recover by HGMS. The nanoparticles used in this thesis have a diameter of approximately 20 nm. While a proof of principle that particles of size above 50 nm can be easily synthesized has been presented in section 4.1.3, it would be important to verify that the mass transfer enhancements attainable are not significantly affected by the particle size. A systematic study of the effect of particle size on mass transfer at constant particle mass fraction would clarify this.

This thesis' research has concentrated on characterization of enhanced mass transfer in turbulent media. Convective effects play a role in *heat* transfer enhancement by nanofluids (Yang *et al.*, 2005), *i.e.* nanofluids increase the heat transfer coefficient by less than the static thermal conductivity. Likewise, it is plausible that nanoparticles increase the diffusion coefficient of gas solutes to a greater extent than they increase k_L. Absorption experiments of oxygen into a stagnant medium would yield values of the effective diffusion coefficient of oxygen in the presence of nanoparticles.

7 REFERENCES

Adlercreutz, P., O. Holst and B. Mattiasson (1982a). "Oxygen-supply to immobilized cells.2. Studies on a coimmobilized algae-bacteria preparation with insitu oxygen generation." Enzyme and Microbial Technology **4**(6): 395-400.

Adlercreutz, P. and B. Mattiasson (1982b). "Oxygen-supply to immobilized biocatalysts - a model study." Acta Chemica Scandinavica Series B-Organic Chemistry and Biochemistry **36**(9): 651-653.

Adlercreutz, P. and B. Mattiasson (1982c). "Oxygen-supply to immobilized cells.1. Oxygen production by immobilized chlorella-pyrenoidosa." Enzyme and Microbial Technology **4**(5): 332-336.

Adlercreutz, P. and B. Mattiasson (1982d). "Oxygen-supply to immobilized cells.3. Oxygen-supply by hemoglobin or emulsions of perfluorochemicals." European Journal of Applied Microbiology and Biotechnology **16**(4): 165-170.

Ali, A. and K. Vafai (2004a). "An investigation of heat and mass transfer between air and desiccant film in an inclined parallel and counter flow channels." International Journal of Heat and Mass Transfer **47**(8-9): 1745-1760.

Ali, A., K. Vafai and A. Khaled (2004b). "Analysis of heat and mass transfer between air and falling film in a cross flow configuration." International Journal of Heat and Mass Transfer **47**(4): 743-755.

Alper, E., B. Wichtendahl and W. Deckwer (1980). "Gas-absorption mechanism in catalytic slurry reactors." Chemical Engineering Science **35**(1-2): 217-222.

Alves, S., C. Maia and J. Vasconcelos (2003). "Gas-liquid mass transfer coefficient in stirred tanks interpreted through bubble contamination kinetics." Chemical Engineering and Processing **43**: 823-830.

Arditty, S., C. P. Whitby, B. P. Binks, V. Schmitt and F. Leal-Calderon (2003). "Some general features of limited coalescence in solid-stabilized emulsions." European Physical Journal E **11**(3): 273-281.

Augenstein, D. C. (1967). Oxygen absorption in fermentors at high power inputs. PhD Thesis, Massachusetts Institute of Technology**:** 130.

Aveyard, R., B. P. Binks and J. H. Clint (2003). "Emulsions stabilised solely by colloidal particles." Advances in Colloid and Interface Science **100**: 503-546.

Aveyard, R., J. H. Clint, D. Nees and V. N. Paunov (2000). "Compression and structure of monolayers of charged latex particles at air/water and octane/water interfaces." Langmuir **16**(4): 1969-1979.

Bailey, J. and D. Ollis (1986). Biochemical engineering fundamentals. Mc Graw Hill, 2nd editon.

Bang, I. and S. Chang (2005). "Boiling heat transfer performance and phenomena of al2o3-water nano-fluids from a plain surface in a pool." International Journal of Heat and Mass Transfer **48**(12): 2407-2419.

Bartholomew, W. and H. Reisman (1979). Economics of fermentation processes. In: Microbial technology, 2nd edition. H. P. a. D. Perlman, Academic Press. New York. **2**.

Bauer, S. and J. Shiloach (1974). "Maximal exponential-growth rate and yield of escherichia-coli obtainable in a bench-scale fermentor." Biotechnology And Bioengineering **16**(7): 933-941.

Bhattacharya, P., S. Saha, A. Yadav, P. Phelan and R. Prasher (2004). "Brownian dynamics simulation to determine the effective thermal conductivity of nanofluids." Journal of Applied Physics **95**(11): 6492-6494.

Binks, B. P. (2002). "Particles as surfactants - similarities and differences." Current Opinion in Colloid & Interface Science **7**(1-2): 21-41.
Binks, B. P. and T. S. Horozov (2005a). "Aqueous foams stabilized solely by silica nanoparticles." Angewandte Chemie-International Edition **44**(24): 3722-3725.
Binks, B. P. and S. O. Lumsdon (2001). "Pickering emulsions stabilized by monodisperse latex particles: Effects of particle size." Langmuir **17**(15): 4540-4547.
Binks, B. P. and C. P. Whitby (2005b). "Nanoparticle silica-stabilised oil-in-water emulsions: Improving emulsion stability." Colloids and Surfaces a-Physicochemical and Engineering Aspects **253**(1-3): 105-115.
Bird, R., W. Stewart and E. Lightfoot (1960). "Transport phenomena." Wiley, New York: 537-542.
Bredwell, M. D. and R. M. Worden (1998). "Mass-transfer properties of microbubbles. 1. Experimental studies." Biotechnology Progress **14**(1): 31-38.
Brilman, D., M. Goldschmith, G. Versteeg and W. Van Swaaij (2000). "Heterogeneous mass transfer models for gas absorption in multiphase systems." Chemical Engineering Science **55**: 2793-2812.
Brilman, D., W. Van Swaaij and G. Versteeg (1998). "A one-dimensional instationary heterogeneous mass transfer model for gas absorption in multiphase systems." Chemical Engineering & Processing **37**(6): 471-488.
Bruining, W., G. Joosten, A. Beenackers and H. Hofman (1986). "Enhancement of gas-liquid mass-transfer by a dispersed 2nd liquid-phase." Chemical Engineering Science **41**(7): 1873-1877.
Buongiorno, J. (2006). "Convective transport in nanofluids." Transactions of the ASME **128**: 240-250.
Calderbank, P. (1958). "The interfacial area in gas-liquid contacting with mechanical agitation." Trans. IChemE **36**: 443-459.
Calderbank, P. H. and M. B. Mooyoung (1995). "The continuous phase heat and mass transfer properties of dispersions (reprinted from chem engng sci, vol 16, pg 39-54, 1961)." Chemical Engineering Science **50**(24): 3921-3934.
Cents, A., D. Brilman and G. Versteeg (2001). "Gas absorption in an agitated gas-liquid-liquid system." Chemical Engineering Science **56**(3): 1075-1083.
Choi, S. (1995). "Enhancing thermal conductivity of fluids with nanoparticles." Developments and Applications of Non-Newtonian Flows: pp. 99-105.
Choi, S., Z. Zhang, W. Yu, F. Lockwood and E. Grulke (2001). "Anomalous thermal conductivity enhancement in nanotube suspensions." Applied Physics Letters **79**(14): 2252-2254.
Clift, J. and M. Grace (1978). "Bubbles, drops, and particles." Academic Press, London.
Damiano, D. and S. S. Wang (1985). "Novel use of a perfluorocarbon for supplying oxygen to aerobic submerged cultures." Biotechnology Letters **7**(2): 81-86.
Danckwerts, P. (1951). "Significance of liquid film coefficients in gas absorptions." Industrial & Engineering Chemistry **43**: 1460.
Danckwerts, P. (1970). Gas-liquid reactions. New York, McGraw-Hill.
Das, S., N. Putra and W. Roetzel (2003a). "Pool boiling characteristics of nano-fluids." International Journal of Heat and Mass Transfer **46**(5): 851-862.
Das, S., N. Putra and W. Roetzel (2003b). "Pool boiling of nano-fluids on horizontal narrow tubes." International Journal of Multiphase Flow **29**(8): 1237-1247.
Das, S., N. Putra, P. Thiesen and W. Roetzel (2003c). "Temperature dependence of thermal conductivity enhancement for nanofluids." Journal of Heat Transfer-Transactions of the Asme **125**(4): 567-574.

Demmink, J., A. Mehra and A. Beenackers (1998). "Gas absorption in the presence of particles showing interfacial affinity: Case of fine sulfur precipitates." Chemical Engineering Science **53**(16): 2885-2902.

Dickinson, E., R. Ettelaie, T. Kostakis and B. S. Murray (2004). "Factors controlling the formation and stability of air bubbles stabilized by partially hydrophobic silica nanoparticles." Langmuir **20**(20): 8517-8525.

Ditsch, A. (2004). Purification of recombinant proteins with magnetic nanoclusters. PhD Thesis, Massachusetts Institute of Technology**:** 158.

Ditsch, A., P. E. Laibinis, D. I. C. Wang and T. A. Hatton (2005a). "Controlled clustering and enhanced stability of polymer-coated magnetic nanoparticles." Langmuir **21**(13): 6006-6018.

Ditsch, A., S. Lindenmann, P. Laibins, D. Wang and T. Hatton (2005b). "High-gradient magnetic separation of magnetic nanoclusters." Industrial & Engineering Chemistry Research **ASAP Article**.

Ditsch, A., D. I. C. Wang and T. A. Hatton (2004). "Magnetic fluids for ion-exchange purification of recombinant proteins." Abstracts of Papers of the American Chemical Society **227**: U211-U211.

Dong, L. C. and D. Johnson (2003). "Surface tension of charge-stabilized colloidal suspensions at the water-air interface." Langmuir **19**(24): 10205-10209.

Drogaris, G. and P. Weiland (1983). "Coalescence behaviour of gas bubbles in aqueous solutions of n-alcohols and fatty acids." Chemical Engineering Science **38**(9): 1501-1506.

Du, Z. P., M. P. Bilbao-Montoya, B. P. Binks, E. Dickinson, R. Ettelaie and B. S. Murray (2003). "Outstanding stability of particle-stabilized bubbles." Langmuir **19**(8): 3106-3108.

Dumont, E. and H. Delmas (2003). "Mass transfer enhancement of gas absorption in oil-in-water systems: A review." Chemical Engineering & Processing **42**(6): 419-438.

Eastman, J., S. Choi, S. Li, W. Yu and L. Thompson (2001). "Anomalously increased effective thermal conductivities of ethylene glycol-based nanofluids containing copper nanoparticles." APPLIED PHYSICS LETTERS **78**(6): 718-720.

Eastman, J., S. Phillpot, S. Choi and P. Keblinski (2004). "Thermal transport in nanofluids." Annual Review of Materials Research **34**: 219-246.

Eastoe, J., M. S. Dominguez, P. Wyatt, A. Beeby and R. K. Heenan (2002). "Properties of a stilbene-containing gemini photosurfactant: Light-triggered changes in surface tension and aggregation." Langmuir **18**(21): 7837-7844.

Einstein, A. (1906). "Zur theorie der brownschen bewegung." Annalen der Physik **19**: 371.

Faour, G., M. Grimaldi, J. Richou and A. Bois (1996). "Real-time pendant drop tensiometer using image processing with interfacial area and interfacial tension control capabilities." Journal Of Colloid And Interface Science **181**(2): 385-392.

Finkle, P. and H. Draper (1923). "The theory of emulsification." Journal of the American Chemical Society **45**: 2780-2788.

Flickinger, M. C. and D. Perlman (1977a). "Application of oxygen-enriched aeration in conversion of glycerol to dihydroxyacetone by gluconobacter-melanogenus ifo-3293." Applied And Environmental Microbiology **33**(3): 706-712.

Flickinger, M. C. and D. Perlman (1977b). "Fermentations with oxygen-enriched air - neomycin and bacitracin." Abstracts Of Papers Of The American Chemical Society **174**(SEP): 35-35.

Flickinger, M. C. and D. Perlman (1979). "Application of oxygen-enriched aeration in the production of bacitracin by bacillus-licheniformis." Antimicrobial Agents And Chemotherapy **15**(2): 282-293.
Frey, A. D. and P. T. Kallio (2003). "Bacterial hemoglobins and flavohemoglobins: Versatile proteins and their impact on microbiology and biotechnology." Fems Microbiology Reviews **27**(4): 525-545.
Frossling, N. (1938). "Evaporation of falling drops." Gerlands Beitage Geophys. **52**: 170-216.
Ghosh, P. (2004). "Coalescence of air bubbles at air-water interface." Chemical Engineering Research and Design **82**(A7): 849-854.
Gibbs, B. F., S. Kermasha, I. Alli and C. N. Mulligan (1999). "Encapsulation in the food industry: A review." International Journal of Food Sciences and Nutrition **50**(3): 213-224.
Gupte, S., S. Advani and P. Huq (1995). "Role of micro-convection due to non-affine motion of particles in a mono-disperse suspension." International Journal of Heat and Mass Transfer **38**(16): 2945-2958.
Hamilton, R. and O. Crosser (1962). "Thermal conductivity of heterogeneous two-component systems." Industrial & Engineering Chemistry Fundamentals **1**: 187-191.
Higbie, R. (1935). "The rate of absorption of a pure gas into a still liquid during a short period of exposure." Transactions of the american nstitute of chemical engineers **31**: 365.
Hinze, J. (1955). "Fundamentals of the hydrodynamics mechanism of splitting in dispersion processes." AIChE Journal **1**: 950.
Holst, O., S. O. Enfors and B. Mattiasson (1982). "Oxygenation of immobilized cells using hydrogen-peroxide - a model study of gluconobacter-oxydans converting glycerol to dihydroxyacetone." European Journal Of Applied Microbiology And Biotechnology **14**(2): 64-68.
Holstvoogd, R., W. Vanswaaij and L. Vandierendonck (1988). "The absorption of gases in aqueous activated carbon slurries enhanced by adsorbing or catalytic particles." Chemical Engineering Science **43**(8): 2181-2187.
Hu, W. S., J. Meier and D. I. C. Wang (1986). "Use of surface aerator to improve oxygen-transfer in cell-culture." Biotechnology And Bioengineering **28**(1): 122-125.
Ibrahim, M. and H. G. Schlegel (1980). "Oxygen-supply to bacterial suspensions of high cell densities by hydrogen-peroxide." Biotechnology And Bioengineering **22**(9): 1877-1894.
Jahanzad, F., S. Sajjadi and B. Brooks (2005). "Comparative study of particle size in suspension polymerization and corresponding monomer-water dispersion." Industrial & Engineering Chemistry Research **44**: 4112-4119.
Jang, S. and S. Choi (2004). "Role of brownian motion in the enhanced thermal conductivity of nanofluids." Applied Physics Letters **84**(21): 4316-4318.
Jeffrey, D. (1973). "Conduction through a random suspension of spheres." Proceedings of the Royal Society of London Series A-Mathematical Physical and Engineering Sciences **335**(1602): 355-367.
Jeon, S. I., J. H. Lee, J. D. Andrade and P. G. Degennes (1991). "Protein surface interactions in the presence of polyethylene oxide.1. Simplified theory." Journal of Colloid and Interface Science **142**(1): 149-158.

Junker, B., T. Hatton and D. Wang (1990). "Oxygen-transfer enhancement in aqueous perfluorocarbon fermentation systems.1. Experimental-observations." Biotechnology and Bioengineering **35**(6): 578-585.
Junker, B., M. Stanik, C. Barna, P. Salmon, E. Paul and B. Buckland (1998). "Influence of impeller type on power input in fermentation vessels." Bioprocess Engineering **18**(6): 401-412.
Kallio, P. T. and J. E. Bailey (1996). "Intracellular expression of vitreoscilla hemoglobin (vhb) enhances total protein secretion and improves the production of alpha-amylase and neutral protease in bacillus subtilis." Biotechnology Progress **12**(1): 31-39.
Kars, R., R. Best and A. Drinkenburg (1979). "Sorption of propane in slurries of active-carbon in water." Chemical Engineering Journal and the Biochemical Engineering Journal **17**(3): 201-210.
Karve, S. and V. A. Juvekar (1990). "Gas-absorption into slurries containing fine catalyst particles." Chemical Engineering Science **45**(3): 587-594.
Kaster, J. A., D. L. Michelsen and W. H. Velander (1990). "Increased oxygen-transfer in a yeast fermentation using a microbubble dispersion." Applied Biochemistry And Biotechnology **24-5**: 469-484.
Kawase, Y., B. Halard and M. Mooyoung (1987). "Theoretical prediction of volumetric mass-transfer coefficients in bubble-columns for newtonian and non-newtonian fluids." Chemical Engineering Science **42**(7): 1609-1617.
Kawase, Y. and M. Mooyoung (1988). "Volumetric mass-transfer coefficients in aerated stirred tank reactors with newtonian and non-newtonian media." Chemical Engineering Research & Design **66**(3): 284-288.
Keblinski, P., S. Phillpot, S. Choi and J. Eastman (2002). "Mechanisms of heat flow in suspensions of nano-sized particles (nanofluids)." International Journal of Heat and Mass Transfer **45**(4): 855-863.
Keller, K. (1971). "Effect of fluid shear on mass transport in flowing blood." Fed Proc **30**: 1591.
Khosla, C. and J. E. Bailey (1988a). "Heterologous expression of a bacterial hemoglobin improves the growth-properties of recombinant escherichia-coli." Nature **331**(6157): 633-635.
Khosla, C. and J. E. Bailey (1988b). "The vitreoscilla hemoglobin gene - molecular-cloning, nucleotide-sequence and genetic expression in escherichia-coli." Molecular & General Genetics **214**(1): 158-161.
Kim, S. and Y. Kang (1997). "Heat and mass transfer in three-phase fluidized-bed reactors - an overview." Chemical Engineering Science **52**(21-22): 3639-3660.
Konz, J. O., J. King and C. L. Cooney (1998). "Effects of oxygen on recombinant protein expression." Biotechnology Progress **14**(3): 393-409.
Koo, J. and C. Kleinstreuer (2004). "A new thermal conductivity model for nanofluids." Journal of Nanoparticle Research **6**(6): 577-588.
Krishnamurthy, S., P. Bhattacharya and P. Phelan (2006). "Enhanced mass transport in nanofluids." Nano Letters **6**(3): 419-423.
Kumar, D., H. Patel, V. Kumar, T. Sundararajan, T. Pradeep and S. Das (2004). "Model for heat conduction in nanofluids." Physical Review Letters **93**(14): Art. No. 144301.
Lamont, G. and D. Scott (1970). "An eddy cell model of mass transfer into surface of a turbulent liquid." Aiche Journal(16): 513-519.

Laurent, A., J. Charpentier and C. Prost (1974). "Etude de la cinetique heterogene globale de l'oxydation catalytique d'une solution aqueuse de sulfite de sodium par l'oxygene gazeux en presence de sulfate de cobalt." Journal de Chimie Physique **71**(4): 613-614.

Lazrak, N., N. Le Bolay and A. Ricard (1998). "Droplet stabilization in high holdup fraction suspension polymerization reactors." European Polymer Journal **34**(11): 1637-1647.

Leal, L. (1973). "On the effective conductivity of a dilute suspension of spherical drops in the limit of low particle peclet number." Chemical Engineering Communications **1**(1): 21-31.

Lee, D., J. Kim and B. Kim (2006). "A new parameter to control heat transport in nanofluids: Surface charge state of the particle in suspension." Journal of Physical Chemistry B **110**: 4323-4328.

Lee, S., S. Choi, S. Li and J. Eastman (1999). "Measuring thermal conductivity of fluids containing oxide nanoparticles." Journal of Heat Transfer-Transactions of the Asme **121**(2): 280-289.

Levich, V. (1962). "Physicochemical hydrodynamics."

Lewis, W. and W. Whitman (1924). "The principles of gas absorption." Ind. Eng. Chem. **16**: 1215.

Linek, V. (1966). Chemical Engineering Science **21**: 777.

Linek, V. and P. Benes (1976). "Study of mechanism of gas absorption into oil-water emulsions." Chemical Engineering Science **31**(11): 1037-1046.

Linek, V. and P. Benes (1978). "Enhancement of oxygen absorption into sodium-sulfite solutions." Biotechnology and Bioengineering **20**(5): 697-707.

Linek, V., M. Kordac and T. Moucha (2005). "Mechanism of mass transfer from bubbles in dispersions - part ii: Mass transfer coefficients in stirred gas-liquid reactor and bubble column." Chemical Engineering And Processing **44**(1): 121-130.

Linek, V. and J. Mayerhoferova (1971). Chemical Engineernig Science **26**: 787.

Linek, V. and V. Vacek (1981). "Chemical-engineering use of catalyzed sulfite oxidation-kinetics for the determination of mass-transfer characteristics of gas-liquid contactors." Chemical Engineering Science **36**(11): 1747-1768.

Liu, S. and D. Li (1999). "Drop coalescence in turbulent dispersions." Chemical Engineering Science **54**: 5667-5675.

Lochiel, A. C., Ph (1964). "Mass transfer in the continuous phase around axisymmetric bodies of revolution." Chemical Engineering Science **19**: 471-484.

Lorenzo-Gonzalez, L. (2005). Experiments conducted as part of a master's thesis under J.F. Hamel, MIT

Lowe, K. (1991). "Perfluorochemicals - blood substitutes and beyond." Advanced Materials **3**(2): 87-93.

Lowe, K., M. Davey and J. Power (1998). "Perfluorochemicals: Their applications and benefits to cell culture." Trends in Biotechnology **16**(6): 272-277.

Lyu, S., T. D. Jones, F. S. Bates and C. W. Macosko (2002). "Role of block copolymers on suppression of droplet coalescence." Macromolecules **35**(20): 7845-7855.

Masuda, H., A. Ebata, K. Teramae and N. Hishinuma (1993). "Alteration of thermal conductivity and viscosity of liquid by dispersing ultra-fine particles." Netsu Bussei (Japan) **4**(4): 227-233.

Mattiasson, B. and P. Adlercreutz (1983). "Use of perfluorochemicals for oxygen-supply to immobilized cells." Annals of the New York Academy of Sciences **413**(DEC): 545-547.

Mattiasson, B. and P. Adlercreutz (1987). "Perfluorochemicals in biotechnology." Trends in Biotechnology **5**(9): 250-254.
Maxwell, J. C. (1873). A treatise on electricity and magnetism. Oxford, Clarendon Press.
Mccurdy, C., E. Stechel, P. Cummings, B. Hendrickson and D. Keyes (2002). "Theory and modeling in nanoscience."
McMillan, J. and D. Wang (1990a). "Mechanisms of oxygen-transfer enhancement during submerged cultivation in perfluorochemical-in-water dispersions." Annals of the New York Academy of Sciences **589**: 283-300.
McMillan, J. D. (1990). Mechanisms of oxygen transfer enhancement during submerged cultivation in perfluorochemical-in-water dispersions. PhD Thesis, Massachusetts Institute of Technology.
McMillan, J. D. and D. I. C. Wang (1987). "Enhanced oxygen-transfer using oil-in-water dispersions." Annals Of The New York Academy Of Sciences **506**: 569-582.
McMillan, J. D. and D. I. C. Wang (1990b). "Mechanisms of oxygen-transfer enhancement during submerged cultivation in perfluorochemical-in-water dispersions." Annals Of The New York Academy Of Sciences **589**: 283-300.
Meguro, K. and A. Yokouchi (1987). "Electrically conductive ferrofluid compostion."
Mehra, A. (1988). "Intensification of multiphase reactions through the use of a microphase.1. Theoretical." Chemical Engineering Science **43**(4): 899-912.
Mehra, A., A. Pandit and M. Sharma (1988). "Intensification of multiphase reactions through the use of a microphase.2. Experimental." Chemical Engineering Science **43**(4): 913-927.
Metkin, V. and V. Sokolov (1985). Zh. Prikl. Khim, **58**: 1132.
Milner, S. T. and H. W. Xi (1996). "How copolymers promote mixing of immiscible homopolymers." Journal of Rheology **40**(4): 663-687.
Mimura, A., K. T and K. R (1969). "Biochemical engineering analysis of hydrocarbon fermentation. I. Oxygen transfer in the oil-water system." J. Ferment. Technol. **47**: 229-236.
Moeser, G., K. Roach, W. Green, P. Laibinis and T. Hatton (2002a). "Water-based magnetic fluids as extractants for synthetic organic compounds." Industrial & Engineering Chemistry Research **41**(19): 4739-4749.
Moeser, G. D., K. A. Roach, W. H. Green, T. A. Hatton and P. E. Laibinis (2004). "High-gradient magnetic separation of coated magnetic nanoparticles." Aiche Journal **50**(11): 2835-2848.
Moeser, G. D., K. A. Roach, W. H. Green, P. E. Laibinis and T. A. Hatton (2002b). "Water-based magnetic fluids as extractants for synthetic organic compounds." Industrial & Engineering Chemistry Research **41**(19): 4739-4749.
Murray, B. S. and R. Ettelaie (2004). "Foam stability: Proteins and nanoparticles." Current Opinion in Colloid & Interface Science **9**(5): 314-320.
Nagaoka, S., Y. Mori, H. Takiuchi, K. Yokota, H. Tanzawa and S. Nishiumi (1983). "Interaction between blood components and hydrogels with poly(oxyethylene) chain." Abstracts of Papers of the American Chemical Society **185**(Mar): 142-POLY.
Nagele, G. (1996). "On the dynamics and structure of charge-stabilized suspensions." Physical Review **272**: 215-372.
Nagy, E. (2003). "On the three-phase mass transfer with solid particles adhered to the gas-liquid interface." Central European Journal of Chemistry **1**(2): 160-177.
Ng, S., P. Warszynski and K. Zembala (1999). Problems Miner. Process. **33**: 143-161.

Nies, D. and H. G. Schlegel (1984). "Use of catalase from escherichia-coli in model experiments for oxygen-supply of microorganisms with hydrogen-peroxide." Biotechnology And Bioengineering **26**(7): 737-741.
Ogawa, S., Y. Shimizu, S. Tone and T. Otake (1982). "Kinetics of the oxidation of aqueous sodium sulfite solutions with air." Journal of Chemical Engineering of Japan **15**(5): 400-402.
Olander, D. (1963). "A hydrodynamic model of mass transfer in a stirred vessel extractor." Chemical Engineering Science **18**: 123-132.
Olander, D. (1964). "A modified model of stirred vessel mass transfer." Chemical Engineering Science **19**: 275-282.
Olle, B., Bromberg, L., Yin, J., Wang, D.I.C., Hatton, T.A. (2005). "Bioprocesses enhanced by fluoropolymer-coated magnetic nanoparticles and methods related thereto", Int. Pat. Appl. WO/2005/063617, Publ. 14/07/2005.
Oyama, Y. and K. Endoh (1955). "Power characteristics of gas-liquid contacting mixers." Chem Eng (Japan) **19**: 2-11.
Pak, B. and Y. Cho (1998). "Hydrodynamic and heat transfer study of dispersed fluids with submicron metallic oxide particles." Experimental Heat Transfer **11**: 151.
Pardieck, D. L., E. J. Bouwer and A. T. Stone (1992). "Hydrogen-peroxide use to increase oxidant capacity for insitu bioremediation of contaminated soils and aquifers - a review." Journal Of Contaminant Hydrology **9**(3): 221-242.
Patel, H., S. Das, T. Sundararajan, A. Sreekumaran Nair, B. George and T. Pradeep (2003). "Thermal conductivities of naked and monolayer protected metal nanoparticle based nanofluids: Manifestation of anomalous enhancement and chemical effects." Applied Physics Letters **83**(14): 2931-2933.
Perry, R. and D. Green (1997). "Perry's chemical engineer's handbook." **7th Edition**.
Pickering, S. (1907). "Emulsions." Journal of the Chemical Society **91**: 2001-2021.
Prasher, R., P. Bhattacharya and P. Phelan (2005). "Thermal conductivity of nanoscale colloidal solutions (nanofluids)." Physical Review Letters **94**(2): Art. No. 025901.
Prime, K. and G. Whitesides (1993). "Adsorption of proteins onto surfaces containing end-attached oligo(ethylene oxide) - a model system using self-assembled monolayers." Journal of the American Chemical Society **115**(23): 10714-10721.
Pugh, R. J. (1996). "Foaming, foam films, antifoaming and defoaming." Advances in Colloid and Interface Science **64**: 67-142.
Pusey, P. (1991). "Colloidal suspensions." In Liquids, freezing, and glass transition, Elsevier, Amsterdam: 763-942.
Quicker, G., A. Schumpe and W. Deckwer (1984). "Gas-liquid interfacial-areas in a bubble column with suspended-solids." Chemical Engineering Science **39**(1): 179-183.
Ramsden, W. (1903). "Separation of solids in the surface layers of solutions and 'suspensions' - preliminary account." Proceedings of the Royal Society of London Series A-Mathematical Physical and Engineering Sciences **72**: 152-164.
Reith, T. and W. Beek (1973). "The oxidation of aqueous sodium sulfite solutions." Chemical engineering science **28**: 1331-1339.
Roco, M. (1999). "Nanoparticles and nanotechnology research." Journal of Nanoparticle Research **1**: 1-6.
Rols, J., J. Condoret, C. Fonade and G. Goma (1990). "Mechanism of enhanced oxygen-transfer in fermentation using emulsified oxygen-vectors." Biotechnology and Bioengineering **35**(4): 427-435.

Rosenberg, M., J. Svitel, E. Sturdik and I. Rosenbergova (1992). "Gluconic acid production by aspergillus-niger with oxygen-supply by hydrogen-peroxide." Bioprocess Engineering **7**(7): 309-313.
Rousseau, D. (2000). "Fat crystals and emulsion stability - a review." Food Research International **33**(1): 3-14.
Rushton, J., E. Costich and H. Everett (1950). "Power characteristics of mixing impellers." Chemical Engineering Progress **46**: 395-404.
Sathyamurthy, N., K. Degaleesan, K. Chandrasekharan and G. Laddha (1979). "Absorption of oxygen by aqueous sodium sulphite solutions." The Canadian Journal of Chemical Engineering **57**: 145-149.
Schlegel, H. G. (1977). "Aeration without air - oxygen-supply by hydrogen-peroxide." Biotechnology And Bioengineering **19**(3): 413-424.
Schutt, E. G., D. H. Klein, R. M. Mattrey and J. G. Riess (2003). "Injectable microbubbles as contrast agents for diagnostic ultrasound imaging: The key role of perfluorochemicals." Angewandte Chemie-International Edition **42**(28): 3218-3235.
Shen, L., P. Laibinis and T. Hatton (1998). "Solution and bilayer structure of surfactant-stabilized magnetic fluids." Abstracts of Papers of the American Chemical Society **216**: U303-U303.
Shen, L., P. Laibinis and T. Hatton (1999). "Aqueous magnetic fluids stabilized by surfactant bilayers." Journal of Magnetism and Magnetic Materials **194**(1-3): 37-44.
Shen, L., A. Stachowiak, T. Hatton and P. Laibinis (2000). "Polymerization of olefin-terminated surfactant bilayers on magnetic fluid nanoparticles." Langmuir **16**(25): 9907-9911.
Shimoiizaka, J. (1977). "Method for preparing a water base magnetic fluid and product."
Shinnar, R. (1961). "On the behaviour of liquid dispersions in mixing vessels." Journal of Fluid Mechanics **10**: 259.
Shinnar, R. and J. Church (1960). "Statistical theories of turbulence in predicting particle size in agitated dispersions." Industrial & Engineering Chemistry **52**(3): 253.
Song, B. H. and J. Springer (1996). "Determination of interfacial tension from the profile of a pendant drop using computer-aided image processing.1. Theoretical." Journal Of Colloid And Interface Science **184**(1): 64-76.
Sonnleitner, B. and U. Hahnemann (1997). "Robust oxygen supply by controlled addition of hydrogen peroxide to microbial cultures." Bioprocess Engineering **17**(4): 215-219.
Sprow, F. (1967). "Distribution of drop size produced in turbulent liquid-liquid dispersion." Chemical Engineering Science **22**: 435.
Srivastava, P., O. Hahr, R. Buchholz and R. M. Worden (2000). "Enhancement of mass transfer using colloidal liquid aphrons: Measurement of mass transfer coefficients in liquid-liquid extraction." Biotechnology And Bioengineering **70**(5): 525-532.
Sundararaj, U. and C. W. Macosko (1995). "Drop breakup and coalescence in polymer blends - the effects of concentration and compatibilization." Macromolecules **28**(8): 2647-2657.
Taylor, G. (1932). "The viscosity of a fluid containing small drops of another fluid." Proc. Roy. Soc **A138**: 41.
Tcholakova, S., N. D. Denkov, D. Sidzhakova, I. B. Ivanov and B. Campbell (2003). "Interrelation between drop size and protein adsorption at various emulsification conditions." Langmuir **19**(14): 5640-5649.

Tobin, T. and D. Ramkrishna (1999). "Modeling the effect of drop charge on coalescence in turbulent liquid-liquid dispersions." The Canadian Journal of Chemical Engineering **77**: 1090-1104.
Van Der Zon, A., P. Hamersma, E. Poels and A. Bliek (2002). "Coalescence of freely moving bubbles in water by the action of suspended hydrophobic particles." Chemical Engineering Science **57**(22-23): 4845-4853.
Van Hemelrijck, E., P. Van Puyvelde, C. W. Macosko and P. Moldenaers (2005). "The effect of block copolymer architecture on the coalescence and interfacial elasticity in compatibilized polymer blends." Journal of Rheology **49**(3): 783-798.
Van Puyvelde, P., S. Velankar, J. Mewis and P. Moldenaers (2002). "Effect of marangoni stresses on the deformation and coalescence in compatibilized immiscible polymer blends." Polymer Engineering and Science **42**(10): 1956-1964.
Van Puyvelde, P., S. Velankar and P. Moldenaers (2001). "Rheology and morphology of compatibilized polymer blends." Current Opinion in Colloid & Interface Science **6**(5-6): 457-463.
Vassallo, P., R. Kumar and S. D'amico (2004). "Pool boiling heat transfer experiments in silica-water nano-fluids." International Journal of Heat and Mass Transfer **47**(2): 407-411.
Vermant, J., G. Cioccolo, K. G. Nair and P. Moldenaers (2004). "Coalescence suppression in model immiscible polymer blends by nano-sized colloidal particles." Rheologica Acta **43**(5): 529-538.
Vilgis, T. A. and J. Noolandi (1990). "Theory of homopolymer block copolymer blends - the search for a universal compatibilizer." Macromolecules **23**(11): 2941-2947.
Vinke, H., G. Bierman, P. Hamersma and J. Fortuin (1991). "Adhesion of small catalyst particles to gas-bubbles - determination of small effective solid liquid gas contact angles." Chemical Engineering Science **46**(10): 2497-2506.
Vinke, H., P. Hamersma and J. Fortuin (1993). "Enhancement of the gas-absorption rate in agitated slurry reactors by gas-adsorbing particles adhering to gas-bubbles." Chemical Engineering Science **48**(12): 2197-2210.
Wakabayashi, S., H. Matsubara and D. A. Webster (1986). "Primary sequence of a dimeric bacterial hemoglobin from vitreoscilla." Nature **322**(6078): 481-483.
Wang, D. Y., H. W. Duan and H. Mohwald (2005). "The water/oil interface: The emerging horizon for self-assembly of nanoparticles." Soft Matter **1**(6): 412-416.
Wang, X., X. Xu and S. Choi (1999). "Thermal conductivity of nanoparticle-fluid mixture." Journal of Thermophysics and Heat Transfer **13**(4): 474-480.
Weber, J. and F. A. Agblevor (2005). "Microbubble fermentation of trichoderma reesei for cellulase production." Process Biochemistry **40**(2): 669-676.
Wen, D. and Y. Ding (2004a). "Effect on heat transfer of particle migration in suspensions of nanoparticles flowing through minichannels." Second International Conference on Microchannels and Minichannels (ICMM2004), Rochester, NY: 939-946.
Wen, D. and Y. Ding (2004b). "Effective thermal conductivity of aqueous suspensions of carbon nanotubes (carbon nanotubes nanofluids)." Journal of Thermophysics and Heat Transfer **18**(4): 481-485.
Wen, D. and Y. Ding (2004c). "Experimental investigation into convective heat transfer of nanofluids at the entrance region under laminar flow conditions." International Journal of Heat and Mass Transfer **47**(24): 5181-5188.

Wen, J., X. Jia and W. Feng (2005). "Hydrodynamic and mass transfer of gas-liquid-solid three-phase internal loop airlift reactors with nanometer solid particles." Chemical Engineering & Technology **28**(1): 53-60.

Wimmers, O. and J. Fortuin (1988a). "The use of adhesion of catalyst particles to gas-bubbles to achieve enhancement of gas-absorption in slurry reactors.1. Investigation of particle-to-bubble adhesion using the bubble pick-up method." Chemical Engineering Science **43**(2): 303-312.

Wimmers, O. and J. Fortuin (1988b). "The use of adhesion of catalyst particles to gas-bubbles to achieve enhancement of gas-absorption in slurry reactors.2. Determination of the enhancement in a bubble-containing slurry reactor." Chemical Engineering Science **43**(2): 313-319.

Xie, H., H. Lee, W. Youn and M. Choi (2003). "Nanofluids containing multiwalled carbon nanotubes and their enhanced thermal conductivities." Journal of Applied Physics **94**(8): 4967-4971.

Xie, H., J. Wang, T. Xi, Y. Liu and F. Ai (2002a). "Dependence of the thermal conductivity of nanoparticle-fluid mixture on the base fluid." Journal of Materials Science Letters **21**(19): 1469-1471.

Xie, H., J. Wang, T. Xi, Y. Liu, F. Ai and Q. Wu (2002b). "Thermal conductivity enhancement of suspensions containing nanosized alumina particles." Journal of Applied Physics **91**(7): 4568-4572.

Xuan, Y. and Q. Li (2000a). "Heat transfer enhancement of nanofluids." International Journal of Heat and Fluid Flow **21**(1): 58-64.

Xuan, Y. and Q. Li (2003). "Investigation on convective heat transfer and flow features of nanofluids." Journal of Heat Transfer-Transactions of the ASME **125**(1): 151-155.

Xuan, Y. and W. Roetzel (2000b). "Conceptions for heat transfer correlation of nanofluids." International Journal of Heat and Mass Transfer **43**(19): 3701-3707.

Xue, L., P. Keblinski, S. Phillpot, S. Choi and J. Eastman (2003). "Two regimes of thermal resistance at a liquid-solid interface." Journal of Chemical Physics **118**(1): 337-339.

Xue, L., P. Keblinski, S. Phillpot, S. Choi and J. Eastman (2004). "Effect of liquid layering at the liquid-solid interface on thermal transport." International Journal of Heat and Mass Transfer **47**(19-20): 4277-4284.

Xue, Q. and W. Xu (2005). "A model of thermal conductivity of nanofluids with interfacial shells." Materials Chemistry and Physics **90**(2-3): 298-301.

Yamada, S., M. Wada and I. Chibata (1978). "Effect of high oxygen partial-pressure on conversion of sorbitol to sorbose by acetobacter-suboxydans." Journal Of Fermentation Technology **56**(2): 29-34.

Yang, J. D. and N. S. Wang (1992). "Oxygen mass-transfer enhancement via fermenter headspace pressurization." Biotechnology Progress **8**(3): 244-251.

Yang, Y., Z. Zhang, E. Grulke, W. Anderson and G. Wu (2005). "Heat transfer properties of nanoparticle-in-fluid dispersions (nanofluids) in larninar flow." International Journal of Heat and Mass Transfer **48**(6): 1107-1116.

Yoshida, F., T. Yamane and Y. Miyamoto (1970). "Oxygen absorption into oil-in-water emulsion: A study of hydrocarbon fermentors." Ind. Eng. Chem. Process Des. Develop. **9**(4): 570-577.

Yu, W. (2003). "Stable and highly conductive nanofluids - experimental and theoretical studies." The 6th ASME-JSME Thermal Engineering Joint Conference.

Yu, W. and S. Choi (2003). "The role of interfacial layers in the enhanced thermal conductivity of nanofluids: A renovated maxwell model." Journal of Nanoparticle Research **5**(1-2): 167-171.
Yu, W. and S. Choi (2004). "The role of interfacial layers in the enhanced thermal conductivity of nanofluids: A renovated hamilton-crosser model." Journal of Nanoparticle Research **6**(4): 355-361.
Zhang, W., Z. H. Li and F. A. Agblevor (2005). "Microbubble fermentation of recombinant pichia pastoris for human serum albumin production." Process Biochemistry **40**(6): 2073-2078.

8 APPENDIX

8.1 Nanoparticle Volume Fraction and Mass Fraction

8.1.1 Oleic Acid-Coated Nanoparticles

The mass fraction of nanoparticles in the experimental samples is determined by drying 5 samples of nanoparticle solution and measuring the wet and dry weight. The determination of the corresponding volume fraction in aqueous solution is made from knowledge of their elemental composition. A sample of dried particles was sent for analysis to *Desert Analytics* and showed the following elemental composition:

%C	*%H*	*%S*	*%Fe*
20.79	3.03	0.05	42.08

from which it can be estimated that the particle is composed of 58.3% magnetite, 18.74% oleic acid and 22.92% Hitenol BC. The magnetite core has a diameter of 7 nm, the oleic acid coating has a thickness of 2.5 nm and the Hitenol BC coating has a thickness of 4 nm approximately. The corresponding volume fraction of the magnetite core in one nanoparticle is 0.04, with a density of 5.3g/mL. The remaining volume fraction of 0.96 corresponds to oleic acid and Hitenol BC. A single nanoparticle will contain $3.74 \cdot 10^{-19}$ g of Hitenol BC and $3.05 \cdot 10^{-19}$ g of oleic acid, which will give an average density of 0.389g/mL for the coating around the nanoparticle. This is a reasonable number considering that the PEO chains in the Hitenol BC coating, which occupy most of the hydrodynamic volume of the particle, are highly solvated. Overall, this gives an average density for the particle 2.57 times lower than that of water. Therefore, the relationship between volume and mass fraction for oleic acid-coated nanoparticles is $\phi_{\text{volume}} = 2.57\phi_{\text{mass}}$

8.1.2 PPO-PEO-Coated Nanoparticles

While the 20 nm oleic acid-coated nanoparticles are single domains with one magnetite core, the 80 nm PPO-PEO-coated nanoparticles are fractal clusters formed by several domains. The polymer coating around each magnetite domain is 7.5 nm thick, which gives a diameter of the fractal core equal to 2a-15, where *a* is the particle radius. With a

fractal dimension of 2, the fraction of the cluster that is magnetite can be estimated as

$$\phi_{\text{magnetite,fractal}} = \frac{7.5}{2a-15}\left(\frac{2a-15}{2a}\right)^2$$

from which the volume fraction of nanoparticles in the medium can be estimated as the ratio of the magnetite volume fraction in the media to the magnetite volume fraction per cluster

$$\phi_{\text{np,volume}} = \frac{\phi_{\text{magnetite}}}{\phi_{\text{magnetite,fractal}}}$$

which renders the following relationship between mass and volume fraction for PPO-PEO-coated nanoparticles

$$\phi_{\text{volume}} = 1.86\phi_{\text{mass}}$$

9 PhDCEP CAPSTONE – COMMERCIALIZATION OF A NOVEL ANTIMICROBIAL PEPTIDE-DESIGN TOOL

EXECUTIVE SUMMARY

Background: Researchers at the Stephanopoulos laboratory at MIT have developed a novel peptide design method that can be used to generate thousands of Antimicrobial Peptides (AmPs) with a high probability of having antimicrobial activity at clinically relevant concentrations. The method allows exploration of a very large sequence space in comparison to current approaches, because it is not limited to natural sequences. Some further development could transform this proof of concept into a commercial drug discovery tool.

Unmet Need: There are 2 million cases per year of hospital infections in the US. These infections result in 20,000 deaths per year and double the mortality risks for Intensive Care Unit patients. Critical care patients are at a very high risk of contracting pneumonia, which causes 135,000 infections per year in the US. Most strains of pneumonia and *Staphylococcus aureus* are currently resistant to penicillin and methicillin respectively. Consequently, there is a critical need for new antibiotics that do not elicit bacterial resistance. This need is especially urgent for antibiotics against Gram-negative infections and for multi-drug resistant organisms. AmPs are the most promising compounds available that can address the pathogen resistance challenge.

Commercialization Strategy: An appropriate commercialization strategy for the innovation would be a hybrid model whereby initially, a partnership is sought to perform contract research on another company's drug candidates using the existing technology platform. The early revenues obtained from the collaboration and from government grants are used to fund the validation of the technology platform. The expertise and credibility gained through the collaboration is then leveraged to obtain a higher valuation in a first round of investment. Once the technology is validated, the focus is shifted towards the internal development of drug candidates through the preclinical stage and possibly Phase I clinical tests. Thereafter, partnerships with pharmaceutical companies are sought. Partners are chosen on the basis of their ability to help navigate the

complicated FDA approval process, and provide marketing and sales expertise once a drug gets approval.

Organizational Structure: The technology platform should be validated by the team currently managing SteriCoat Inc., a company spun from the Stephanopoulos and Langer labs at MIT that develops AmP-coated medical devices. The SteriCoat team has already established the proof of principle around the technology platform; with one more year of experimentation, several key risks associated with the technology could be mitigated. Following this, a first round of investment could be obtained. The current SteriCoat team would have the wrong skill set to continue the development at this stage. An expert management team in drug development should then be hired and the business should be spun off from SteriCoat Inc. This new management team should identify and pursue the best therapeutic application for the technology. The downside of this proposed organizational structure is that the SteriCoat founders have to surrender the control of the technology platform. The upside is avoiding insufficient resources and lack of focus in developing the two businesses in parallel, which could lead to doing a poor job at both.

ACKNOWLEDGEMENTS

SteriCoat's team members Joel Moxley and Chris Loose gave me the opportunity to collaborate in this exciting project, and have provided me with access to information sources and valuable advice. Tanguy Chau, a PhDCEP student in the Stephanopoulos lab, has contributed to the compilation of competitive intelligence data.

I thank professor Michael Zasloff (Professor of Surgery and Pediatrics, Georgetown University, and founder of Magainin Pharmaceuticals, Inc.), professor Frank Douglas, (Executive Director of the MIT Center for Biomedical Innovation), and professor Rebecca Henderson (George Eastman Kodak LFM Professor of Management) for taking the time to meet with me and providing helpful insights.

Through informal conversations, Daphne Zohar (CEO, PureTech Ventures), Kevin Pojasek and Eric Elenko (senior associates, PureTech Ventures), and Robert Bitterman (President & CEO, Cutanea Life Sciences), have also contributed helpful insights.

9.1 Background

9.1.1 What Are Antimicrobial Peptides (AmPs)?

AmPs are one of nature's most ancient ways of combating bacterial infections. [1] These molecules are produced by animals, plants, and certain bacteria. They have a high affinity for the bacterial membrane because of its positively charged groups and hydrophobicity. This allows these peptides to kill bacteria by disrupting their membrane. Bacteria cannot completely change the properties and structure of their cytoplasmic membrane [1], which makes them less likely to develop resistance to AmPs.

Bacteria have evolved resistance mechanisms against some peptides, but not all. For example, bacteriocin-producing bacteria show resistance to the peptides they produce, which enables them to out compete other microorganisms. [2] The mechanisms of resistance evolved by bacteria include proteolytic cleavage, production of external AmP-binding molecules, AmP-specific drug exporters, alteration of the electrostatic properties of the bacterial cell surface, and biofilm formation, among others. [1]

Yet, despite these mechanisms of resistance, AmPs have remained a remarkably successful strategy for the inhibition of growth of microorganisms. This is intriguing given how effective bacteria are at building resistance against modern antibiotics. [1] Nature has evolved some ways to circumvent bacterial resistance to AmPs, such as protease-resistant AmPs, or the combination of several antimicrobial mechanisms in one molecule. While many bacteria have developed resistance to a specific mechanism, none has developed resistance against all mechanisms.

9.1.2 The Therapeutic Use of AmPs

The clinical value of AmPs has not been yet fully proven. While they are the most innovative new family of antibiotics that has been developed in the last two decades, the only clear clinical success to date in the area has been the lipopeptide daptomycin (marketed in the US by Cubist Pharmaceuticals under the trade name Cubicin), which acts against multidrug resistant Gram-positive organisms. Daptomycin is similar to AmPs (it has a pore forming/ion leakage mechanism) but it is not strictly an AmP, but a

lipopeptide. Several other peptides are in clinical trials. Table 9-1 shows a list of AmPs in commercial development..

Table 9-1. Antimicrobial peptides in development [3], [4]

Compound	Company	Stage of development
Talactofeerin	Agennix	Phase II
hlF-1-11	AM-Pharma	Phase II
CSA-13	Ceragenix	Preclinical
Locilex	Genaera	Complete, rejected by FDA
HB-50, HB-107	Helix Biomedix, Inc.	Preclinical
IMX942	Inimex	Preclinical
NA	Lytix Biopharma AS	Preclinical
MBI-594, MX-226	Migenix	Phase IIIb, Phase II
Mersacidin	Novacta Biosystems, Ltd.	Preclinical
NA	Novobiotics	Preclinical
Plectasin	Novozymes A/S	Preclinical
PAC113	Pacgen	IND approved
113D	Par Advance Tech., Inc.	Preclinical
PTX001 to PTX007	PepTx	Preclinical
NA	Polymedix	Preclinical
Neuprex	Xoma	Phase III
CZEN-002	Zengen	Phase IIb

The main impediments that have prevented the clinical success of AmPs are their high cost of manufacturing, their short half-life in the human body (they get quickly degraded by proteases), and more generally, the lack of understanding of the pharmacodynamics and pharmacokinetics of these compounds when administered systemically.

9.1.3 Advantages of AmPs Over Traditional Antibiotics

Several characteristics of AmPs make them attractive compounds for commercial exploitation as antibiotics. First and foremost, bacteria are less likely to develop resistance against them. Second, AmPs exhibit a broad activity spectra against both

Gram-positive and Gram-negative bacteria, and can kill multi-drug resistant bacteria at concentrations similar to traditional antibiotics. [3] Third, they kill bacteria very rapidly, through a mode of action that is bactericidal (as opposed to simple growth inhibition), and that can target several bacteria at the same time. Finally, they can be used alone or in combination with existing antibiotics to increase their efficacy.

9.2 Description of the Business

9.2.1 The Company. SteriCoat Therapeutics?

Chris Loose and Kyle Jensen in the Stephanopoulos laboratory at MIT discovered that AmPs contain many semi-conserved motifs in their primary sequence.[5] They hypothesized that these motifs could be arranged in novel ways to produce active AmPs. They then were able to prove that the new, non-natural peptides synthesized by manipulation of these motifs were active against a range of Gram positive and Gram negative bacteria *in vitro*. Almost 50% of the newly designed sequences had moderate antimicrobial activity at clinically relevant concentrations (256 μg/ml or better), and 2 out of 40 leads generated had high activity (in the range of 2-16 μg/ml). It is hoped that a bigger screen and more optimization would quickly lead to many molecules with activity at 4 μg/ml or below. A patent application was filed and the method was recently featured in *Nature*. [5] One of the advantages of this design method is that it allows exploration of a very large sequence space in comparison to the space covered by current approaches, which is limited to natural sequences.

This new method can be used to generate thousands of AmPs, which could then be screened against clinically relevant bacteria and assayed for toxicity. The inventors believe that some further development could transform this proof of concept into a commercial drug discovery tool.

Chris Loose is a co-founder of SteriCoat Inc., a startup from the Stephanopoulos and Langer labs that will produce AmP-coated medical devices to treat infections associated with implants and catheters. The SteriCoat team, which initially included Chris Loose (Chief Technology Officer), David Lucchino (Chief Executive Officer), and Joel Moxley

(Chief Operations Officer), and the staff is currently growing, has been involved in obtaining a strong IP position around this invention. The next step for the team, and the focus of the present study, is to formulate a commercialization strategy for the technology.

The team will also need to decide whether this technology can be pursued best under SteriCoat's roof, as a therapeutics division, or whether it should be pursued as an independent business. On the one hand, it is clear that the invention has a direct application to SteriCoat's main line of business: newly synthesized AmPs could be tethered to medical devices using SteriCoat's coating technology. Furthermore, there are clear people synergies in having the inventor of both technologies (the coating method used by SteriCoat and the peptide-design tool described in this work) work directly on their development. On the other hand, the medical device business currently pursued by SteriCoat and the drug discovery business are quite different; they require different assets and skills. The lack of focus in trying to pursue the two innovations in parallel could be detrimental to SteriCoat, which is currently focused on developing medical devices only.

9.2.2 The Need

During the past 40 years only three new classes of antibiotics have been discovered, and all of them targeted Gram-positive bacteria. Because the use of existing antibiotics has inevitably lead to the emergence of resistant bacteria, there has been a continuing need for new types of antibiotics. The pharmaceutical industry has attempted to meet this need by making iterative, synthetic modifications to existing antibiotic families, most of which were discovered half a century ago. [6]

According to the Centers for Disease Control and Prevention, there are 2 million cases per year of nosocomial infections in the US. This type of infections results in 20,000 deaths a year and double the mortality risks for ICU patients. Catheter-related infections cause 70,000 deaths per year. Critical care patients are at a very high risk of contracting pneumonia, which causes 135,000 infections per year in the US; unfortunately nearly 30% of the pneumonia strains are currently resistant to penicillin. [7] Similarly, most strains of *Staphylococcus aureus* are becoming resistant to methicillin. There is a critical need for new antibiotics that do not elicit bacterial resistance. This need is especially

urgent for antibiotics against Gram-negative infections and for multi-drug resistant organisms. [8] Gram-negative pathogens such as *Acetinobacter* and *Pseudomonas* are the highest concern among medical specialists because there is no effective treatment against them. [9]

9.2.3 Previous Failures and One Success

Several failures have influenced heavily the commercial outlook of AmPs, leading to the disappearance of a number of startups and a generalized skepticism among investors and professionals of the pharmaceutical industry alike. Magainin Pharmaceuticals, founded by professor Michael Zasloff,[2] did not get approval from the FDA for an AmP for the treatment of infected diabetic foot ulcers. In a very controversial ruling, its lead compound was found to be no more efficacious than existing treatments. IntraBiotics Pharmaceuticals abandoned the clinical trials for its peptide Iseganan and is now facing extinction. PPL Therapeutics, which had worked on transgenic methods for production of peptides decided to sell its intellectual property. [10] Some industry experts are skeptical about the future of AmPs because, although they have shown promise as antimicrobials without eliciting resistance, its understanding has not improved significantly.

The only success story to speak of in the field of AmPs is the market introduction of Cubicin (daptomycin) by Cubist Pharmaceuticals. Cubist licensed this molecule from Eli Lilly in 2003 and by 2006 had turned it into a business with sales of $190 million a year.[10],[11] In December 2005, ziconotide (Prialt) was approved for the treatment of severe chronic pain, but limited to the treatment of patients that do not tolerate morphine.

9.3 Opportunity and Market Overview

9.3.1 The Global Market for Therapeutic Peptides

Therapeutic peptides have found applications in oncology, cardiovascular diseases, infections, metabolic diseases, and central nervous system disorders. The global market for therapeutic peptides is currently estimated at $1 billion. [12] The US accounts for 65% of the market, Europe for 30% (mainly led by Germany and the UK), and Japan

[2] Prof. Zasloff, who is one of the leading experts in AmPs, will be joining the advisory board of SteriCoat

accounts for most of the Asian market. It is expected that this market will grow at around 10.5% a year until 2010. [12] Currently, there are over 40 peptides marketed worldwide, 270 in clinical phases, and nearly 400 in advanced preclinical phases. The group of approved peptide drugs includes vancomycin, oxytocin, and cyclosporine among others.

Within infectious diseases, the fastest growing segments are antivirals and antimicrobials. The proof of concept for the technology analyzed in the present work focused on infectious bacterial agents, which constitute a very urgent market need. While not necessarily the most lucrative long-term market, this market would likely adopt novel, safe and efficacious therapeutic peptides quickly.

Oncology, which initially would not be a business target, is the largest segment of the therapeutic peptide market. It accounts for 60% of the European market (similar data for the US is not available), followed by cardiovascular diseases (15%), infections (10%), metabolic diseases (10%), and central nervous system disorders (5%). Eli Lilly & Co., which has a strong focus on diabetes, and Roche have been very active in the therapeutic peptide market

9.3.2 The US Market for Critical Care Antibiotics

The US market for critical care antibiotics is $3.14 billion and is growing at 4% per year. Nearly 5 million prescriptions for critical care antibiotics are written annually, at an overall average daily cost of $62.5 per prescription. [7]

Four main families of antibiotics account for 75% of the market. These four families include the Cephalosporins (a beta-lactam antibiotic), which account for 29% of the US market for critical care, and have grown marginally in recent years. Their growth, and that of Penicillins (another beta-lactam antibiotic), which account for 15% of the market, will remain stagnant because there are no new drugs in the respective pipelines. Quinolones have taken market share from Cephalosporins and today account for 33% of the market. It is estimated that they will continue to grow at 7% since promising products are in the pipeline. Carbapenems account for 8% of the US market but are the family that is growing fastest, at 11%. [7] AmPs constitute a new family of antibiotics, and their market size is largely determined by the sales of Cubicin. Today, they account for less than 1% of the critical care antibiotics market.

9.3.3 Antibiotics: a Good Business?

The global market for oral antibiotics is $25 billion, of which the US accounts for $8.5 billion. [13] The large market size, combined with the growing antibiotic resistance problem and the threat of bioterrorism has fueled demand for new antibiotics. However, several forces are acting to oppose growth of this market, the most important of which are uncertainty around regulations and the inability of incumbents of obtaining good margins on their products. A summary of pros and cons of the antibiotics business is shown in Table 9-2.

Table 9-2. Pros and cons of the antibiotics business

Market Upside ↑	Market Downside ↓
Large market size: oral antibiotics market is $25 B	Success may limit opportunities (effective antibiotics may be put in restricted drug list)
Federal Incentives for antibiotic research; Bioterrorism grant money available, SBIR	"Me-too" = low returns (affects reimbursement policies, limits ability to achieve good returns)
Clear rules for approval (↓ regulatory risk)	Regulatory issues: possible change of standards? (retrospective changes to superiority trials, scare investors)
Short clinical trials (<10 years), easy patient recruiting (non-inferiority trials), and small number of patients needed for trials	Few marketing/sales partners (Big Pharma left)
Scientific risk known early, minimize time to failure (great if seeking VC investment)	Low confidence on computational tools for new target identification (genomics, bioinformatics, high throughput)
Pharma retreated from the market (<$1B)	

On the upside, the main market drivers, along with the large market size, are

- Government incentives for pursuing research in the area

- Clear rules for approval (at least until recently), which provide a clear path for developing new compounds. As a result, regulatory risks are lower than with drug development in other therapeutic areas.

- Shorter clinical trials with unambiguous endpoints. As stated by an expert in the area "Basically, the drug either kills the bug or not, and subsequent questions deal only with safety and the most appropriate dose and treatment schedule"[13]. As a result, human clinical trials tend to be shorter than for other types of drugs, and the total time for a drug to reach the market is generally under 10 years. Furthermore, patient recruiting for trials is easy because the FDA only requires (at least until recently) non-inferiority trials.

- Scientific risk is known early because the clinical trials are shorter. As a result, time to failure can be minimized, which makes this type of investment more attractive to venture capital.

- Big pharma retreated from this market because the typical antibiotic product does not have the potential to become a blockbuster, *i.e.,* to have more than $1 billion in sales. [13] For example, the best selling antibiotic, Pfizer's Zithromax, had revenues of $2.01 billion in 2003. This is far from blockbusters used to treat chronic diseases, which are taken for life (*e.g.*, Pfizer's Lipitor had sales of $9.23 billion in 2003). Companies that left the market include Sanofi-Aventis and Bayer. This opened up the opportunity for small biotech companies to compete for lucrative niches.

On the downside, the key restraints for the development of this market are:

- The success of an antibiotic may in fact limit its opportunities. If a new antibiotic is very effective, hospitals may decide to put it in a restricted drug list and only use it as a last line of defense when all else fails. This limited use makes it very difficult for a company to make profits on its drug.

- Possible regulatory changes. The FDA is considering proposing placebo-based clinical trials or superiority trials instead of the current standard of non-inferiority

trials. This would make it more difficult for an antibiotic to satisfy an efficacy endpoint in a clinical trial. [13]

- Reimbursement policies limit the ability to achieve large returns. Most antibiotics are small modifications on existing families of compounds and reimbursement agencies tend to place them under "me-too" categories that offer low reimbursement rates. [13]

- Lack of partners for clinical trials, marketing and sales activities. The exodus by Pharma companies has opened many opportunities for small biotech firms, but at the same time has left a void in expertise in downstream activities such as marketing and sales. This makes it difficult for small companies to find partners that can give them resources to support costly clinical trials or access to distribution channels.

- Computational tools have underdelivered in drug discovery. Genomics, bioinformatics, and high-throughput screening approaches have provided very few leads for antibacterial drugs. [13] Some companies are returning to traditional approaches involving evaluation of natural products and chemical modifications.

AmPs have the potential to address two of the main key restraints of the antibiotics market. Since they do not elicit significant bacterial resistance, there would be no reason for doctors to limit their use by putting them in restricted lists. Furthermore, since they would constitute an entirely new class of antibiotics, they would most likely receive a more generous reimbursement by the reimbursement agencies.

9.4 Product Offering

9.4.1 Technology Platfrom

The technology platform[3] at the core of this business opportunity is a novel method to synthesize peptides with desired properties. One of these properties can be antimicrobial activity. The method identifies motifs associated with a certain characteristic of interest, such as antimicrobial activity, by applying a pattern recognition procedure to a database of peptides. The method can then be used to generate new, non-natural peptide sequences that incorporate the patterns associated with the characteristic of interest.[5] The novel peptides synthesized by the method have a very high probability (~50%) of being active against bacteria, and the number of new peptides that can be synthesized is only limited by the available equipment (*e.g.,* peptide synthesizers) and manpower. Since any given compound needs to satisfy many criteria to become a drug, having access to an essentially unlimited pool of peptides that are likely to have antimicrobial activity increases the odds of success.

This technology platform can be monetized in several ways. First, novel peptide leads that show promise can be developed through internal programs or outlicensed to pharmaceutical or biotechnology companies. Second, the platform can be used to optimize existing peptide-based drugs or drug candidates from other companies. Third, the database of old and newly synthesized compounds with known efficacy against bacteria could be quickly scanned to respond to a bioterror threat.[11] Lastly, the IP around the technology platform could be licensed out to third parties that do not compete in the same space.

9.4.2 Stage of Development

The inventors have established a proof of concept around using the peptide design method to impart antimicrobial activity to new sequences. They designed over 40 sequences, 50% of which were moderately active against both Gram positive and Gram

[3] What is usually meant by the term "technology platform" is an IP-protected invention, frequently developed in an academic setting, that makes possible the development of other products. The technology platform itself is not a product, but enables discovery of new products.

negative bacteria, and 2 out of 40 of which had activity at clinically relevant concentrations. Table B in the Appendix summarizes data on the minimum inhibitory concentrations of the designed AmPs on different Gram positive and Gram negative microorganisms.

The next stage of development will involve characterization of the toxicity of the new peptides. This information will be used to identify patterns associated with toxicity, which will then be incorporated into the design method. This will enable the method to yield increasingly safer compounds. [11]

9.4.3 Initial Market

The antibiotics market will be an appropriate initial market for the following reasons:

First, the technology platform has already proven effective at generating large numbers of effective leads *in vitro.* The approach, however, does not incorporate yet parameters that are essential for *in vivo* activity. This makes this technology a better fit for antiinfectives (as opposed to chronic diseases, for example), because once a compound has proven effective against a pathogen, it is likely that it will also be effective against this same pathogen *in vivo*. Once a compound has shown efficacy against pathogens in animal models, the path to market is more straightforward than in other therapeutic areas. For this reason, companies developing antibacterials can be more attractive to investors, than, for example, companies developing cancer drugs. Of course, efficacy alone is not enough; the compounds must also be non-toxic and have favorable pharmacokinetics – as is the case in any other therapeutic area.

Second, there is an urgent, unmet need in the antibiotics market. An AmP against multidrug resistant pathogens would not be an incremental improvement, but rather a must-have breakthrough drug that reimbursement agencies would most likely support.

9.5 Customers

9.5.1 Key End-User Groups

Users will include hospital in-patients and healthcare providers. Hospital in-patients groups will need the product in the Intensive Care Unit, in critical care, dialysis, treatment of infections, surgery, and intravenous nutrition. Healthcare providers, including specialists, physicians, surgeons, and nurses, will adopt AmP-based drugs because bacteria are less susceptible to develop drug resistance against them. AmPs would alleviate the pressure on hospitals to monitor infections from resistant pathogens and reduce their liability.

9.5.2 Customer Access

Critical care antibiotics are generally distributed directly to hospitals. Wholesale distribution is done through manufacturers and hospital pharmacies. [7]

9.6 Business Strategy

9.6.1 Possible Business Models

The motif discovery technology platform can be commercialized using a variety of business models. Figure 9-1 presents a number of the options available, from simply licensing the technology upfront to becoming an integrated company that develops, manufactures, and sells its own drugs. A multitude of variants of each of the options presented in Figure 9-1 exists in the marketplace. At a basic level, the choice of a specific business model involves a tradeoff between the risk that the company is willing to bear and the amount of value it expects to capture[4]. The choice of a business model should be guided by the existing IP position and by the complementary assets (technological assets, people assets, marketing & sales assets, etc) owned by the company. Since most companies do not own all the assets necessary to bring a drug to the market, it will generally be the case that only a few of the options presented in Figure 9-1 are sensible

[4] "Value capture", as used in business strategy argot, refers to the fraction of the value created that a business manages to retain for itself. The remaining portion of the value is captured by the competition and by the rest of participants in the value chain. For example, licensing a technology early on bears a much lower risk than developing a drug and taking it through the FDA approval process. However, a company

choices. It is also often the case that the optimal business model evolves and changes as a company grows, since the company can acquire new complementary assets.

Licensing: Licensing is typically pursued for innovations developed in academic labs, since the complementary assets do not have to be developed or bought. While licensing is a component of many hybrid models that are being pursued by companies in the AmP and antiinfectives space, it rarely is the case that a company licenses only its core technology. In general, licensing is sought on proof of concept products.

Life Science Technology Company (LSTC): LSTCs in the AmP space can be built around IP (IP around technology platforms or IP around compounds), products, and services (*e.g.*, contract research). LSTCs built around selling information (e.g., data mining) also exist but are less common. An example of an LSTC in the AmP space is Polymedix Inc., which has a computational platform licensed from the University of Pennsylvania to generate proprietary crystal structures of membrane-bound protein receptors.

Drug Development Company: Becoming an integrated drug development company from R&D to marketing and sales is an unrealistic scenario. However, in many cases, companies have started by licensing a technology or offering a service and then transitioned to a hybrid business model that includes development of their own drug candidates. Companies choose to in-license drugs to strengthen their portfolios in certain therapeutic areas (*e.g.*, Cutanea Life Sciences*)*, out-license drugs, and in some cases, sell option agreements for their IP (*e.g.*, Genaera with Dupont). Partnerships with pharmaceutical companies usually provide the startup company with immediate cash, access to expertise and resources around the FDA regulatory process, and access to distribution channels. Typically, the pharmaceutical company makes an upfront payment and attaches further milestone payments to the progress of the technology or product developed by the startup. If a product is successfully marketed, the licensor receives royalties.

---

licensing a technology that will yield a marketed drug will have to share the profits generated by the drug with its downstream partners (manufacturing, distribution, marketing, and sales).

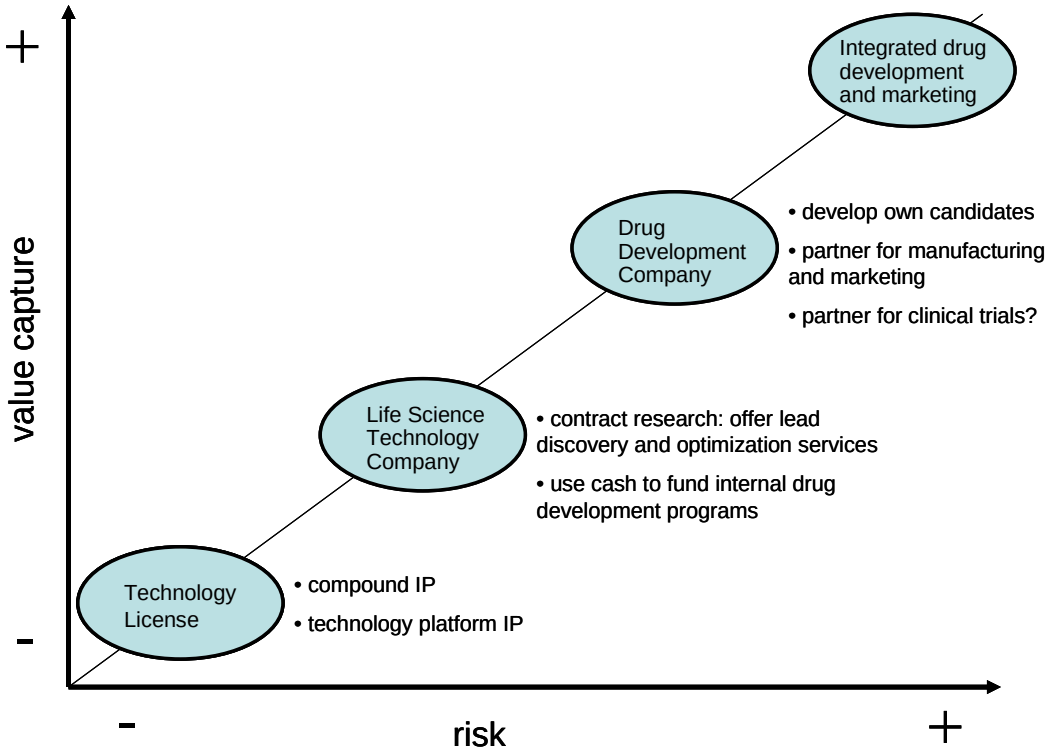

Figure 9-1: Value capture as a function of the risk incurred for several business models

9.6.2 Recommended Business Model

A suitable business model would be a hybrid model whereby:

- Initally, a partnership is seeked to perform contract research on another company's drug candidates using the existing technology platform.

- The early revenues obtained from the collaboration and from government grants are used to perform the additional experiments necessary to validate the technology platform, and to jumpstart internal development of 1 or 2 drug candidates in the antiinfectives area. The expertise and credibility gained through the collaboration is leveraged to validate the technology platform and obtain a higher valuation in a first round of venture capital funding or in an equity placement by a pharmaceutical company.

The internal drug candidates could be taken through the preclinical stage, which would involve performing absorption, distribution, metabolism, excretion, and toxicity tests in animal models. These tests typically last for approximately 1 year. Thereafter, the costs

for clinical trials may be prohibitive and it may be best to seek partnerships with pharmaceutical companies, at least for Phase III trials and possibly for Phase II as well. The partners of choice would help navigate the complicated and bureaucratic FDA approval process, and provide marketing and sales expertise once a drug was approved. It would also be necessary to seek a manufacturing partner. Peptide manufacturing is a relatively competitive business, and therefore it should not be excessively difficult to obtain good terms in a partnership. Since the competitive advantage of the technology is not related to the manufacturing process of the peptides, granting the manufacturing rights to an outside party should not be a major cause of concern.

The following support the choice of this business model:

- First, the inventors have already been approached by a pharmaceutical company interested in using the technology platform to optimize one of its products. A research contract with this company not only would offer early access to cash, but would also be an ideal showcase for validating the technology platform. It is likely that investors such as venture capitalists would assign more credibility to the platform if it were validated using somebody else's compound (they may be suspicious of a platform validated using one's own compounds, since these could have been carefully selected to portray the technology in the best possible light). On the downside, exclusivity issues would have to be dealth with carefully, and the the two parties would need to agree clearly on what terms would establish the termination of the collaboration.

- Second, the current source of competitive advantage is the IP around the peptide design platform. This asset can be leveraged best in the preclinical R&D operations. The company does not have the complementary assets needed to bring a drug through clinical trials and to the market; it would be necessary to rely on other parties.

9.6.3 Technology Platform vs. Product

Why not stay purely as a technology platform, as opposed to venturing into drug development? It makes sense to start purely as a technology platform doing contract research for pharmaceutical clients, since this is the main source of competitive

advantage and the team has no expertise in drug development. However, in the long term, contract research platforms have rarely worked as a standalone business. [14] Furthermore, since early-stage drug development is very risky, investors place very low valuations on early stage drug development companies with a technology platform unless they have a product in clinical trials. Capital markets, finding it difficult to compare and valuate different platforms, have become fixated on clinical trials as a valuation metric for progress; as a result, the valuation assigned to enterprises has become largely a function of the net present value of its leading drug candidates. [15] Furthermore, pharmaceutical companies have, by and large, stopped doing collaborations with startups that have technology platforms but no products.

9.6.4 The First Partnership

Ideally, the first partnership could be in place this year if the ongoing conversations with a pharmaceutical company are formalized. The partner would most likely offer an upfront payment to cover the research costs in exchange for services to optimize one of its compounds. Although it is unlikely that royalties on the drug could be obtained, [8] the partnership would still offer an attractive avenue to validate the technology platform, and would constitute most of the company's operating revenue during the first years of operation. PharmOptima is an example of a company in the antiinfectives area that has supported its Gram-negative discovery program through contract research contracts with partners and also through government funds.

9.6.5 Future Partnerships

A successful collaboration with the first partner would open the possibility for further partnerships. Possible candidates could be companies in the antiinfectives area that have a major patent about to expire or companies that have had to abandon once promising peptide compounds because of unwanted side effects. In both cases, development of improved variants using the peptide design method could be an attractive option.

9.7 Competition and Competitive Advantage

9.7.1 The Competition

Several companies have peptide therapeutics development programs. Nearly half of them have a focus on antimicrobials (shown in boldface in Table 9-3). The rest have programs in cancer, inflammation, immune diseases, cardiovascular diseases, osteoporosis, artherosclerosis, and HIV. The main competitors with alternative technology platforms for the development antimicrobials are:

Ansata Therapeutics, Inc.: Ansata has an AmP technology platform to develop new therapeutics for dermatological applications. The company seeks to develop and commercialize technologies that allow drug molecules to effectively penetrate into cells and target the drugs specifically to the nucleus.

Arris Pharmaceutical: Arris develops computer-enhanced peptide therapeutics. It follows a structure-based, rational design approach which combines molecular biology, x-ray, crystallography, NMR, combinatorial chemistry and artificial intelligence.

Inimex Pharmaceuticals, Inc.: Inimex has a technology platform for the development of drug therapies that control the innate immune response. The company is currently validating is platform testing compounds in animal models.

Migenix, Inc.: Migenix develops and commercializes drugs in the areas of infectious and degenerative diseases. Its most advanced clinical program is in Phase III.

Polymedix: Polymedix's technology platform generates proprietary crystal structures of membrane protein receptors and novel drug designs that mimic proteins. Its leads are non-natural peptides that mimic the structure of magainins. Its platform has been validated showing activity of the lead compounds and satisfactory pharmacokinetics.

SelectX Pharmaceuticals, Inc.: Operates a platform technology based on combinatorial genetics, directed evolution and target screening.

Other important competitors developing antimicrobials with less of a focus on a technology platform are:

Agennix: Develops lactoferrin, a natural human protein with antimicrobial properties. The company has core clinical programs in oncology and respiratory disease, and a number of additional indications in development. Its most advanced compound is in Phase II clinical trials.

AM-Pharma: Develops lactoferrin-based peptides. The company operates in the segments of lipopolysaccharide -mediated diseases and infections of viral, fungal and bacterial origin.

EntoMed SA: Develops insect-derived AmPs.

Genaera Corporation: Develops therapeutic products for the treatment of infectious diseases by isolating therapeutic compounds from animals.

Novozymes A/S: Has isolated and developed the peptide plectasin from a fungus. This peptide has shown promise for the treatment of systemic infections.

Pacgen Biopharmaceuticals: Develops innovative peptide therapeutics the treatment of infectious diseases and immune system diseases.

Rx3 Pharmaceuticals, Inc: Applies structure-based drug design technologies to antimicrobial programs.

Xoma, Ltd.: Develops and manufactures recombinant proteins and peptides, in partnership with large pharma companies. Its most advanced compound is in Phase III.

Table 9-3. Competitors with peptide therapeutic development programs (companies in boldface have antimicrobial programs).

Company Name	Country	Status	Founded	Amount Invested ($ millions)
Agennix, Inc.	US	Active Investment	*	49.6
Alba Therapeutics Corporation	US	Active Investment	2004	42.5
AM-Pharma Holding BV	Netherlands	Active Investment	2000	13.0
Ansata Therapeutics, Inc. (FKA: Rubicon Pharm. Inc)	US	Active Investment	2002	5.5
Aphton Corporation	US	Went Public	1981	14.8
Arizona Engineered Therapeutics Inc. (aka; AzERx)	US	Pending Acquisition	2003	0.2
Arris Pharmaceutical	US	Went Public	1989	35.2
Biointerface Technologies, Inc.	US	Active Investment	1987	0.2
BioLineRx Ltd. (FKA: Bioline Therapeutics)	Israel	Went Public	2003	24.0
Celtrix Pharmaceuticals, Inc. (FKA: BioGrowth)	US	Went Public	1983	42.8
Chemokine Therapeutics, Inc. (FKA: PTM Mol. Biosys.)	Canada	Went Public	1998	1.8
Connetics Corp.	US	Went Public	1993	55.6
COR Therapeutics, Inc.	US	Acquisition	1988	20.7
Diatide, Inc. (FKA: Diatech, Inc.)	US	Went Public	1990	41.7
Digilab BioVisioN GmbH (FKA: BioVisioN AG)	Germany	Acquisition	1997	29.6
Discovery Laboratories, Inc.	US	Went Public		13.2
EntoMed SA	France	Defunct	1999	26.0
Genaera Corporation (FKA: Magainin Pharmaceuticals)	US	Went Public	1987	18.1
Immune Response Corporation (The)	US	Went Public	1986	26.9
InfiMed Therapeutics, Inc.	US	Acquisition	1998	32.0
Inimex Pharmaceuticals, Inc.	Canada	Active Investment	2001	11.6
Migenix, Inc. (FKA: MitoKor)	Canada	Went Public	1993	0.0
NanoBio Corporation	US	Active Investment		10.0
Nobex Corporation (FKA: Protein Delivery)	US	Bankruptcy - Ch.11	1993	90.5
Pacgen Biopharmaceuticals Corporation	Canada	Went Public		0.0
Pasteur Merieux Serums & Vaccins (AKA: PMs&v)	France	Acquisition		0.3
Proteolix, Inc.	US	Active Investment	2003	40.8
RedCell, Inc.	US	Acquisition	1993	10.1
Rx3 Pharmaceuticals, Inc.	US	Active Investment	2004	1.4
Schering-Plough Corporation	US	Went Public		
SelectX Pharmaceuticals, Inc.	US	Active Investment	2002	8.0
Trimeris, Inc. (FKA: SL-1 Pharmaceuticals, Inc.)	US	Went Public	1993	38.3
Westgate Biological Ltd.	Ireland	Active Investment		0.0
Xigen SA	Switzerland	Active Investment	2002	21.2
Xoma, Ltd.	UK	Went Public		

Source: VentureXpert

The average amount invested in the group of companies presented in Table 9-3 (before they went public, or to date if they are private) is $22 million. The average amount invested in the subgroup of companies focusing on antimicrobials is slightly lower, at $13.5 million.

9.7.2 Competitive Advantage

The main advantages of the technology are:

Ability to explore a much larger portion of the peptide sequence space than the competition. The approaches followed by the competitors are limited to the study of peptides encountered in nature or to incremental modifications of existing peptide sequences. As a result, the sequence space they can explore is only a minuscule fraction of all the possible combinations of aminoacids, most of which are non-natural.

Less laborious than existing methods. Current methods require laborious screening of organisms for the presence of novel AmPs. Instead, large numbers of new peptides with a high probability of efficacy can be quickly synthesized with the present method.

Ability to quickly scan a diverse library of AmPs to respond to the emergence of a bioterror threat. Many companies have a library of variants of 1 or 2 molecules, but they do not cover a very diverse space, which would be important fighting a new pathogen.

9.8 Development Plan

9.8.1 Main Risk-Mitigating Steps During Year 1

Initially, a licensing agreement with the MIT Technology Licensing Office (TLO) will be necessary in order to secure the rights to pursue the commercialization of the technology platform. The MIT TLO usually takes an equity stake, a deferred payment, and around 5% on royalties on sales.

Following the licensing agreement with the TLO, the team will complete a series of experiments directed at eliminating the risk associated with the design tool and at validating the technology platform before seeking a first round of investment (Figure 9-2). The following experiments will be funded with research grants in collaboration with the Stephanopoulos laboratory at MIT:

- Characterization of the activity of all known linear AmPs against the most clinically relevant bacterial targets. This will allow weighting of the AmPs in the motif discovery tool to favor those most likely to offer the desired activity spectra

(the work carried out to date has used as a starting point a published list of AmPs that did not include information on activity spectrum and toxicity [16]).

- Characterization of the *in vitro* toxicity of the AmPs by performing hemolysis tests on red blood cells. This will allow to filter out the motifs associated with human toxicity from the motif discovery tool

A database with increasingly powerful and selective lead sequences will be developed by incorporating the outcomes of these experiments to the motif discovery tool.

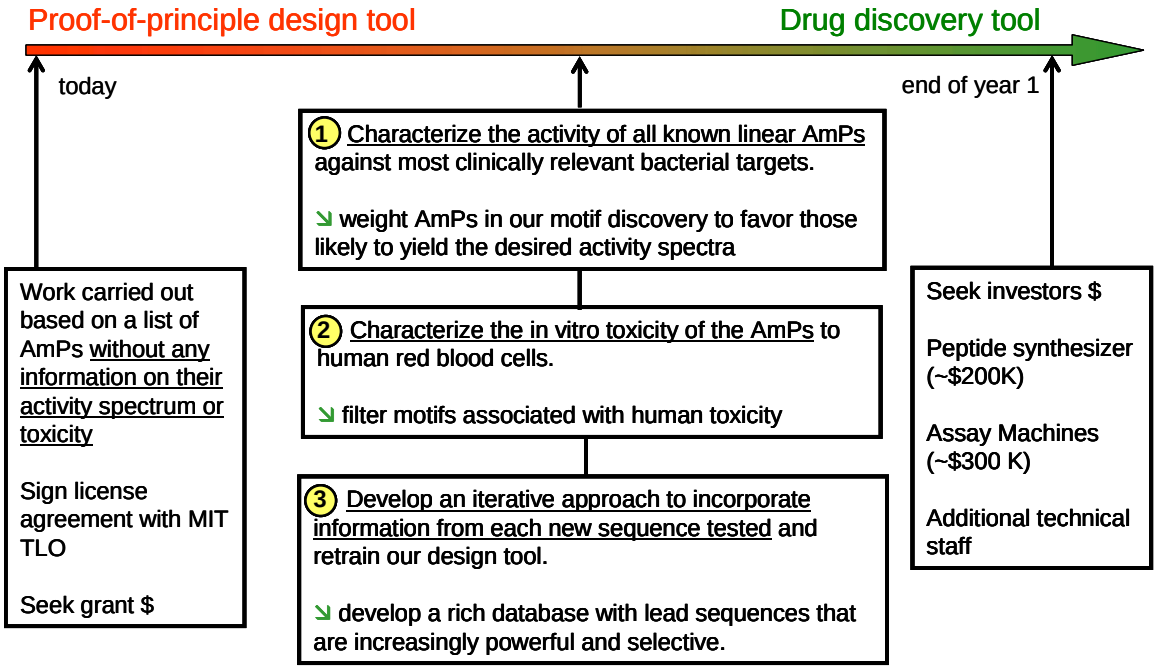

Figure 9-2: Proposed development plan for the first year of operations

9.8.2 Key Milestones after Year 1

After the risk mitigation steps proposed in Figure 9-2 are met, an injection of capital of around $1 million (500 K in equipment) will be necessary to scale up the technology platform. Assuming that at this point the platform has been validated and development on one or more drug candidates has started, it may be possible to attract a first round of investment. Revenues from a possible research contract with a pharmaceutical company

or additional research grants (*e.g.,* SBIR grants) may be a financial alternative to sustain the business. The key milestones through the next round of funding will be:

- Creating a scaled-up process that integrates all the different design, synthesis, and analysis steps, which would be capable of testing tens of thousands of sequences a year.

- Signing 2 to 3 additional corporate partnership agreements to generate leads for other companies or optimize their existing compounds.

- Hiring a management team with the necessary expertise to lead a drug candidate through the drug approval process. Hire a strong chemistry group for the internal drug development program.

- Creating a product pipeline that looks appealing to future investors. Have at least one drug candidate in clinical trials by the time a second investment round is needed. This second round of investment could come from venture capitalists or from a partner in the pharmaceutical industry (*e.g.,* Novozymes took its compound plectasin through Phase I clinical trials and then sought a partner for further development).

9.9 Risks

The most important risks that the company will be exposed to are:

Product risk: there is a risk that a drug product cannot be created. This risk is inherent to most biotechnology enterprises and part of doing business in this area. This risk is mainly driven by uncertainty around the technology. It is generally accepted [17] that the main hurdles that have prevented the success of AmPs in the past have been manufacturing, delivery, low metabolic stability, and *in vivo* toxicity:

- Manufacturing by chemical synthesis can be prohibitively expensive for large peptides. The company's technology offers the freedom to keep the peptide sequences relatively short (~20 aminoacids). Peptides of size in the vicinity of 20

aminoacids would have a cost of goods sold of approximately $400/gram when manufactured by chemical synthesis. [17]

- Delivery through patient-friendly routes has proven difficult for AmPs. Other companies have bypassed this problem by focusing on topical applications instead of pursuing a systemic or oral delivery route.

- Metabolic stability is low because peptides are degraded by a variety of proteases. Other competitors seem to be better positioned to address this issue. Lytyx and Helix Biomedix are addressing it explicitly by creating small peptides with low charge and with chemical groups that protect them from degradation.

- AmP candidates that have shown promise *in vitro* could be toxic *in vivo.* With the exception of daptomycin, despite promising *in vitro* results, AmPs have not shown good efficacy in animal models. Transforming the leads obtained with the motif discovery method into drugs that work *in vivo* will be on of the most challenging aspects of the business and will require hiring expert personnel and partnering.

Market risk: the market risk for antibiotics is inexistent because there will always be consumers that need them. However, it is still unclear what the market acceptance of AmPs will be like. It is expected that reimbursement policies for AmP-based antibiotics will be more favorable than for existing families of antibiotics, as long as they fulfill their promise of not eliciting bacterial resistance. It will most likely be the case that when AmPs are widely commercialized no resistance emerges. Experiments have shown that resistant mutants are unlikely to emerge, and when they actually emerge, they have severely decreased viability that makes them unlikely to survive. [18] However, it is still unclear whether mutants will emerge to *non-natural* peptides. Existing natural peptides do not cause new selection pressure, because the resistance mutations that could occur already occurred. [18] Slightly modified, or non-natural peptides might entail some new selection pressure. However, mutants to *combinations* of peptides, whether natural or non-natural, are very unlikely to emerge.

Partner risk: the exodus of Big Pharma from the antibiotics space has left a void in expertise in downstream activities such as marketing and sales. This will make it difficult

for small companies to find partners that can give them resources to support costly clinical trials or access to distribution channels.

Regulatory risk: the FDA is considering proposing placebo-based clinical trials or superiority trials instead of the current standard of non-inferiority trials. This would make it more difficult for an antibiotic to satisfy an efficacy endpoint in a clinical trial and would scare investors. [13]

People risk: hiring and retaining management with deep expertise in drug development will be crucial. Having access through the Scientific Advisory Board to Michael Zasloff, one of the world's experts in development of AmPs, may help establish contacts with industry professionals.

Financial risk: there is a risk that the company will not be able to secure to funding needed to complete the validation of the platform. Platform companies often have insufficient resources to develop both a product and a platform, and risk doing a poor job at both. [15] By focusing the efforts during the first year only on validating the platform, some of this risk should be mitigated.

Competitive risk: A blocking patent application on both the methodology and the range of compositions within the design space (product by process) has been filed. Still, there is an obvious risk that competitors may devise superior methods of developing AmPs.

9.10 Financing

9.10.1 Financing Strategy

Research grants will be sought to fund the first year of development at MIT, after which the team expects to have convincing data to pitch the start up opportunity to the investor community.

During the first year of operations, financing options include SBIR grants and upfront payments from contract research work. The National Institutes of Health (NIH) and the

Department of Defense (DoD) are the main supporters of antibacterial development programs.[5]

Typically, financing for technology platforms has involved the following steps: [15]

- Raise a Series A of $3 to $5 million (after transferring the technology from the academic institution where it was developed, and identifying areas for R&D).
- Raise a Series B of $15 to $20 million (after securing partnerships and collaborations and initiating internal development of drug candidates).
- Raise a Series C of $20 to $50 million, which is usually the last round before exit.

Lately, this model has changed because pharmaceutical partners and investors are no longer interested in partnering or investing until a platform has been validated. This transfers all the early risk before the delayed Series A to the company founders.

9.10.2 Exit Opportunities

Companies in the antibiotic space have realized exits both through public offerings and through acquisition. A detailed list of valuations of public, private, and acquired companies is presented in Figure 9-3 and in Table A in the appendix. Figure 9-3 shows that valuations depend strongly on the clinical phase of the company's leading drug candidate (for private companies, the valuation corresponds to the amount invested; for public companies, to the current market capitalization; for acquired companies, to the acquisition price). Figure 9-3 also shows that acquisitions in the antibiotic space are unlikely at an early stage. Possible acquirers consider early stage companies in this area too risky an investment. In general, acquirers look for target companies that have products in the market, since that can help boost their revenues right away and meet the growth expectations from their shareholders. Companies that have promising technology platforms but no product in clinical trials (*e.g.* Polymedix, Helix Biomedix, Ansata) are unlikely acquisition targets. The figure also shows that from preclinical studies to Phase

[5] Anadys Pharmaceuticals received a $1.2 million NIH SBIR grant in 2004 to develop antibacterials. In October 2006, the DoD awarded $24.7 million to Achaogen for a program to develop a treatment for anthrax

II, with few exceptions, most companies stay private, and that from Phase III onwards most companies go public. This can be due to two factors: first, public markets only place attractive valuations on companies that have eliminated most of the risk associated with clinical trials; second, in order to raise the substantial amounts of cash needed to manage Phase III trials and market a drug, companies can no longer rely on private investors and look for funding in the public markets.

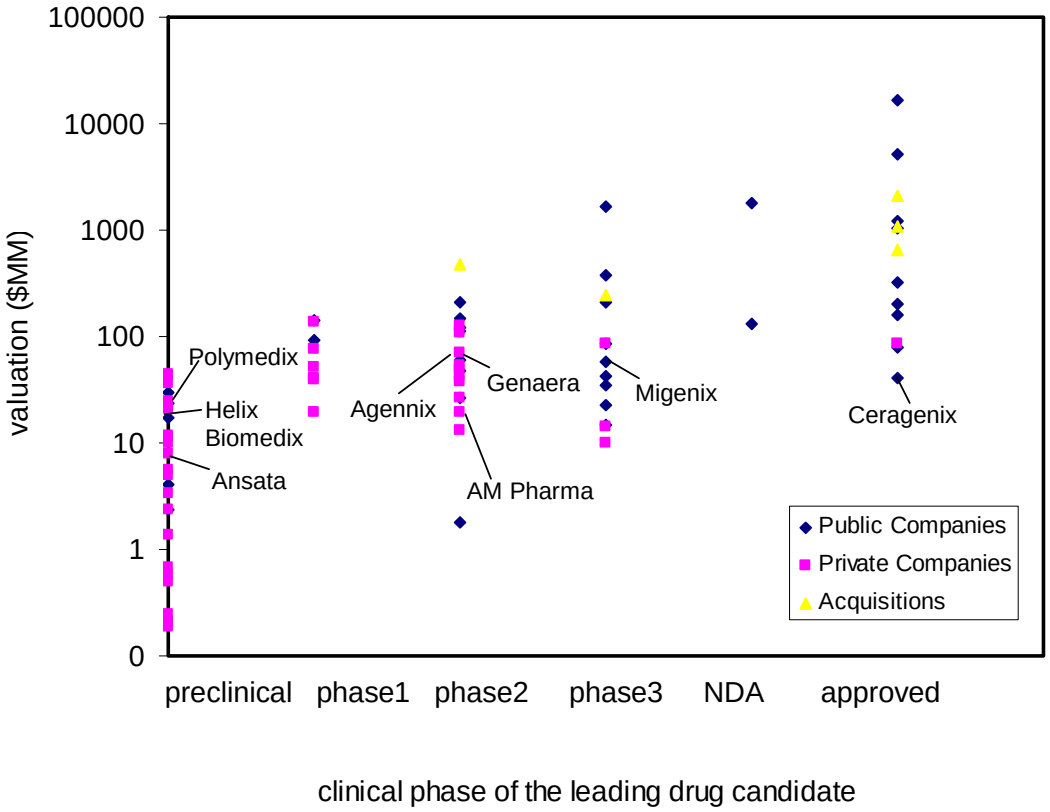

Figure 9-3: Valuations of public, private, and acquired companies in the therapeutic peptide and antibiotic spaces as a function of the clinical phase of their leading drug candidate

Exits through public offerings: Antibiotic companies that have exited through public offerings have, today, a median market capitalization value 3.5 times larger than the amount that was invested in the company before it went public (Table A in the Appendix). In other words, the most common return for private investors that kept their stock when the company went public is x3.5).

Exits through acquisition: Antibiotic companies that have been the target of acquisitions have received acquisition premiums in the range of x2.5 to x52.8. Table 9-4 shows a selection of recent acquisitions in the antibiotics space including the acquisition premium multiples (ratio of the price paid by the acquirer over the amount invested in the target company before being acquired). The multiples range from x2.5 to x52.8. The average time to exit for the group of companies presented was 7.8 years, which is on the long end for venture capital investments. However, these companies are not ideal comparables because they are not purely focused on the AmP space; however, they are the closest approximation we can get given the fact that no acquisitions of "pure-play" companies focused on AmPs have occurred yet.

Table 9-4. Selected information on acquisitions in the antibiotics space.

Target name	Acquirer name	Date announced	Phase of leading candidate	Amount invested ($ millions)	Deal value ($ millions)	Deal value / Amount invested
OraPharma, Inc.	Johnson & Johnson	11/14/2002	approved	33.9	85	**2.5**
Peninsula Pharm., Inc.	Johnson & Johnson	6/30/2005	3	88.26	245	**2.8**
Cerexa, Inc.	Forest Laboratories	1/11/2007	2	50	480	**9.6**
Connetics Corp.	Stiefel Laboratories	12/28/2006	approved	55.55	640	**11.5**
COR Therapeutics, Inc. (acquired by Millenium)	Millenium	2/12/2002	approved	20.65	1090	**52.8**

Source: VentureXpert and Internet research

Figures 9-4 and 9-5 show box plots of company valuations organized by clinical phase of the company's lead drug candidate, for both companies in the general antibiotics space and companies focusing on peptide therapeutics. Table 9-5 summarizes the statistics in Figures 9-4 and 9-5. It can be seen that, at each clinical phase, valuations on companies focusing on therapeutic peptides are substantially lower than valuations on companies focusing on the general category of antibiotics (which includes also all companies pursuing traditional, chemistry-based antibiotic discovery). It appears that both the public markets and private investors apply a discount factor to companies pursuing therapeutic peptide-based approaches, and that this discount factor gets larger as the drugs progress through the clinical phases. When the drugs are in preclinical stages, investors do not seem to differentiate between the two types and consider both just as risky (compare the mean valuations of $15 million vs. $18 million in Table 9-5). In Phase I, valuations on peptide-based drug command a 45% discount ($74 million *vs.* $41 million), in Phase II, a

67% discount ($92 million *vs.* $30 million), and in Phase III an 83% discount ($219 million *vs.* $38 million). This is consistent with the general view, held among industry professionals, that the investment community is still skeptical about the promise of therapeutic peptides – perhaps rightly so, given the lack of successes to date. Some industry professionals believe that the outlook for the therapeutic peptide business, and more specifically for AmPs, will change drastically once (or if) the compounds currently in Phase III get FDA approval. [19]

Table 9-5. Summary statistics of valuations as a function of the clinical phase of the lead drug candidate for companies in the antibiotics space and for companies focusing on therapeutic peptides

Companies in the antibiotic space

	Preclinical	Phase I	Phase II	Phase III	NDA	Approved
Sample size	32	8	19	13	2	13
Mean valuation ($ million)	15	74	92	219	971	535
standard deviations ($ million)	23	45	108	443	1186	645

Companies focusing on therapeutic peptides

	Preclinical	Phase I	Phase II	Phase III	NDA	Approved
Sample size	9	1	6	3	4	3
Mean valuation ($ million)	18	41	30	38	45	191
standard deviations ($ million)	11	NA	20	22	61	170

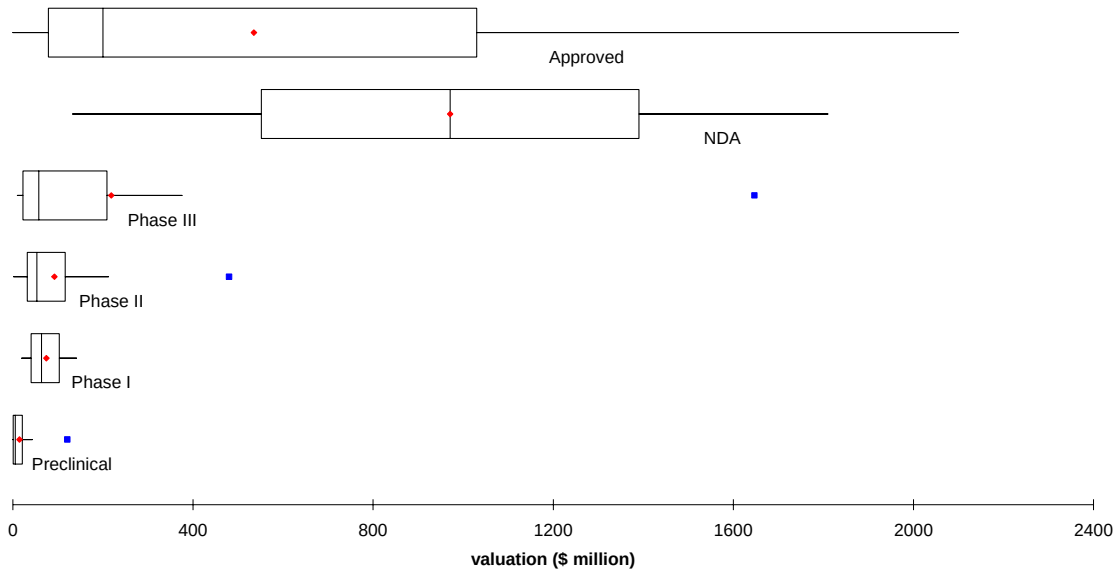

Figure 9-4: Box plots of the valuations of companies in the antibiotics space as a function of the clinical phase of their lead candidate

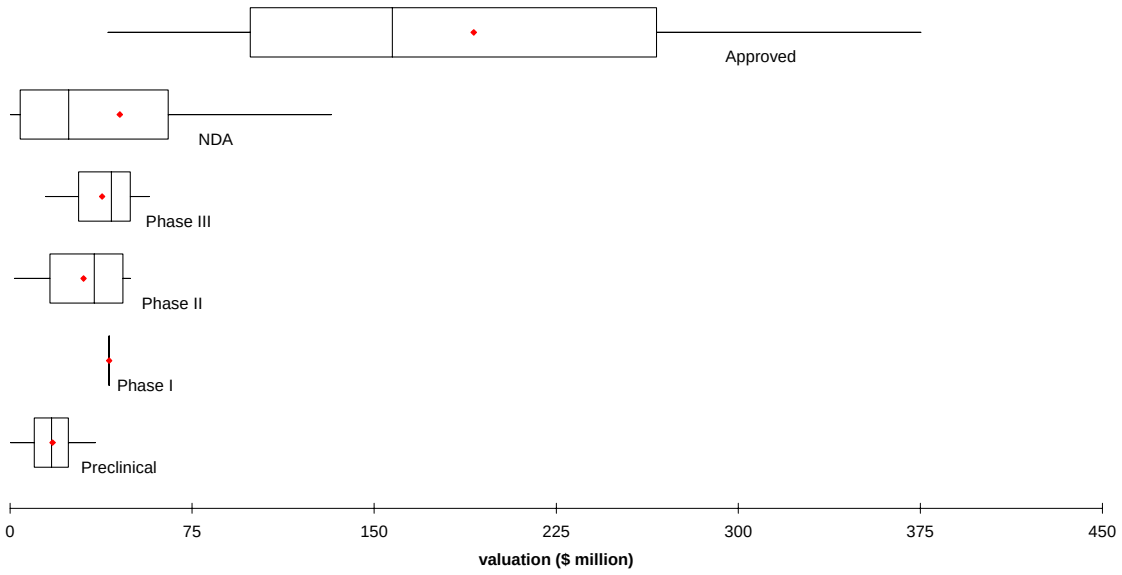

Figure 9-5: Box plots of the valuations of companies in the therapeutic peptides space as a function of the clinical phase of their lead candidate.[6]

[6] Connetics and COR Therapeutics, which were acquired respectively for $640 million and $1090 million, are not included in the chart since they had multiple other development programs that obscure the comparison

9.10.3 Who are the Likely Buyers?

The company could achieve an exit through acquisition by a market leader in the antibiotics space looking to strengthen its antibiotics portfolio, or looking to make up for lost revenues in mature products with expired patents. The key market players in the antibiotics market are Pfizer and GlaxoSmithKline (GSK). Other important players are AstraZeneca, Merck, Eli Lilly, Johnson&Johnson, Merck, and Wyeth. Both Pfizer and GSK could be potential acquirers; Pfizer dominates the market with strong products like Zyvox and Zithromax. Its merger with Pharmacia expanded its hospital antibiotics portofolio, and currently it has an important collaboration with Vicuron Pharmaceuticals. GSK ranks second in sales but many of its products are mature and facing strong pressure from generics. Since GSK's pipeline does not have any products in advanced clinical phases, GSK will be looking for acquisitions if it wants to maintain a presence in this market. Some key patent expirations that might lead to acquisition activity are presented in Table 9-6.

There is also a second tier of smaller companies that are building deep portfolios, including Vicuron Pharmaceutica, Basilea Pharmaceutica, and Cubist Pharmaceuticals, that could be possible acquirers.

Table 9-6. Key patent expirations of antibiotics

Compound	Company	Expiration
Avelox	Bayer	2009
Cipro	Bayer	2004
Levaquin	Ortho-McNeil	2010
Tequin (recalled in 2006)	GSK	2007
Ivanz	Merck	2013
Merrem	AstraZeneca	2010
Zyvox	Lytix Biopharma AS	2014
Zythromax	Migenix	2005

9.11 Go / No Go

If the main risk-mitigating development steps outlined in section 9.8 are completed satisfactorily, the opportunity to seek investment and start a business should be considered. At that point, the essential requirements to make this business successful would be in place: an urgent market need, a promising technological innovation with adequate IP protection, and a very strong team of people that have the entrepreneurial passion needed, that will be able to inspire it in others, and that have surrounded themselves with some of the World's leading experts in the field. Still, the downsides merit a sober examination (Figure 9-6):

No-go	Go
Reality test: • A multi-drug-resistant superbug epidemic has not yet hit • There are still enough traditional antibiotics that can be tweaked to meet the growing resistance problem.	When resistance becomes a real problem, there will be no issue
Incumbents have strong advantages over newcomers: • Ease of development • Toxicology knowledge	Broad, blocking patent applications on both methodology and range of compositions within design space (*Product by process)*
Remaining technological hurdles: • Manufacturing • Stability • Delivery	Have started industry dialogue Very strong advisory group and energetic team

Figure 9-6: Arguments in favor and against of pursuing the business opportunity

First, a multi-drug resistant superbug epidemic has not yet hit, and thus far pharmaceutical companies have managed to tweak the existing families of antibiotics to meet the growing resistance problem. However, the specialists predict that this will indeed become a real problem, and then there will be no issue as to whether AmPs must be developed aggressively. AmPs will not only mitigate the resistance issue, but will also enjoy higher margins in the market than conventional antibiotics because they are not "me- too" products, and can therefore benefit from higher reimbursements.

Second, large pharma incumbents have historically had strong advantages over newcomers in the antibiotics area. They have the toxicology knowledge and the

development skills to turn around new drugs quickly. Large pharma companies have gradually abandoned the antibiotics field in order to focus on the more lucrative chronic diseases, which fit better their business model. However, competition is still intense because there are a large number of smaller companies in the area (Table 9-3).

Third, several technological hurdles still remain, including high manufacturing costs, low metabolic stability of AmPs, and the need for novel delivery techniques that allow systemic administration (Figure 9-7). Although no competitor has addressed all these hurdles, some competitors have distinctively targeted some. For example, Polymedix has addressed the issue of high manufacturing cost of peptides by using cost-effective starting materials, and the issue of low metabolic stability by making small AmPs that are less prone to protease degradation. AM-Pharma and Inimex have addressed the issue of *in vivo* toxicity by stimulating the host to combat pathogens using small, non-toxic fragments of AmP analogs. The technology platform presented in this work would partly address the manufacturing issue, since the size of the non-natural peptides synthesized can be decided at will (and therefore be kept small enough to make manufacturing by chemical synthesis feasible). It is unclear whether the stability issue would be addressed; it has been suggested that non-natural sequences may be more stable to degradation. [17] It would not address the delivery issue, but this would not be a factor preventing the introduction of a product in the market (an oral antibiotic is ideal, but if need be, doctors can administer it by injection).

Problems with AmPs	Does this approach address them?
1. Manufacturing	**Partly** • Short peptides (20 aa.) can be manufactured by chemical synthesis. • Manufacturing costs for peptides are decreasing
2. Low metabolic stability	**Unclear** • Unnatural sequences may exhibit higher metabolic stability in vivo? (Latham, *Nature* 1999) • Competitors addressing it explicitly: create small peptides with low charge protected from degradation by protecting groups (Lytyx, Biomedix)
3. Delivery	**No** But delivery issues won't prevent introduction
4. Toxicity associated with size and charge	**Unclear** Can keep peptides below 20 aa. in size

Figure 9-7: Main technological hurdles restraining the progress of AmPs.

9.12 Under What Roof?

The SteriCoat team will face the decision of whether this technology should be pursued under SteriCoat's organizational structure, as its therapeutics arm, or as an independent business.

I believe the best approach would be to have the SteriCoat team manage the validation of the technology platform throughout the first year of experimentation, and then hire an expert management team in drug development and spin it off as a separate business.

Initially, there are benefits in validating the technology at SteriCoat. First, the inventors of the technology, currently managing SteriCoat, would work directly on the development. Second, the invention has a direct application to SteriCoat's main line of business: newly synthesized AmPs can be tethered to medical devices using SteriCoat's coating technology. The biggest problem with this approach is that working on validating the technology will divide the focus of the SteriCoat management team at a time when they will have their hands full with the medical device business. The alternative, however, is to expect a third party to acquire the technology and develop it, which would not bring much value to the SteriCoat founders since acquirers will not be willing to pay a good price until it is validated.

After the platform is validated, it will be best to hire an expert management team in drug development and spin it off as a separate business. This new management team should identify the best therapeutic application for the technology and pursue it. The current SteriCoat team would have the wrong skill set at this stage. Separation is convenient because SteriCoat may have insufficient resources to pursue both the medical device business and the drug development business, and risks doing a poor job at both. It is also convenient because the very high cost and complexity of developing a drug would force the drug development business to focus on one single product, [15] exposed to a high likelihood of failure in the clinical trials. If trials did fail and the two businesses had not been separated, the next round of financing would be a down round that would wash out the SteriCoat founders and put the medical device business in jeopardy as well. The drawback of separating the businesses is that the SteriCoat founders have to surrender the control of the technology platform, which might in fact have a higher upside market potential than the medical device business.

9.13 Appendix

Table A: Valuations of public, private, and acquired companies in the antibiotics and therapeutic peptides space as a function of the clinical phase of their leading drug candidate.

Company Name	Phase of leading candidate	Status	Amount Invested ($ millions)	Market Cap (for public companies) ($ millions)	Acquisition Price ($ millions)
Acambis (FKA: OraVax, Inc.)	2	Public	40.3	147.5	
Achaogen, Inc.	preclinical	Private	42.28		
Achillion Pharmaceuticals, Inc.	preclinical	Public	120.86	105.4	
ActivBiotics Canada, Inc.	3	Private	10		
ActivBiotics, Inc. (FKA: Merlin Technologies, Inc.)	2	Private	53.34		
Adaptive Therapeutics, Inc.	NA	Private	9		
Advanced Life Sciences, Inc.	3	Public	11.47	85.06	
Advanced Viral Research	3	Public		22.29	
Advancis Pharmaceutical Corp.	2	Public	99.76	112.52	
Aegis Pharmaceutical, Ltd.	NA	Private	0.36		
Affinity Biotech, Inc.	defunct	Public	1.4		
Affinium Pharmaceuticals (FKA: Integrative Proteomics, In	preclinical	Private	36.15		
Agennix, Inc.	2	Private	49.57		
AgION Technologies, Inc.	NA	Private	27.7		
Alba Therapeutics Corporation	2	Private	42.45		
Allelix Biopharmaceuticals	3	Private			
Allergan	approved	Public		16840	
Alpharma Inc. (FKA: A.L. Laboratories, Inc.)	NA	Public	0.13		
Amoebics	preclinical	Private	0		
AM-Pharma Holding BV	2	Private	12.95		
Amura Therapeutics Limited	preclinical	Private	0		
Anamax, Inc.	NA	Private	0		
Ansata Therapeutics, Inc.	preclinical	Private	5.5		
Aphton Corporation	3	Public	14.75	0.154	
Ardea Biosciences, Inc.	NA	Public	86.15		
Arizona Engineered Therapeutics Inc. (aka; AzERx)	preclinical	Private	0.21		
Arpida Ltd.	3	Public	99.09	209	
Arris Pharmaceutical	preclinical	Acquisition	35.15		
Ash Access Technology, Inc.	NA	Private	15		
Athelas SA (Merge w/ Merlion Pharma)	preclinical	Merger	2.36		
Basilea Pharmaceutical	3	Public		1647	
Biointerface Technologies, Inc.	NA	Private	0.17		
BioLineRx Ltd. (FKA: Bioline Therapeutics)	preclinical	Public	24		
Bionest Company, Ltd.	NA	Private	0		
Biophage Inc.	preclinical	Acquisition	0.47		
BioRelix, Inc.	preclinical	Private	0.25		
Biovertis AG	preclinical	Private	21.21		
Celtrix Pharmaceuticals, Inc. (FKA: BioGrowth)	NA	Public	42.77		
Cempra Pharmaceuticals, Inc.	3	Private	14		
Ceragenix	approved	Public		40.4	
Cerexa, Inc.	2	Acquisition	50		480
Chaperone Technologies	preclinical	Private	0		
Chem Tech Research, Inc.	NA	Private	5.28		
Chemokine Therapeutics, Inc.	2	Public	1.8		
China Chemical Synthesis Industrial Co. Ltd.	NA	Private			
Confarma S.p.A.	NA	LBO	0		
ConjuGon, Inc.	preclinical	Private	3.3		
Connetics Corp.	approved	Acquisition	55.55		640
COR Therapeutics, Inc. (acquired by Millenium)	approved	Acquisition	20.65		1090

Appendix (continued)

Company Name	Phase of leading candidate	Status	Amount Invested ($ millions)	Market Cap (for public companies) ($ millions)	Acquisition Price ($ millions)
Crea BioPharma Inc.	NA	Private	0.75		
Cubist Pharmaceuticals, Inc.	approved	Public	36.28	1210	
Cumbre Pharmaceuticals, Inc. (FKA:Cumbre Inc.)	1	Private	38.89		
Daiichi Sankyo	3	Private			
Demegen, Inc. (FKA: Demeter BioTechnologies, Ltd)	preclinical	Public	4		
Diatide, Inc. (FKA: Diatech, Inc.)	3	Public	41.73		
Digilab BioVisioN GmbH (FKA: BioVisioN AG)	NA	Acquisition	29.6		
Discovery Laboratories, Inc.	NDA	Public	13.21	132.4	
Elitra Pharmaceuticals, Inc. (FKA: RajyaBiotics, Inc.)	defunct	Private	45.85		
EluSys Therapeutics, Inc. (FKA: E-Site Therapeutics)	2	Private	70.24		
Emergent Biosolutions (FKA: Microscience, Ltd.)	approved	Public		326.85	
Enanta Pharmaceuticals, Inc.	2	Private	107.26		
EntoMed SA	defunct	Defunct	25.98		
EntoMed SA	defunct	Defunct	25.98		
Entopharm Company, Ltd.	NA	Private	0.77		
Exponential biotherapies	2	Private	37		
FASgen, Inc.	preclinical	Private	0.5		
Genaera Corporation (FKA: Magainin Pharmaceuticals)	2	Public	18.11	47.9	
Genetic Systems Diagnostics Partners	NA	Acquisition	2.8		
Glykoz Pty Ltd.	preclinical	Private	43.34		
Great Lakes Pharmaceuticals, Inc.	NA	Private	0.3		
Hedral Therapeutics, Inc.	NA	Private	0		
Hedral Therapeutics, Inc.	NA	Private	0.08		
Helix Biomedix, Inc	preclinical	Public		17.09	
Imagilin Technology, LLC	approved	Private	0.08		
Immune Response Corporation (The)	2	Public	26.9	11.98	
InfiMed Therapeutics, Inc.	NA	Acquisition	31.97		
Infusion Systems Corporation	NA	Acquisition	7.5		
Inimex Pharmaceuticals, Inc.	preclinical	Private	11.64		
Innate Pharmaceuticals AB	preclinical	Public	2.37		
Intralytix	approved	Private			
ioGenetics LLC	preclinical	Private	0.2		
Ipsat Therapies Oy	2	Private	19.11		
Ivex Pharmaceuticals, Ltd.	NA	Acquisition	0		
Korea United Pharm, Inc.	approved	Public	0.24		
KOSAN Biosciences, Inc.	2	Public	52.54	212.37	
Libragen	preclinical	Private	0.68		
LTB4 AB	NA	Private	0		
Lyphomed, Inc.	recalled	Acquisition	2.38		
Lytix Biopharma AS	preclinical	Private			
Mayne Pharma, Pty. Ltd. (FKA: Faulding FH & Co.)	approved	Acquisition	0.04		
Medication Delivery Devices	NA	Merger	6.1		
Mediphore-Biotechologie AG	NA	Bankruptcy - (	2.61		
Microban International, Ltd.	NA	Private	65.88		
Microbiotix	preclinical	Private	5		
Microscience Ltd.	NA	Acquisition	62.4		
Midway Pharmaceuticals, Inc.	preclinical	Private	0.57		
Migenix, Inc. (FKA: MitoKor)	3	Public	0	57.29	
MithraGen, Inc. (FKA: MithraTech, Inc.)	NA	Private	3.06		

Appendix (continued)

Company Name	Phase of leading candidate	Status	Amount Invested ($ millions)	Market Cap (for public companies) ($ millions)	Acquisition Price ($ millions)
Morphochem AG	NA	Acquisition	91.77		
Mpex Pharmaceuticals, Inc. (FKA: Mpex BioScience)	1	Private	19.7		
Mutabilis	preclinical	Private	11.25		
Nabriva Therapeutics Forschungs GmbH	1	Private	50.82		
NanoBio Corporation	preclinical	Private	10		
Nectar Lifesciences, Ltd. (FKA: Surya Medicare Ltd)	NA	Private	1.37		
Neogen Corporation	NA	Public	6.15		
NeuTec Pharma PLC	3	Public	10.1	35.4	
Nobex Corporation (FKA: Protein Delivery)	NA	Bankruptcy - (	90.49		
Novacta Biosystems	NA	Private			
Novexel S.A.	1	Private	135.16		
Novobiotics	NA	Private			
Novozymes	preclinical	Public			
Oculus Innovative Sciences, Inc.	approved	Public	55.48	78.8	
Optimer Pharmaceuticals, Inc.	approved	Public	67.25	200	
OraPharma, Inc.	approved	Acquisition	33.9		85
Oscient Pharmaceuticals	2	Public		59.9	
Oxoid Holdings, Ltd.	NA	Acquisition	0		
Pacgen Biopharmaceuticals Corporation	1	Public	0		
Par Advance Technologies	preclinical	Private			
Paratek Pharmaceuticals, Inc.	1	Private	76.6		
Pasteur Merieux Serums & Vaccins (AKA: PMs&v)	NA	Acquisition	0.32		
Peninsula Pharmaceuticals, Inc.	3	Acquisition	88.26		245
Peptide Technologies	NA	Private			
PepTx, Inc	preclinical	Private			
Pharmoptima	none	Private			
Polymedix	preclinical	Public		30.41	
Prolysis, Ltd.	preclinical	Private	20.77		
Pro-Med AG	NA	Private	7.49		
Proteolix, Inc.	1	Private	40.8		
Protez Pharmaceuticals	2	Private	26.86		
Receptagen Corp (FKA: VitaMed Inc)	defunct	Private	1		
RedCell, Inc.	NA	Acquisition	10.05		
Remedyne Inc.	NA	Defunct	3.2		
Replidyne, Inc.	1	Public	126.5	141.4	
Rib-X Pharmaceuticals, Inc.	2	Private	124.5		
RNL Life Science	NA	Private	0.73	9.9	
Rx3 Pharmaceuticals, Inc.	preclinical	Private	1.37		
Sam Chun Dang Pharm Co., Ltd.	NA	Public	0		
Schering-Plough Corporation	NA	Public			
SciClone Pharmaceuticals	2	Public		120.26	
SelectX Pharmaceuticals, Inc.	preclinical	Private	7.95		
Siga Technologies	1	Public		92.4	
Smart Drug Systems, Inc.	NA	Private	12.79		
SoloPak Pharmaceuticals, Inc.	NA	Private	78.46		
Suntory	NA	Public			
Targanta Therapeutics, Inc. (FKA: PhageTech, Inc.)	3	Private	85		
Tetraphase Pharmaceuticals, Inc.	preclinical	Private	10.04	25	
Theravance, Inc. (FKA: Advanced Medicine, Inc.)	NDA	Public	244.58	1810	
Trimeris, Inc. (FKA: SL-1 Pharmaceuticals, Inc.)	approved	Public	38.28	157.5	
Trine Pharmaceuticals, Inc.	NA	Private	87.48		
Triosyn Corporation	NA	Private	6.21		
Ulysses Pharmaceuticals Products Inc.	preclinical	Private	0.19		
Vertex Pharmaceuticals, Inc.	approved	Public	13.54	5060	
ViroPharma, Inc.	approved	Public	13.99	1030	
Westgate Biological Ltd.	NA	Private	0		
Xigen SA	preclinical	Private	21.17		
Xoma, Ltd.	3	Public		375.6	
Zengen	2	Private			

Note: Public valuations are given by current market capitalizations (2007). Private valuations correspond to the amount invested (*Source: VentureXpert and Internet research*)

Table B: Minimum Inhibitory Concentrations of designed peptides against bacterial targets.

Class	*E. Coli* (gram negative)		*B.Cereus* (gram positive)		*E. Coli* or *B. Cereus* MIC≤256μ/ml
	MIC≤256μ/ml	MIC ≤ 64μ/ml	MIC≤256μ/ml	MIC ≤ 64μ/ml	
Designed	16/40	4/40	8/40	4/40	18/40
Shuffled	1/38	0/38	2/38	1/38	2/38

Source: Loose et al., Nature, 443 (19), 2006
Note: "Shuffled" peptides were peptides randomly selected from the middle of non-antimicrobial proteins. They are intended to serve as a negative control.

9.14 References

[1] D. Kraus and A. Peschel (2006) "Molecular mechanisms of bacterial resistance to antimicrobial peptides", in Antimicrobial Peptides and Human Disease, M. Shafer (Ed.), Springer, 231-250

[2] M.A. Riley, J.E. Wertz (2002) "Bacteriocins: evolution, ecology, and application. Annual Review of Microbiology **56:** 117-137

[3] A.K Marr, W.J. Gooderham and R.E.W. Hancock, (2006), "Antibacterial peptides for therapeutic use: obstacles and realistic outlook", Current Opinion in Pharmacology, **6**: 468-472

[4] L. Zhang, T.J. Falla, (2006), "Antimicrobial peptides: therapeutic potential", Expert Opinion in Pharmacotherapy, **6**: 468-472

[5] C. Loose, K. Jensen, I. Rigoutsos and G. Stephanopoulos (2006), "A linguistic model for the rational design of antimicrobial peptides", Nature, **443**(19): 867-869

[6] J. Clardy, M.A. Fischbach and C.T. Walsh (2006), "New antibiotics from bacterial natural products", Nature Biotechnology, **24**(12): 1541-1550

[7] Frost & Sullivan, US critical care antibiotics market, May 2003

[8] Phone conversation with Michael Zasslof, Professor of Surgery and Pediatrics, Georgetown University, founder of Magainin Pharmaceuticals, Inc. (March 2007)

[9] J.L. Fox (2006), "The business of developing antibacterials", Nature Biotechnology, **24**(12): 1521-1528

[10] V. Marx (2005), "Watching peptide drugs grow up", Chemical & Engineering News, **83** (11): 17-24

[11] Press release by Cubist Pharmaceuticals, January 24, 2007 http://www.vcall.com/IC/GenRelease.asp?ID=112420

[12] Frost & Sullivan, Strategic analysis of the therapeutic peptides market in Europe, October 2004

[13] R.E. Christoffersen (2006), "Antibiotics-an investment worth making?", Nature Biotechnology, **24**(12): 1512-1514

[14] Conversation with Daphne Zohar, Eric Elenko, and Kevin Pojasek, PureTech Ventures (April 2007)

[15] J.J. Fleming, "Platform versus Product Strategies", presentation at the MIT Sloan School of Management as part of course 15.363, Strategic Decision Making for the Life Sciences, April 2007

[16] C. Loose, J.F. Moxley, "Discovery and evaluation of antimicrobial peptides", document submitted to the innovation grant program at the Deshpande Center, MIT, 2006

[17] P. W. Latham (1999), "Therapeutic peptides revisited", Nature Biotechnology, **17**: 755-757

[18] H.G. Boman, (2003), "Antibacterial peptides: basic facts and emerging concepts", Journal of Internal Medicine, **254**: 197-215

[19] Conversation with Robert Bitterman, President & CEO of Cutanea Life Sciences, (May 2007)